ALUMINA - SILICON CARBIDE COMPOSITES FROM KAOLINITE-CARBON

PRECURSORS BY HOT-PRESSING

by

MADHUSUDHAN R. PENUGONDA

B.Tech(Ceramic Engineering), Institute of Technology - Banaras Hindu University, India,

1985

A THESIS SUBMITTED IN PARTIAL FULFILMENT OF

THE REQUIREMENTS FOR THE DEGREE OF

MASTER OF APPLIED SCIENCE

in

THE FACULTY OF GRADUATE STUDIES

Department of Metals and Materials Engineering

We accept this thesis as conforming

to the required standard

THE UNIVERSITY OF BRITISH COLUMBIA

December, 1987

In presenting this thesis in partial fulfilment of the requirements for an advanced degree at the University of British Columbia, I agree that the Library shall make it freely available for reference and study. I further agree that permission for extensive copying of this thesis for scholarly purposes may be granted by the head of my department or by his or her representatives. It is understood that copying or publication of this thesis for financial gain shall not be allowed without my written permission.

Department of <u>Metals and Materials Engineering</u>

The University of British Columbia
1956 Main Mall
Vancouver, Canada
V6T 1Y3

Date <u>March 4, 1988</u>

DE-6(3/81).

ABSTRACT

The system kaolinite – carbon black consisting of cheap precursors has been investigated, in terms of its potential to form Al_2O_3 – SiC composites. The carbothermal reduction process of mullite and silica was studied, in detail, in the range $1275°$ to $1810°C$ and over different periods, both under sintering as well as hot–pressing conditions. It was established that the reduction of mullite and silica starts around $1450°C$, where the rate of reaction is very slow. Until about $1800°C$ during the reduction of mullite, SiO_2 gets preferentially reduced, thus forming a composite ceramic consisting of SiC and Al_2O_3 phases.

The kinetics of the formation of SiC + Al_2O_3 were followed in the range $1590°$ – $1660°C$ and it was noted that under hot–pressing conditions they follow a contracting cylinder model. The rate of reaction increased with the increase in temperature and followed a parabolic path with time because of the geometry of the hot–pressed specimens at each temperature. This indicated that the gas diffusion in and out of the system along the edges of the cylindrical specimens is the rate controlling step. The activation energy of the reduction process was calculated to be 922 KJ/mole. The application of pressure prior to the carbothermal reduction process seemed to be not favourable for the formation of SiC and Al_2O_3, however, when applied after the beginning of soaking period, this greatly improved the densities and formation of SiC and Al_2O_3.

The microstructure of the samples was analysed using SEM and TEM. It was found that the grain size of the composite ceramic was of the order of 0.2μm. SiC was

present mainly in the form of fine platelets.

Finally, the isothermal compaction behaviour of the system was studied under a constant pressure in the temperature range $1200^{\circ}C - 1800^{\circ}C$, during which the formation and carbothermal reduction of mullite and silica took place. A mathematical model based on the least squares fitting was used to fit the compaction curves. Due to the complex nature of the compaction data an empirical approach was used to interpret the data and a viscoelastic model was developed. It was found that the interactive–double–Kelvin unit having two elastic and two viscous components explained the type of compaction behaviour observed in the kaolinite + C system. One of the viscous components (η_1) and one of the elastic components (M_1) were found to be temperature sensitive.

It is concluded that starting from the cheap precursors (kaolinite and carbon black) a particulate composite of Al_2O_3–SiC can be produced by hot–pressing technique. SiC–whisker formation is not encountered in this system. The very fine grain size of the particulate composite, resulting in a small flaw size, should provide the composite ceramic with good mechanical properties.

TABLE OF CONTENTS

List of Tables

List of Figures

ACKNOWLEDGEMENT

1. INTRODUCTION

1.1. General Review

1.1.1. Importance of Structural Ceramics

This may be called *Ceramic Fever*[1] or *Industrial and Cultural Revolution through High-Tech Ceramics.*[2] The interest in technical ceramics has grown tremendously over the last decade and will continue to increase. *The Promise of Ceramics*[1] is leading the materials engineer into the *Age of Dynamic Ceramics.* That's because these materials offer a truly unique set of properties that could allow them to perform functions that no other families of materials can. Their novel functions include electrical/electronic, structural/mechanical, magnetic, optical, chemical and biological applications. The United States Senate in a recent bill described ceramics as being *economic strategic materials* because they are expected to have a significant impact on the economy in the future.

Structural applications of ceramics range from automotive heat engines to military armor. Applications of ceramics in heat engines offer many advantages. Some of them are (i) increase in engine efficiency, (ii) decrease in the specific fuel comsumption, (iii) lighter weight engines and (iv) reduction of pollution. In addition, since ceramics have better wear properties than metals, friction is reduced. Ceramics will also open the way for engine options such as the turbine and stirling. These engines could be used in automotive, aerospace and military applications. Turbine blades, rotors, vanes, shrouds, combuster, combuster liners and other parts are candidates for ceramics.

1.1.2. Importance of Reliability

The incorporation of brittle ceramics in engines in the place of more ductile metals has necessitated a new perspective on engine design and a dialogue between engine designers and ceramists. The primary design criterion is reliability which includes probability of survival, short-term reliability against catastrophic failure and long-term reliability against wear, corrosion, creep (high temperature deformation under stress), and creep fracture (high temperature slow crack growth). Thermal shock and environmental degradation are also considered in design. Future requirements for high temperature structural materials are, therefore, the systems which retain their strength, toughness, creep resistance and corrosion resistance to increasingly high temperatures for the service life of a particular component.

1.1.3. Limitations of Monolithic Ceramics

Advanced ceramic materials – silicon carbide, silicon nitride, partially stabilized zirconia (PSZ), and SiAlON, because of their excellent chemical and physical properties, have been seriously considered for use as structural components in heat engines and high-temperature energy conversion systems. One severe limitation, however, is the relatively low fracture toughness (K_{IC}) of these materials. With the exception of PSZ (K_{IC} = 7 MPa.m$^{1/2}$), monolithic ceramic materials including SiC, Si_3N_4, Al_2O_3 and mullite have a fracture toughness of the order of 3 to 5 MPa.m$^{1/2}$.

The other limitation is the high temperature degradation phenomenon that exists and which influences both performance and reliability. For example, the strength of a

monolithic ceramic typically diminishes at elevated temperatures (Fig. 1)[3], initially owing to the diminished potency of toughening mechanisms[4] and subsequently, following the onset of creep.[5]
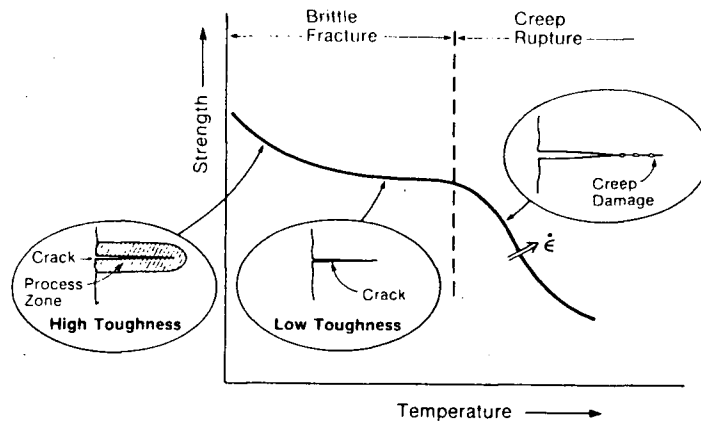
Fig. 1. A schematic illustrating trends in strength with temperature: the trends at lower temperature, in the brittle range, reflect the temperature dependence of the toughness: the trends at high temperature involves creep and creep rupture (after A.G.Evans[3]).

The most important of silicon carbide materials, in technology suitable for industrial production, is the reaction-bonded silicon carbide. Its flexural strength is only moderate in comparison with its hot-pressed counterparts ($\simeq$ 450MPa as compared to $\simeq$ 750MPa), and its toughness is still insufficient for most applications.

In the case of Si_3N_4 its use is limited by its relatively low fracture toughness and by the fact that its mechanical properties begin to deteriorate at temperatures above $1200°C$ due to the glassy phase formed by the sintering aid normally introduced to obtain densification.[6]

1.1.4. *Ways to improve reliability*

Ceramists are pursuing a number of avenues to improve the reliability of ceramics. One of them is to identify the sources of strength–degrading flaws and to develop new processing methods to *eliminate* the defects (i.e., reduce the size of the largest flaw). This involves production of ceramics with very uniform microstructure and very high strength, so that the design stresses can always be kept well below the failure stresses. Substantial advances have been made with this approach during the past 10 years.

However, the most satisfactory approach is to design ceramic microstructures with resistance to fracture, and hence some tolerance to defects. This at best (to the present knowledge) can be achieved by the incorporation of a second phase in the form of discrete particles or whiskers (short fibres) or fibres in a ceramic matrix. This, rather recent feature of the engineering ceramics sector – the *deliberate* construction of multiphase structures in the quest for enhanced physical or other novel properties, has led to what is known as *ceramic matrix composites.*

The great majority of ceramics are multiphase, i.e., comprising more than one solid phase in addition to porosity as may by retained. So it may be appropriate to distinguish the ceramic matrix composites as a separate class of materials from the traditional ceramics, the multiphase nature of which is a consequence of the use of raw materials of relatively low purity.

1.1.5. Ceramic matrix composites

Ceramic matrix composites are an active, expanding field of development. The increasing number of publications in various ceramic and other related journals only confirm the wide interest in the study and development of ceramic matrix composites. This interest has resulted from the increasing promise that such composites show for significantly enhanced mechanical reliability, which the monolithics does not. As there has been no work done in this Department on ceramic matrixcomposites, a detailed review of the status of ceramic matrix composites is included in this thesis.

Within the last year Japan and the U.S. had revised their goals for real-life monolithic automotive ceramic structural applications to year 2000, with ceramic-matrix composites being commercialized around 2010. But most suppliers and potential suppliers of ceramics to the automakers feel that the really practical materials will be found among the ceramic-matrix reinforced composites under development today, and that commercial applications for these ceramic-composite materials are likely to be the first.[7] In fact a sintered silicon-carbide reinforced with titanium-diboride particulates is currently undergoing field tests by Standard Oil Engineered Materials Co. and soon may become commercially available. This composite is 50 to 75% tougher than monolithic silicon carbide and is said to be extremely abrasion resistant. Shown in Fig. 2. are valve-train components, including guides, roller follower, and rocker-arm pads, the prototypes made from their proprietary Hexoloy. These provide the potential for super-hot running engines and extremely low wear.

Fig. 2. Sintered a-SiC/TiB$_2$ particulate ceramic composite valve-train components, including guides, roller follower, and rocker-arm pads, provide the potential for super-hot running engines and extremely low wear (Produced from Sohio Engineered Materials).

1.1.6. Classification of Ceramic Matrix Composites

It may first be pointed out that the state-of-the-art of polymer-matrix and metal-matrix composites is far more advanced than that of ceramic composites. However, in terms of the mechanical behaviour and especially in terms of high temperature use, all-ceramic systems go well beyond reported capabilities. Also work on the processing of metal matrix composites seems to be more restricted in scope than that on the processing of ceramic matrix composites.[8] This review will deal only the ceramic matrix composites, as the subject of uses of ceramic fibers such as glass, graphite, Al$_2$O$_3$, or SiC in polymeric (and more recently in metal) matrices is extensive.

Further classification of ceramic matrix composites can be made on the basis of

the type of the matrix material (non-oxide, oxide, glass or, glass-ceramic) and on the basis of the type of the filler material (carbon, oxide or non-oxide) and of its form (long fibers, whiskers - which are short fibers and often single crystals, and particles).

1.1.6.1. Long Fiber reinforced Ceramic Matrix Composites: General Discussion

The reinforcement of brittle materials with high-strength fibers to yield composites of very high toughness was first demonstrated using carbon fibers in ceramic and glass matrices.[9-10] However, these composites are vulnerable to degradation in oxidizing environments at relatively low temperatures. The commercial availability of continuous-polymer derived SiC fibers (Nicalon),[11] which are more oxidation resistant than carbon fibers and are chemically compatible with many ceramic matrices, has rekindled interest in the development of ceramic matrix composites.[12] A range of other fibrous ceramic materials potentially suitable for ceramic matrix reinforcement (eg. SCS-6 Nextel 312 and FP) are commercialy available along with Nicalon fibers, but only Nicalon has received the most attention. Its favoured status results from the in-situ formation of a carbon-rich interface layer when processed in a number of ceramic matrices, especially oxides. It is currently believed that if a carbon-rich layer is developed at the fiber-matrix interface during the processing of these composites, they fail in a non-catastrophic fashion. This interface is strong enough to transfer load from the matrix to the fibers, yet weak enough to fail preferentiallly prior to fiber failure. The composite can thus accumulate significant local damage without failing catastrophically. That interface layer permits composite toughening by "fiber debonding" and "pull out" but is also the likely cause of oxidative instabilities.

A critical issue for utilization of the aforementioned fibers is their thermal stability. (The assesment of thermal stablility of fiber must be made with the fiber in a composite and not from the data on virgin fibers). It was reported that none of these fibers are likely to provide adequate long term reinforcement at $>1200^\circ$C, and that most would experience problems at $>1000^\circ$C.[13] A satisfactory approach to alleviate the oxidation problem or to improve thermal stability is to protect the fibers by coating them with a suitable material. Such a coating must be chemically compatible with both fiber and matrix, must itself be oxidation resistant, and must provide an interface mechanically suited for composite toughening. A number of organizations have begun to use this approach and have reported favourable composite behaviour at room temperature.[14 – 15]

Recognizing the need for more refractory ceramic fibers, fiber suppliers have been working toward improved products. The new fibers that are now commercially available are Tyranno (Si, Ti, C, O), MPDZ (47 Si, 30 C, 15 N, 8 O) and Nextel 440 (70 Al_2O_3, 28 SiO_2, 2 B_2O_3) and also in developmental quantities the PRD–166 (Al_2O_3, 15–25 ZrO_2). Others that are researched on a laboratory basis are Avco's (Si, C), HPZ (59 Si, 10 C, 28 N, 3 O), MPS (69 Si, 30 C, 1 O) and Nextel 480 (70 Al_2O_3, 28 SiO_2, 2B_2O_3).

It is very encouraging to note that fiber manufacturers are actively pursuing advanced fiber development. It is unlikely that one single fiber will provide the desired mechanical and thermal attributes in addition to being chemically compatible with a wide range of ceramic matrices. Continued efforts by the fiber development community are therefore a critical need to achieve the limits of ceramic composite applications.

1.1.6.2. Whiskers

Whisker reinforcement also has the potential of dramatically improving high temperature properties of ceramics. Silicon Carbide whiskers are now commercially available and the incorporation of these whiskers resulted in ceramic composites with very high toughness values ($K_c \simeq 12$ MPa.m$^{1/2}$) (egs. Al_2O_3 [16] and Si_3N_4 [17] reinforced with SiC whiskers). This interest in whisker reinforcement is stimulated in part by the higher Young's Moduli that can be obtained in whiskers because of their favourable crystal orientations, eg. $\simeq 630$ GPa ($\simeq 90$ million psi) in β – SiC whiskers, which commonly grow in the <111> direction.

Further, there are also other important reasons for interest in short fibers in composites, especially whiskers. The first is the very high strength of the whiskers, eg., the whiskers grown at the Los Alamos National Laboratory frequently have strengths of the order of 10 GPa (>1 million psi).[16]   Another fundamental reason for the interest in whiskers is their single crystal give them the potential of providing the highest temperature capability for ceramic fiber composites.

1.1.6.3. Particulate Addition

There have been a number of reports showing that proper dispersion of second–phase particles can increase the mechanical properties and wear resistance of ceramics.[18 – 21] An advantage of these particulate composites is that they offer increased flexibility for unique material property tailoring.

1.1.6.4. Matrices

Depending upon the application foreseen for these composites, nearly all ceramic materials are potential matrix materials. Important attributes for matrix selection are refractoriness, compatibility with reinforced fibres, whiskers, or particulates, and composite fabricability.

Potential matrices include glass and glass-ceramics, crystalline oxides, carbides, borides, and nitrides. For fiber reinforcement only glass and glass-ceramics have been widely used owing to their relative ease of composite fabrication by hot-pressing.

On the other hand, with whisker and particulate reinforcement a variety of refractory oxides and nitrides have been utilized. This wide choice of matrix materials that whisker and particulate reinforcement can have also adds to the advantages that it has over long fiber reinforcement in ceramic matrices.

1.1.7. Toughening Mechanisms

While the focus of most discussion will be on fracture toughness as a major factor in improved reliability, it should be recognized that this is not the sole criterion. The concept of toughness should be taken in a broader concept of resistance to crack propagation and/or fracture, since there are a variety of circumstances under which one wishes to avoid fracture which may not be directly, if at all, dependent upon the conventional concepts of fracture toughness.[22]

1.1.7.1. Mechanisms most common to ceramic particulate composites

Substantial improvements in toughness have been achieved by creating microstructures containing second phases that somehow resist crack growth (for example by undergoing stress-induced transformations near the tip of cracks)[23] and by adding high strength whiskers.[24]

Numerous mechanisms have been proposed to account for the observed toughening: crack deflection, microcracking, residual stresses, crack pinning, crack bridging and transformation toughening.

Although advanced fracture mechanics analyses have been developed for many of these mechanisms, there is still argument in many composite systems over which mechanisms are responsible for the observed toughening. Moreover, it is likely that several mechanisms operate simultaneously in many materials.[25]

a) Crack Deflection Toughening:

Cracks can be deflected by fracture-resistant second phase particles, or residual stress fields. The reorientation of the crack plane away from normal to the applied stress causes a reduction in the crack driving force which is manifested as an increased fracture toughness.

Faber[26] has made a fairly comprehensive analysis of toughening due to crack deflection. Her results, as summarized in Fig. 3 show that toughening increases in the

order of particles, platelets, to rods or short fibers and that the aspect ratio (length to diameter) is the most important parameter for rods or fibers. An important characteristic of this toughening mechanism is its independence of *temperature and particle size.*
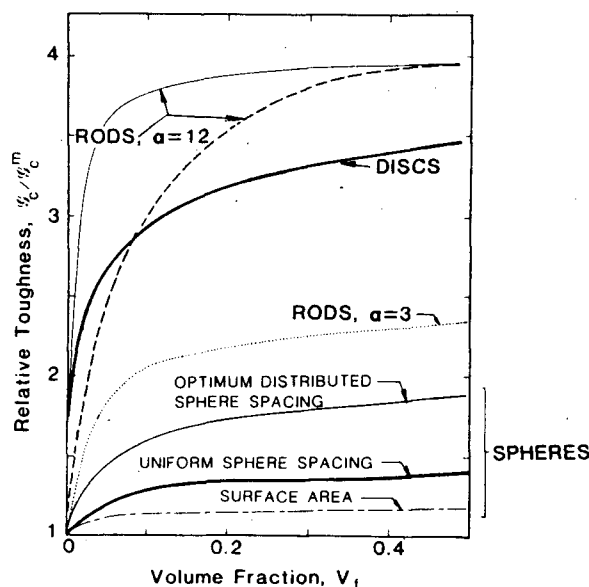
Fig. 3. Summary of analytical modeling of toughening from crack deflection (after K.T.Faber[26]).

b) Microcrack toughening

Ceramic microstructures that contain localized residual stresses are susceptible to microcracking. Such residual stresses can arise from second phase inclusions that undergo transformation or have different thermal expansion or elastic properties than the matrix. The toughening then arises mainly from a crack–tip shielding process, the dilation induced by microcracking. Fracture mechanics analyses[27] of this toughening mechanism indicate that there is generally a size effect in microcracking and that toughening arises only from

particles within a narrow size range (about a factor of two below the critical size for spontaneous microcracking). Consequently, there are strict requirements on microstructural dimensions and uniformity to achieve large increases in toughness by microcracking. (Fig. 4) It should be noted that microcrack toughening is very sensitive to temperature because the thermal expansion "misfits" that give rise to residual stresses are reduced at high temperature.
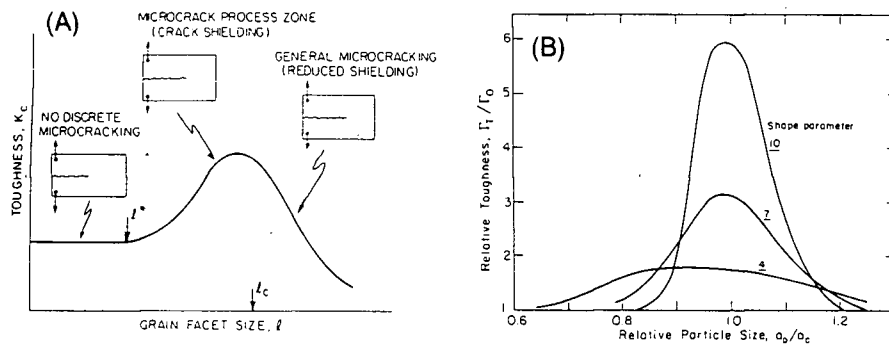
Fig. 4. Effect of (A) grain size and (B) particle size on toughness of microcracking brittle materials (after A.G.Evans[27]).

c) Transformation Toughening

Tetragonal ZrO_2, incorporated in a controlled manner, as a second phase effectively shields crack propagation. This shielding is exemplified by stress–induced martensitic transformation from its high temperature tetragonal structure to the room temperature monoclinic structure which accompanies $\simeq$ 4% volume increase and $\simeq$ 7% shear distortion. Transformation toughening has been achieved by incorporating ZrO_2 precipitates or particles in many matrix materials (Al_2O_3[28] and mullite[29]). There are strict requirements on microstructural dimensions and uniformity because the critical stress for transformation is sensitive to particle size.

1.1.7.2. Toughening Mechanisms in Whisker Composites

The toughening mechanism in whisker composites has not been well identified, but preliminary observations suggest that crack bridging[25] is important. Also crack deflection and whisker pullout were suggested to be the possible toughening mechanisms in whisker reinforced ceramic composites (SiC-whisker reinforced Alumina[30]).

The crack bridging mechanism for improving resistance to brittle fracture is independent of temperature and should also operate in the creep fracture region. Recent experiments have shown that the creep rate of Al_2O_3 reinforced by SiC at high temperatures is reduced by several orders of magnitude.[31] Crack bridging seems to be the likely mechanism of creep inhibition in this case. Further studies of this mechanism are expected to yield large gains in understanding creep processes and in developing improved creep resistance.

1.1.8. Processing and Fabrication of Ceramic Matrix Composites

The critical role of processing and fabrication of a composite in the realisation of its material properties cannot be over emphasized. The whole field of composites is at a stage where the level of processing expertise is often the factor controlling their development.[24]

Fiber reinforced glasses and glass-ceramics can be fabricated in a manner totally analogous to that used for resin matrix composites (hot-pressing, matrix transfer molding and injection molding techniques).[32] Alternate fabrication techniques such as chemical

vapour infiltration[33], melt infiltration and reaction bonding[8,34] can be used for fiber reinforced carbide, silicate and nitride ceramics.

For whisker reinforcement the problem of mixing whisker (or short fibre) and matrix powder brings difficulty with the avoidance of clustering and whisker damage, and the fibre loading is consequently limited[35,36] to some 30 volume percent. The dispersibility of whiskers which translates into improved strength[24] of the composite can be improved both by the ultrasonic dispersion techniques and by the use of a finer-particle, less-agglomerated matrix powder.[24,37] For the fabrication of these composites the most effective technique has been hot-pressing. There have been, however, attempts to use more industrially favoured ceramic fabrication techniques. Pressure-less sintering was used for SiC-whisker reinforced alumina with considerable success.[36] At Max-Planck-Institute fur Metalforschung, W.Germany slip casting of SiC whisker(20 vol%) reinforced Si_3N_4 was done which, after pressureless sintering produced a homogeneous, well dispersed microstructure with improved properties.[38] A recent, not so well established fabrication technique, microwave sintering was used to fabricate SiC and Si_3N_4 whisker reinforced composites of ZrO_2 and Al_2O_3, and full sintered density was reported for alumina.[39]

For powder dispersed ceramic matrix composites the usual ceramic fabrication techniques can be easily employed once the second phase is well dispersed in the composite powder.

1.1.9. Ceramic Matrix Composites Under Development

In previous sections, the emphasis was on concepts rather than specific, i.e., aspects of mechanisms. In this section, however, the specific compositions that have been tried with varying degrees of success and the improved properties of the composites are briefly discussed. Ceramic matrix composites with Al_2O_3 as the matrix phase are described in a full section as these are very related to the present project. However, Table I. summarizes the details of raw materials, fabrication procedure and mainly the improved properties of some composites that have been manufactured recently, without involving alumina matrix.

Table I. Some ceramic matrix composites that have been studied.

Sl. No.	Composition	Matrix phase	Filler phase	Processing details	Fabrication details	Toughening mechanisms suggested	Properties /remarks	Ref.
1	SiC-15vol% TiB2	SiC	TiB2 particles	Powders vibro milled, then wet mixed.	Hot-pressed at 2000 C for 45 mins at 35MPa (96.5% Th. density)	Crack deflection and branching	Mean strength increased by 28%(from 379 to 485MPa). Mean fr. toughness increased by 45%(from 3.1 to 4.5MPa m. Oxidation problems >1200 C.	18
2	SiC-16vol% TiB2	SiC	TiB2 particles	Blended and dried by spl. non-aqueous method.	Sintered at >2000 C in inert atm. (98-99% Th. density)	Crack deflection	Flexural strength increased by 30%(to 478 MPa). Fr. toughness inreased by 90% (to 8.9 MPa m). Thermal shock resistance enhanced. Composite electric-discharge machinable.	19
3	SiC-24.6 vol% TiC	SiC	TiC particles (1 m)	Wet mixed in alcohol	Hot-pressed at 2000 C in vacuum(1.3MPa) at 70MPa. (99% Th. density)	Crack deflection	Critical fr. toughness increased (to 6MPa.m) High flexture strength < 680MPa), both properties increasing with volume fraction of TiC.	20
4	Si3N4-30vol% TiC	Si3N4	TiC particles		Hot-pressed	Not understood	Toughness increased (to 4.3 MPa m) Abrasive wear resistance improved, compared to harder alumina based ceramics.	21
5	Si3N4-0.4wt% SiC	Si3N4 (.5 m)	SiC particles	With sint. aids mixed in attritor mill & CIPped at 630 MPa.	Sintered at 1850 C under 0.1MPa nitrogen and HIPped.	-	Fracture strength improved distinctly. Fracture toughness degraded slightly.	40
6	Si3N4-30vol% SiC	Si3N4	SiC-whiskers	Si + Si3N4 + additives wet mixed in ethanol for 90 hrs. CIPped, nitrided at 1200 C (1hr.)& at 1350 C(3hrs)	Sintered at 1850 C, or HIPped at 1700 C, 200 MPa Ar pressure	-	Ave. strength dropped from 900 to 600Mpa with 10 or 20 vol% whiskers. Fr. toughness decreased slightly. Degradation in properties attributed to metal impurities.	41
7	Si3N4-30vol% SiC	Si3N4 (.5 m)	SiC-whiskers (aspect ratio 33)	Whiskers dispersed in methanol & added to Si3N4,additives	Hot-pressed to <1800 C, in Nitrogen atmosphere	Whisker pull out & Crack deflection	Fracture toughness increased by 40% (to 6.4MPa m). Fracture strength increased by 25%.	17

17

1.1.10. Alumina matrix ceramic composites

Alumina as a matrix material for ceramic composites is receiving renewed attention mainly because its potential as a high temperature engineering material has been realized by the recent SiC-whisker reinforcement.

Several attempts have been made, earlier, to improve the poor high temperature mechanical properties of alumina by second phase dispersions. McHugh et al.[42] and Rankin et al.[43] reported some strength increase by a metallic (Mo) dispersion, but they explained the results by the refinement in grain size which was obtained when Mo particles were added to the alumina powder before sintering/hot-pressing. The strong effect of Mo fibers[44,45] on the work of fracture was attributed to fiber pull-out, necking and rupture. However, the whole research area of metal additions was not pursued further.

Various carbide phases including SiC, Mo_2C, WC, TiC[46] and ZrC[47] have been tried as dispersed phases in Al_2O_3 matrix, but with limited success. Investigations of the effect of titanium carbide dispersion showed only a minor influence on K_{IC}, but a distinct increase in strength. This was attributed to grain size refinement in the presence of TiC particles during fabrication. In the case of ZrC, low carbide contents improved toughness and strengh, again due to the grain refinement, but high carbide contents caused the mechanical properties to fall due to the poor sintering ability of the carbide. Hot-pressed Al_2O_3-TiC composites possess high wear resistance and are widely used as tool materials for very high-speed cutting/grinding of hard materials.

Hasselman et al.,[48] reported improved thermal shock resistance and toughness for an Al_2O_3 composite with BN inclusion. The relatively much lower Young's modulus of BN improved the mechanical properties of Al_2O_3.

Strengthening alumina by transformation toughening has been studied primarily by Claussen and co–workers.[23,28,49 − 51] Though an extensive study has been made, yet, the basic concept of transformation toughening is disputed in the literature. The 2–3 fold increase in fracture toughness achieved by transformation toughening, however, undisputably makes this as one of the most promising approaches of toughening.

Though very high toughness values are achieved in $Al_2O_3 - ZrO_2$ composites, however, no increase in strength is achieved. On the contrary, the more the volume content or the size of the ZrO_2 particles increased, the more the strength decreased.

1.1.11. Alumina−−SiC−Whisker Composites

1.1.11.1. Enhanced High Temperature Mechanical Properties

Results on hot–pressed $Al_2O_3 - SiC$–whisker composites (summarized in Fig. 5)[52,53] show that when SiC whiskers are added to an Al_2O_3 matrix, both the fracture toughness and strength are significantly improved compared to monolithic Al_2O_3. The improved strength and fracture toughness are retained to $\simeq 1200°C$.[53] In addition, the $Al_2O_3 - SiC$–whisker composites are very resistant to slow crack growth,[53] high temperature creep,[31,54] thermal shock,[37] and are very hard even at $1200°C$.[54] The increase in fracture toughness is due to crack deflection and bridging by the SiC
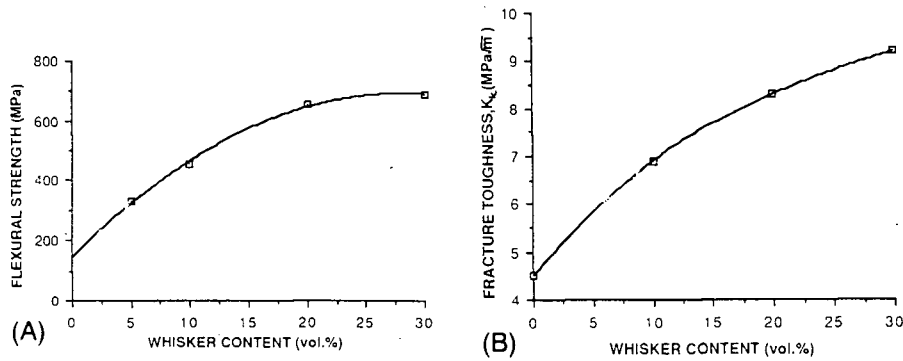
Fig. 5. Both flexural strength (A) and fracture toughness (B) of Al_2O_3 are increased with additon of SiC whiskers. Data are for hot-pressed composites (after T.N.Tiegs[52] and P.F.Becher[53]).

whiskers.[30,35,36,52,53,55] Interestingly enough, Jenkins et al.,[55] using a chevron-notched three-point-bend specimen evidenced a rising R-curve and an increasing K_I value with crack length for the toughening mechanism of a 25 wt% SiC-whisker-reinforced Al_2O_3 ceramic. That means the strength is no longer related uniquely to an initial flaw size.

The reports on SiC-whisker-reinforced Al_2O_3 matrix composites are so encouraging that the product has already been marketed by various manufacturers of ceramic components. For example, Sandvik Coromant Co., Fair Lawn, N.J. markets an Al_2O_3/SiC whisker cutting tool material, designated cc670. Developed for turning and boring nickel-based alloys at high speeds, this material exhibits greater tool life than conventional tungsten carbide inserts. Greenleaf Technical Ceramics, Hayward, CA markets the product under designation WG.300 which has a fracture toughness value, K_c of 8.8 $MPa.m^{1/2}$ and Vickers (10 Kg load) hardness of 8100. Other property data of this material, as supplied are shown in Table I. ARCO Advanced Materials Division, Greer, SC supplies a product designated SA - 25 which is a 25 wt% SiC-whisker distributed in a

Table II. Property data of the SiC – Whisker – reinforced alumina composite supplied by Green Leaf Technical Ceramics.

GREENLEAF CORPORATION

| WG··300 |

TYPICAL PHYSICAL PROPERTIES

PROPERTY	UNITS	COMPOSITE
Microstructure	-	2 Phase Polycrystalline
Crystalline Phases	-	Alumina matrix + Silicon Carbide Whiskers
Density	G/CC	3.74
Porosity	-	Gas Tight
Melting Point	°C	2040
Color	-	Grey/Green
Hardness R_A	-	94.5
Vickers (10Kg Load)	-	8100
Modulus of Rupture (4PT - as machined)	PSI	100,000 ± 6,000
Young's Modulus	PSI	57×10^6
Modulus of Rigidity	PSI	83×10^6
Poisson's Ratio	-	.23
Characteristic Strength	PSI	103,000
Wiebull Modulus (2 parameter)	-	13
Fracture Toughness K_c	KSI $\sqrt{IN}$	8.0
Thermal Expansion (25-500°C)	IN/IN °C	6.0×10^{-6}
Volume Resistivity	OHM-CM	700

polycrystalline alumina matrix.

1.1.11.2. Processing and fabrication of SiC-whisker reinforced alumina composites

a) Raw Materials

SiC-whiskers that have been used by various workers for the reinforcement in Al_2O_3 composites are typically those produced from rice hulls,[56] the microstructure of which was described by Nutt.[57] The whiskers are typically < 1 μm in diameter and about 30 μm in length and are predominantly of alpha form. The whiskers may contain extraneous materials, such as unreacted rice hulls, which have to be removed by sedimentation[32] prior to incorporation into the composites.

Al_2O_3 powder used in these composites is a commercial high purity grade material and often in the submicron size range (0.3 to 0.5 μm).

b) Importance of Processing

Becher et al.,[30] and Shalek et al.,[58] found that processing flaws limited the strength in both the Al_2O_3 matrix composite and the Si_3N_4 matrix composite. The processing flaws observed in the composites are primarily "nests" of whiskers, devoid of matrix Al_2O_3 and Al_2O_3, "prior hard agglomerates" which, after processing, are devoid of whiskers. It is critically important that such processing flaws be eliminated in the final product. The ideal microsructure would contain a uniform distribution of whiskers within the matrix phase.

Very eloborate processing techniques involving flotation or sedimentation from *dispersions* of the components were found to be effective in eliminating the potential flaw types.[46,59] Al_2O_3 powder and SiC whiskers were added together [59] or separately [54] to water and pH of the slurry adjusted for good deflocculation. The slurry was blended and ultrasonically dispersed. The pH of the slurry was then adjusted to flocculate. The slurry was simultaneously heated and stirred[59] or centrifuged[54] to increase the weight fraction of the solids. When separate dispersions were made for SiC whiskers and Al_2O_3 powder, they were mixed in correct proportions, the pH was adjusted, and the mixed slurry was ultrasonicated[8] prior to pressure filtration.[54] Composites fabricated using the material obtained by the above process were found to have homogeneous microstructure, devoid of obvious processing flaws.

c) Importance of fabrication technique

Pressureless sintering was found by Porter et al.,[54] to be ineffective for densification of slip cast components with a 15 wt% whisker loading at 1550°C in vacuum for 30 min. This is due to effective locking of the structure at whisker intersection nodes caused by Al_2O_3 sintered into small aggregates located at the intersections of whiskers.

Tiegs et al.,[37] have recently investigated the various possibilities to overcome the limitations of pressureless sintering and reported not much success. They found that

— lowering the aspect ratio of the whiskers and/or using smaller diameter Al_2O_3 particles would improve the green density and thus lead to increased final densities

— at higher whisker loading ($\geq$ 10 vol%), particle rearrangement during densification

was severely inhibited, resulting in low final densities

— MgO and Y_2O_3 as liquid phase sintering additives greatly improved the sintering for the 10–vol%–SiC–whisker composites

Pressure sintering methods have enabled high densities to be achieved. Porter et al.,[54] obtained full density for a 15 vol%–SiC–whisker–Al_2O_3 composite by vacuum hot–pressing at 1500°C and 24 MPa. With higher SiC–whisker loading (at 30–vol%) J.Homeny et al., achieved theoretical density by the process of hot–pressing for 60 min in ultra high purity Ar atmosphere at 1900°C and 31.2 MPa.

Hot–pressing essentially causes the whiskers to be oriented randomly, with their length in a plane perpendicular to the hot–pressing axis.[30] Due to this the fracture toughness and fracture strengths of a pressure–sintered composite exhibit an orientation dependence. With the crack plane oriented perpendicular to the plane of the whisker axis, large increases in both these values can be observed.

1.1.12. Some Material Sources for SiC – Whiskers.

SiC–whiskers used by various workers[30,37,54,59] for the production of SiC–whisker–reinforced alumina composites are those made by a process involving the pyrolysis of silica and carbon produced from ground rice hulls. The process is potentially inexpensive and two kinds of SiC are formed.[56,60] The bulk of the product contains clusters of extremely fine SiC ($\simeq 0.1\mu$m) and only a small portion ($\simeq 10\%$) contain SiC whiskers (0.1 to 0.5 μm in dia and with aspect ratio of >100). These whiskers are not perfect and contain small internal cavities[57] which would be expected to reduce the

intrinsic whisker strength.

So far, only the whiskers produced by this method are under commercial production and larger whiskers (having higher strengths) grown by a vapour–liquid–solid chemical vapor deposition process at Los Alamos National Laboratory[16] are at the development stage. The later process by its very nature tends to be costly and is not very suitable for industrial production!

For any material that would be used as a heat engine ceramic, cost of production is indeed a major constraint. In a recent survey by Massachusetts Institute of Technology of automotive manufacturers (including General Motors, Ford, Chrysler, Volks Wagen, Daimler Benz and Porshe) to determine the value of altering engine performance characteristic by using ceramics, it was found that the *primary constraint*, over and above any of the other benefits, is that the part must be produced at no additional cost, with cost being the "go/no–go" constraint.

Keeping the above factor in mind, it would be worthwhile to explore the avenues that could lead to potentially inexpensive manufacturing processes.

1.1.13. Kaolinite -- A Potential Raw Material for SiC-Alumina composites

In the case of producing SiC and/or SiC–whisker reinforced Al_2O_3 composites a potentially inexpensive process could be the carbothermal reduction of kaolinite. A typical natural kaolinite is $\simeq$ 45 wt% SiO_2, 38 wt% Al_2O_3 rest moisture and impurities and is an abundant, cheap raw material. Carbothermal reduction of the clay produces typically a

mixture of Al_2O_3 and SiC phases. Bechtold et al.,[61] found that the SiC formed is in the form of whiskers that grow around Al_2O_3 particles. In their investigation however, the main aim was to separate Al_2O_3 as a pure phase from the SiC whiskers. The possibility of producing a dense composite body retaining both the Al_2O_3 and SiC (especially in the form of whiskers) phases would be worth investigating as there has been no such study. It may be noted that carbothermal reduction of kaolinite in the presence of nitrogen is a well established process used for the production of β'–SiAlON ($Si_3Al_3O_3N_5$) powder. This process was first described by Lee and Cutler[62], and very recently by Van Dijen et al.,[63] and Higgins and Hendry.[64]

The feasibility of producing SiC–Al_2O_3 composites by the process of carbothermal reduction of clay can also lead to some additional benefits. These could be

— uniformity in microstructure or very good dispersion of SiC–whiskers within the Al_2O_3 matrix leading to good high temperature mechanical properties.

— higher whisker loading in the composite, and

— possible ease of fabrication

1.1.14. Action of heat on kaolinite(clay)

The thermal decomposition of kaolinite has been studied extensively and continues to be a subject of active interest not only for ceramists but also for mineralogists and crystallographers. This is partly because of the industrial applications, but also due to the complexity of the mineral reactions involved and the difficulties in characterising the phases.

$$Al_2O_3 \cdot 2SiO_2 \cdot 2H_2O \quad \xrightarrow{\simeq 600°C} \quad Al_2O_3 \cdot 2SiO_2 \; + \; 2H_2O \qquad \text{........ 1}$$

kaolinite   metakaolinite
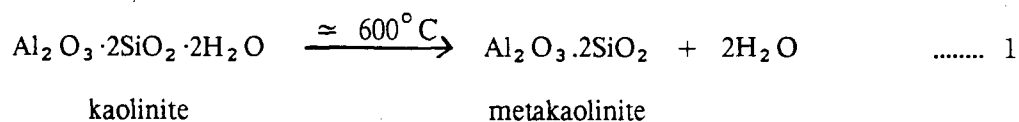
During this reaction, no morphological change of the hexagonal platelets of kaolinite particles could be observed in the hot-stage of an electron microscope.

On further heating, an exothermic event occurs at about 980°C leading to the formation of spinel plus an alumina phase – the nature and significance of which is still debated. The disagreement on the nature of this phase centers on whether it is γ-alumina or an Al-Si-spinel, or some combination of both. The latest investigations of this reaction involved techniques such as infrared study, RED study, RED study combined with structural X-ray spectroscopy, ^{29}Si and ^{27}Al solid-state nuclear magnetic resonance[65]. All of these investigations support γ-alumina formation. They conceed, however, that some spinel may be formed.

With the current knowledge it can be stated that primary mullite(alumina deficient mullite) and spinel phases form at about 980°C in parallel reactions, the relative efficiency of which probably varies from clay to clay. The silica that separates out from metakaolinite is of amorphous nature and does not show up in the XRD analysis. At higher temperatures the spinel may dissociate into silica to form more mullite and the remaining silica gets converted to cristobalite.

1.1.15. Formation of Alumina and Silicon Carbide Phases

Heating a mixture of kaolinite and carbon leads, after the successive phase transformations of kaolinite, to a mixture of mullite, silica and carbon. Further heating of this mixture leads to the carbothermal reduction of the silica phase.

Mullite $(3Al_2O_3 \cdot 2SiO_2)$ is an aluminosilicate consisting of alumina and silica.

The equilibrium reactions in the first stage reduction of silica and alumina may be written as

$$SiO_2 \ (s) \ + \ 3C \ (s) \ = \ SiC \ (s) \ + \ 2CO \ (g) \qquad \text{........ 2}$$

$$2Al_2O_3 \ (s) \ + \ 3C \ (s) \ = \ Al_4O_4C \ (s) \ + \ 2CO \ (g) \qquad \text{....... 3}$$
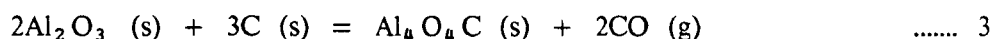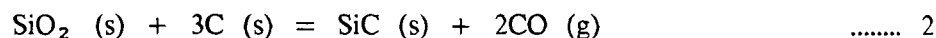
It is seen from Fig. 6 (of ref. 66) that the equilibrium pressure of CO in the reduction of silica is about two orders of magnitude higher than that in the reduction of alumina. As a consequence, in the reduction of mullite, the silica will be preferentially reduced.[61,66,67]

$$Al_6Si_2O_{13}(s) \ + \ 6C \ (s) \ = \ 3Al_2O_3(s) \ + \ 2SiC(s) \ + \ 4CO(g) \qquad \text{........ 4}$$
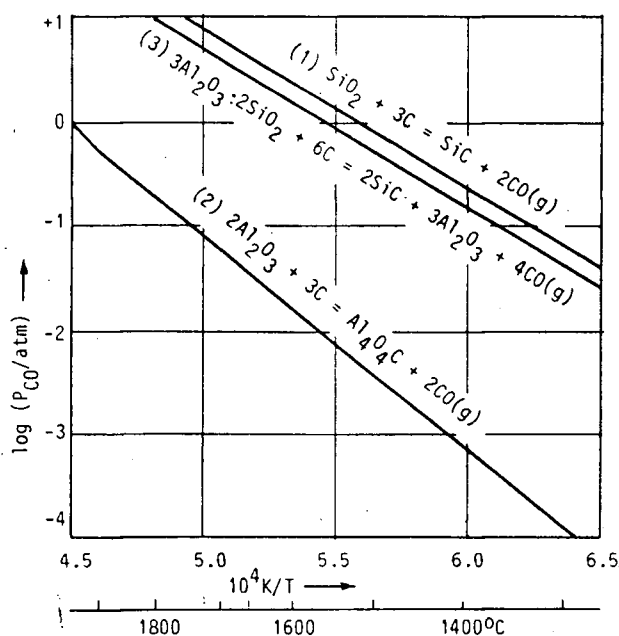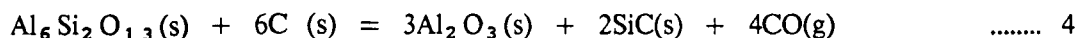
Fig. 6. Equilibrium pressures of CO in the first reaction between carbon and silica and in the first reaction between carbon and alumina (after Siri Bentsen[66]).

It has been well established that the reduction of silica proceeds through gaseous intermediates of CO and SiO. the likely reactions[61],[66] are
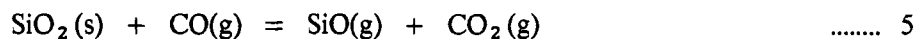
$$SiO_2(s) + CO(g) = SiO(g) + CO_2(g) \qquad \text{........ 5}$$

$$CO_2(g) + C(s) = 2CO(g) \qquad \text{........ 6}$$

$$SiO(g) + 2C(s) = SiC(s) + CO(g) \qquad \text{........ 7}$$

The initial CO gas for Reaction (5) can be obtained from reaction at the solid-solid contacts between carbon and silica particles.[68]

$$SiO_2 + C = SiO + CO \qquad \text{........ 8}$$

Once the reaction is initiated, carbon will regenerate CO through Reaction (6).

1.2. Objectives of the present study

It was mentioned that there is a greater need to look into the processes and methods that make use of the cheaply available raw materials to produce structural ceramics. Bechtold and Cutler[61] devised a scheme to separate alumina from the surrounding SiC whiskers, formed by the carbothermal reduction of clay(kaolinite). As a broad objective, in the present study, a scheme was devised to produce an intimate mixture of Al_2O_3 and the SiC formed during the carbothermal reduction of kaolinite, in order to obtain a composite ceramic.

To clarify the reduction temperatures of silica and alumina from the varied

reports available in the literature, a series of sintering and hot-pressing experiments were performed on kaolinite + C mixtures. The kinetics of the formation of SiC and Al_2O_3 were followed at various temperatures and the reaction mechanism involved was studied.

The effect of pressure, on the nucleation of alumina, formation of SiC and on the densification of the product was studied. The samples were analyzed for the composition, density, phase distribution, grain size and the shape of the particles.

Also, the isothermal compaction behaviour of kaolinite + carbon black mixtures was studied under a constant pressure in the temperature range $1200^{\circ} - 1800^{\circ}C$ during which the formation and carbothermal reduction of mullite and silica took place. Also the effect of excess carbon in the system kaolinite + C was studied. The data obtained were interpreted using mathematical and mechanical models.

2. EXPERIMENTAL

2.1. Materials

The raw materials used in this study were *kaolinite* and *carbon black* which are abundantly available and cheap. The kaolinite of Georgia, North Carolina was supplied by Estrin Ceramic Suppliers under its trademark name of "Ajax". This kaolinite is very pure and has SiO_2 (53.8 wt%) and Al_2O_3 (44.4 wt%) with total impurities below 1%. This is a calcined kaolinite and has the loss on ignition(LOI) of only 0.8% and has a pyrometric cone equivalent(PCE) of cone 36. The kaolinite is of −325 mesh.

It may be noted that kaolinite is a naturally occurring mineral that contains a variety of associated mineral impurities and other ions substituted in its crystal lattice and is far from being consistent either physically or chemically. Common impurities are quartz, mica, TiO_2, Fe_2O_3 and others. Impurities such as quartz and mica tend to have larger particle sizes and can be separated from the kaolinite. However, TiO_2 which is the main impurity in the present kaolinite tends to have a small particle size and distribute itself throughout this mateiral. Also the degree of crystallinity varies from kaolinite to kaolinite mainly as a consequence of its impurities.[69] The impurities present and the degree of crystallinity have marked effect on the thermal transformations and the high temperature behaviour of kaolinite.[65,70,71] For these reasons, a very pure and well known kaolinite (Georgia Kaolin) with minimal impurities was selected for the present study.

The source of carbon was carbon−black, known also as lamp black. It was selected in preference to graphite powder because it is finer and can be very intimately

mixed with clay and it is also more reactive. In addition this material is cheaper than graphite. It may be noted that the selection of the source of carbon is important in that i) the more intimate and reactive the carbon is with clay particle the more favourable is the formation of SiC[66] ii) the morphology of the C precursor might be reflected in the morphology of the SiC formed.[72]

2.2. Mixing

To prepare the kaolinite—carbon black samples, 20g mixtures of the kaolinite and carbon black were weighed in stoichiometric proportions (or in desired proportions) and dry mixed in a vibratory/shaker mixer for 10 mins. The kaolinite—carbon black mixture was then wet mixed thoroughly in an agate mortar and pestle using ethanol as the liquid medium. The amount of ethanol added was just enough to obtain a viscous paste which holds by itself and that no settling of the particles occurred. Wet mixing was found to be very effective in breaking the clusters of the particles of the ingredients and in obtaining a very homogeneous mixture of kaolinite and carbon black.

The viscous mass was dried in an oven at $80^\circ C$ for at least 6 hrs and was further ground into a free flowing powder.

2.3. Hot—Pressing

In order to investigate the feasibility of fabricating alumina—silicon carbide composites from kaolinite—carbon black precursors, initially isothermal compaction experiments and later a set of reaction kinetic experiments were performed. These

experiments were conducted in a hot pressing unit, a schematic diagram of which is shown in Fig. 7.

The powder mixtures were placed inside a high quality graphite die, which served also as the susceptor in a 12 kw induction generator used for heating. The die assembly shown in Fig. 8. consists of a set of floating plungers that can slide inside a graphite sleeve which itself is inserted in the die. The graphite sleeve, tapered outside is finely split along its length which facilitates easy removal of the compact after hot-pressing. Graphite discs (spacers) were placed between the compact and the plungers. The clearance between the plungers and sleeve wall was sufficient to allow the gas phase produced during reaction to escape. Initially the loose powder mixture was put in the die and was precompacted at 20MPa. After the precompaction the plungers and spacers were removed and any excess powder trapped between the sleeve wall and plungers was scraped off. This helped in avoiding the friction between the plungers and sleeve wall.

The whole die assembly was enclosed in a quartz tube containing thick fiberfrax insulation inside and two water cooled copper disks on its top and bottom ends. To prevent oxidation of the graphite die the system was purged continuously with argon.

The load was applied by a pressurized nitrogen cylinder connected to the press. The loading rate can be controlled using a leak valve which allows a linear build-up of pressure in the piston chamber. The loading rate used in all the experiments was approximately 1.3 MPa/sec. The load was recorded with the help of a Houston force washer(Model 2754 v-2k, S/N 5781-001) situated at the bottom of the die assembly. The force-washer was connected to one of the channels of a Kipp and Zonen BD-41 dual
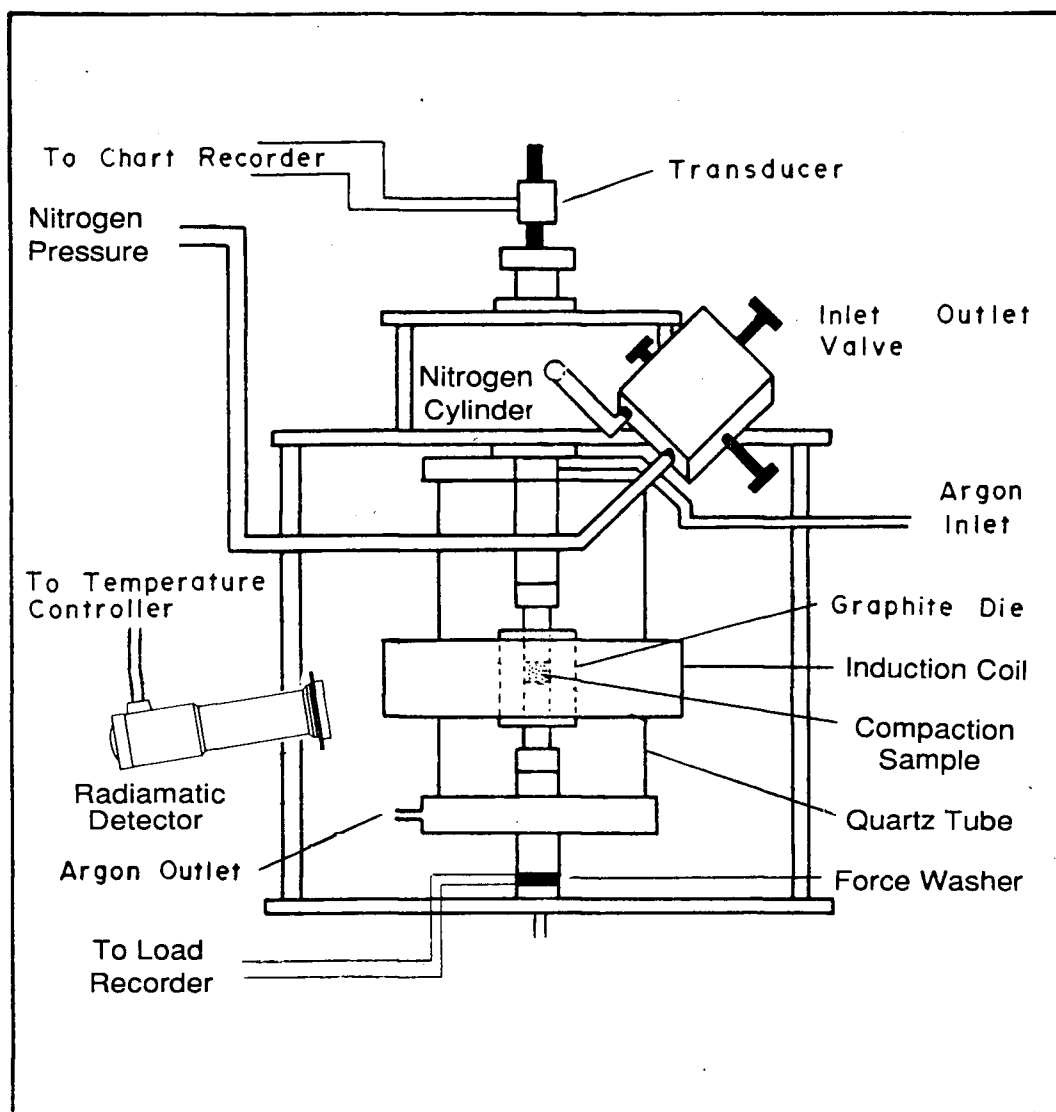
Fig. 7. Schematic diagram of the hot-pressing equipment.
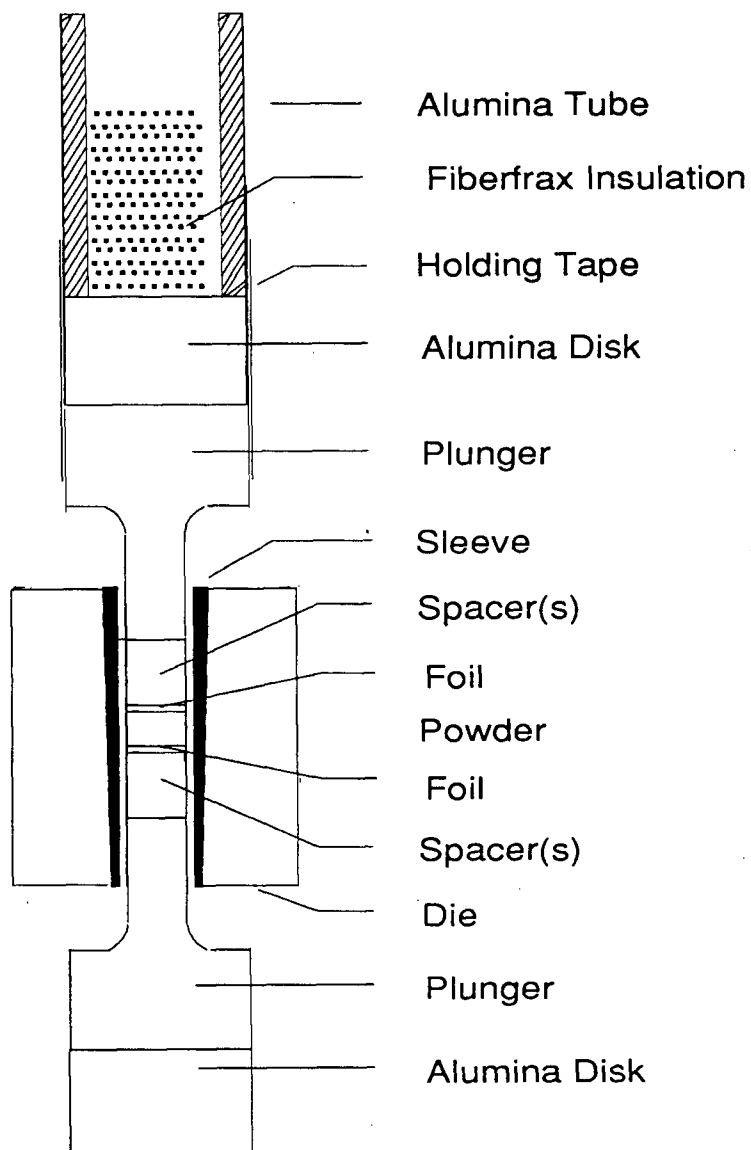
Fig. 8. Die assembly shown in vertical cross-section.
All materials are graphite unless specified.

channel chart recorder set to a 2000 pound full scale load. The force washer was previously calibrated using an Instron testing machine.

The linear dimensional change was monitored by an inductive displacement transducer connected to a strain gauge bridge and to the second channel of the chart recorder.

The temperature was measured using a small target radiamatic detector (Model RI − 3) which was located about twelve inches away from the surface of the graphite die. The detector was levelled and positioned so that it could detect the heat from the central part of the die. For the radiation (from the hot graphite die) to reach the detector a hole was drilled through the quartz tube and its insulation which was fitted with a removable quartz window. The detector was fixed onto a tripod stand which provided a free movement both horizontally and vertically and this facilitated the accurate focus through the window.

2.4. Sintering

The formation of SiC and $a-Al_2O_3$† phases during the kaolinite−carbon black reaction was also studied by pressureless sintering. For these experiments a Centorr furnace with a tungsten resistance heating element was used. In order to avoid contamination from any vapour species of tungsten, the specimens were enclosed in an alumina/graphite crucible with cover. Before sintering, the furnace chamber (and its reservoir) was was thoroughly purged with argon. The argon atmosphere was maintained

---

† Henceforth, all references of Al_2O_3 in the text represent $a-Al_2O_3$.

throughout the sintering experiments.

2.5 Hot-pressing of Kaolinite–carbon black mixtures

The carbothermal reduction of kaolinite–carbon black mixtures leading to the formation of Al_2O_3 and SiC was studied in detail.

2.5.1. Compaction Vs Temperature

Firstly, the compaction behaviour of the reaction mixture, kaolinite + carbon black was investigated as a function of temperature under constant pressure. Similar work on pure clay was earlier reported by Chaklader[73] who also performed isothermal compaction experiments in the temperature region $894 - 1022^\circ C$ covering the transformation of metakaolinite to spinel/$\gamma-Al_2O_3$.

In the present study the effect of carbon (as carbon black) on the compaction behaviour of kaolinite was studied using a mixture of kaolinite and carbon black. These data were then compared with that obtained on pure clay. Two different clay–carbon black mixtures were prepared. In the first mixture(M1) the carbon content was mixed in stoichiometric proportion with the SiO_2 content of kaolinite $(Al_2O_3 \cdot 2SiO_2 \cdot 2H_2O)$. In the second mixture(M2) 22.5 wt% excess carbon was added in addition to that in M1.

About 1.0g of the powder mixture was precompacted (by hand) in the graphite die. The die assembly was then placed in the hot–press and heated at an average heating rate of $25^\circ C/min$. A pressure of 20MPa was applied at room temperature and

was maintained during heating. The linear dimensional change ΔL, during compaction and the corresponding temperatures were recorded. The data were normalized with respect to the initial length and plotted to obtain the compaction curves for both the powder mixtures M1 and M2.

2.5.2. Isothermal Compaction

From the compaction curves of the kaolinite–carbon black mixtures three distinct regions of enhanced compaction were identified. It was mentioned in the earlier works[61,66] that the carbothermal reduction takes place only in the temperature region after the third enhanced compaction step which is also the region of mullite formation. So this temperature range was selected to carry out a series of isothermal compaction experiments. The temperatures selected were 1200, 1300, 1400, 1500 and 1600°C. The compositions selected were the same as M1 and M2.

About 1.0g of the powder mixtures was precompacted (by hand) in the graphite die and was heated in the hot–press at an average heating rate of 32°C per min. Before heating, a pressure of 20MPa was applied on the powder compact and was maintained for 2 mins, until the mechanical equilibrium was reached. This application of pressure was important in two ways; a) to remove any slack present in the die assembly and b) to precompact the loosely held powder which otherwise might contribute to the compaction measured during the mullite formation. After the release of the pressure the heating was started and the temperature raised uniformly noting the linear dimensional change ΔL and the temperature. Once the temperature was about 800°C the pressure (20MPa) was reapplied, slowly and was maintained for 2.0 minutes. The purpose of this

application of pressure was to eleminate the enhanced compaction that normally takes place during the dehydroxylation of kaolinite (500–660°C) which has been reported previously.[74]

Once the pressure was released the heating was continued until the desired temperature was reached. There it was held for 2.0 minutes to attain temperature equilibrium and then a pressure of 20MPa was gently applied and maintained for 10 minutes while the compaction was recorded as a function of time. The pressure was then released and the power was switched off. The time vs ΔL profile on the chart was digitized to obtain a set of ΔL vs time values to obtain an isothermal compaction curve. The initial length value of the specimen was obtained by adding the final length to the total compaction measured from the chart.

2.5.3. Carbothermal reduction of mullite and silica

The initial formation of mullite, especially at low temperatures has been reported to be very sluggish.[71] The amorphous silica separated during the transformation process of metakaolinite to γ–alumina/spinel is not very reactive.[75] Mullite reacts with carbon 2.0 to 2.5 times slower when compared to silica.[66] Due to these reasons the carbothermal reduction of mullite and silica is very slow and the 10 minutes soaking time used during the isothermal compaction experiments would not be sufficient for SiC and Al_2O_3 to form.

In order to study the correlation between the time and temperature needed for the formation of SiC and Al_2O_3 several hot–pressing and sintering experiments were

carried out for much longer times than 10 minutes. Two of the powder mixtures selected for testing were the same as M1 and M2. The third mixture selected contained 10 wt% quartz powder added to kaolinite which is mixed with enough carbon to reduce both the parent and added silica.

Temperatures in the range 1460 – 1800°C and pressures in the range 20 – 50MPa were used for hot-pressing experiments whereas temperatures in the range 1400 – 1800°C were used for sintering experiments. In some of the cases the hot-pressed specimens were further sintered at higher temperatures.

2.5.4. Kinetic Studies

After a basic understanding of the carbothermal reduction reactions of kaolinite(mullite + silica) a more systematic study of the reaction was done in order to follow the kinetics of the reduction process. Four different temperatures 1590, 1620, 1640 and 1660°C were selected and at each temperature experiments were done for varying times. The experimental procedure followed was the same as described in section 2.5.2. Care was taken to use the same die assembly as the variation in the annular space between the sleeve wall and the plungers (plus spacers) affected the rate of compaction.[74] This was due to the gas phase reactions that were involved during the carbothermal reduction process. The hot-pressed specimens obtained were typically of 0.96cm dia and 0.4 – 0.5cm thick.

2.5.5. Characterization

2.5.5.1. Phase Identification

The X-ray diffraction analyses (XRD) were carried out to characterize the sample compositions. Most of the samples were analyzed by XRD to find the various phases present in them. Some difficulty was encountered in distinguishing between the various polymorphic phases of SiC that are present in the samples. This is because of the very similar nature of their 2Θ values.

The bulk density of the specimens was calculated from the dimensions and weight of the specimen. The apparent density and percentage apparent porosity values were calculated using the liquid displacement techniques. Water was used as the liquid medium and the specimens were soaked in water under vacuum (for about 5 hrs) in order to fill all the open pores in the specimen.

2.5.5.2. Microstructure Analysis

Efforts to identify the various phases present and their distribution in the microstructure using a scanning electron microscope (SEM) with an attached energy dispersive X-ray analyser (EDX) were not successful. However, photomicrographs at high magnifications were obtained by SEM to look at the morphology of the specimens.

More importantly, the transmission electron microscopy (TEM) was used to look at the orientation of various grains and phases present in the composite. Most of the

emphasis was on the study of the shape and distribution of the SiC phase(s) present in the system. Though good results were expected from TEM analysis, the specimen preparation was found to be very difficult. The specimens were drilled to produce 3mm disks using an 'abrasive slurry drill'. Thin slices (0.3mm thick) were cut from the disks using a diamond wheel. They were further thinned and polished to approximately 100 μm thick using a disk polisher. Those specimens were carefully mounted using mounting wax on the dimpler stage. The specimens were dimpled in order to thin down the center of the specimen to an approximate thickness of 20 μm. Diamond slurries of 1 μm and 5 μm were used during the dimpling operation. It was found to be most difficult to thin the whole specimen to about 10 μm thick and still retain the strength of the specimen for handling because of its brittle nature. It was also reported that long ion milling causes preferential sputtering.[76] So the dimpling operation was found to be very essential.

The specimens were ion milled in a micro ion mill (of Technics Inc.) using Ar as the ion source. Voltage of 6 KV (DC) and total gun current of 1 mA (DC) were used. The specimens were aligned at $15°$C to the ion beam. The last few hours of the ion milling operation were carefully guarded, so that the perforation once made in the centre of the specimen, was not milled further. The ion milling times needed were typically in the range 60 to 70 hrs. for specimens dimpled to $\simeq$ 15 μm thick. Because of many difficulties involved the success ratio in preparing the specimens useful for TEM analysis was 1:6. When ion milling was found to introduce artifacts in the specimen, mechanical micro-thinning was used to prepare the TEM specimens.

3. RESULTS

3.1. Effect of carbon on the compaction of kaolinite

The application of pressure during the successive phase transformations of kaolinite leads to enhanced compaction at each transformation.[73] This phenomenon has been used to study the temperature ranges and the extent of this enhanced compaction of kaolinite–carbon black mixture. A compaction curve obtained for a mixture of kaolin + 28(wt%)C that was heated at a rate of $25°C/min$ under a constant pressure of 20MPa is shown in Fig. 9. The carbon was present in the form of carbon black and was in molar equivalent of the SiO_2 content of the kaolinite. The compaction behaviour of this mixture seems very similar to that of pure kaolinite. The compaction at around $650°C$ is due to the dehydroxylation of kaolinite and at about $970°C$ is due to the formation of $\gamma-Al_2O_3$ (and/or spinel) and amorphous silica.

To see the effect of carbon content, two reaction mixtures with different carbon contents were selected and the compaction curves were obtained. These compaction plots are shown in Fig. 10. Also included in this figure is another compaction curve of pure clay[73] for comparison. It may however, be noted that the comparison is only qualitative as the experimental conditions and parameters are not the same.

The presence of carbon did not seem to affect the phase transformations but its thermal inertness certainly reduced the total compaction of the mixture. An interesting observation to be made from the figure is that above $1450°C$ the compaction subsided for pure kaolinite, whereas it continued for kaolinite + carbon mixtures.
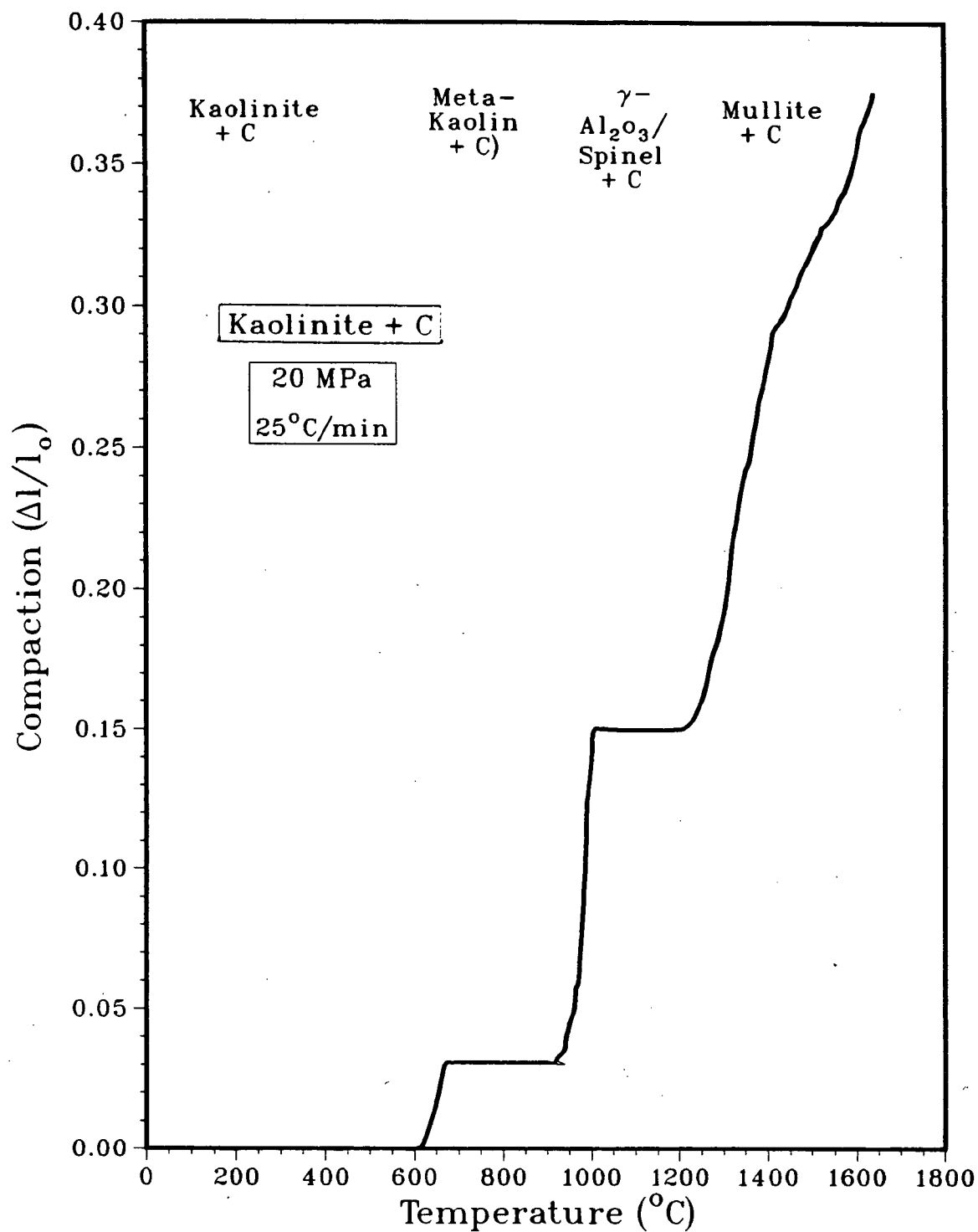
Fig. 9. Compaction curve during the successive phase transformations of kaolinite + carbon black.
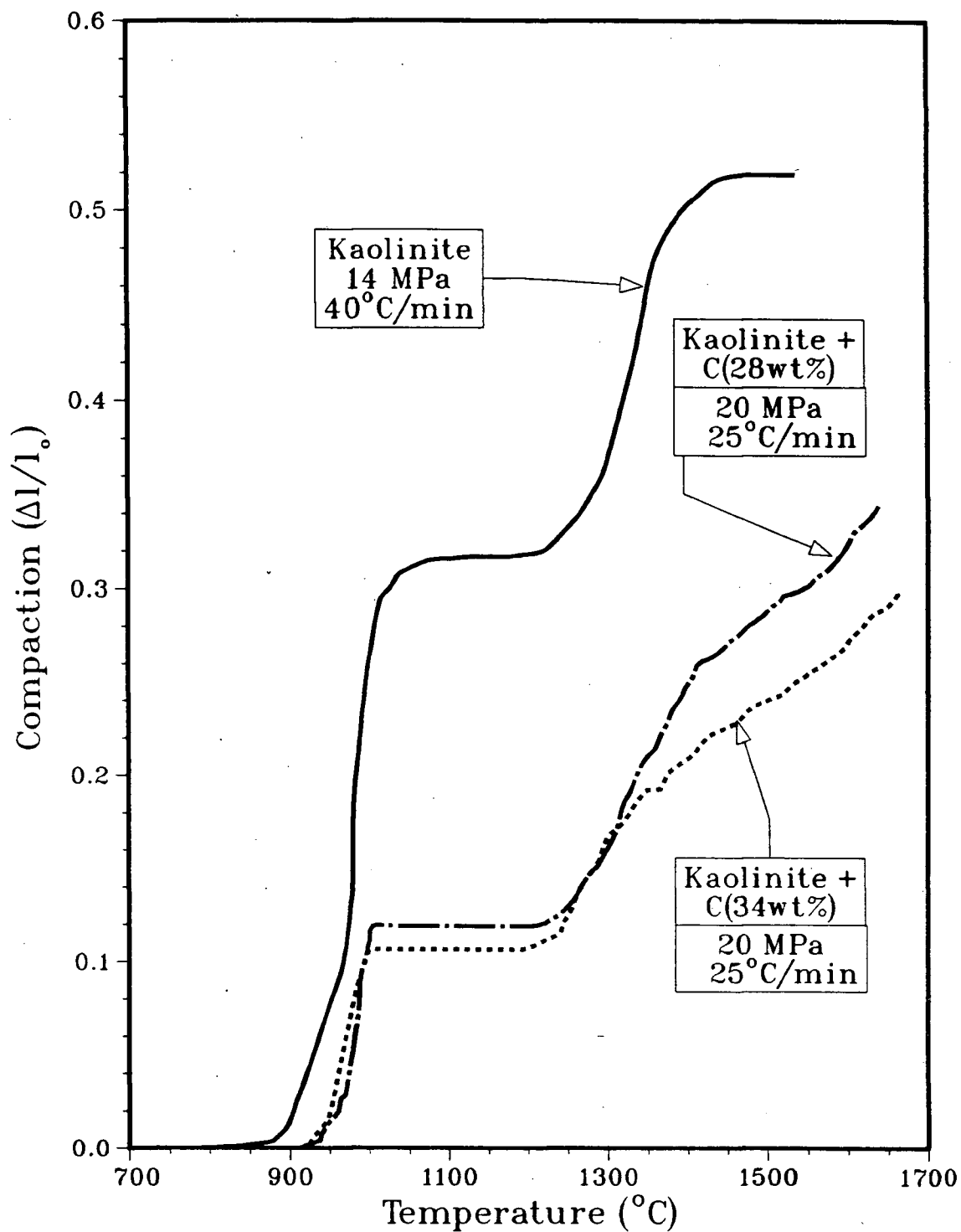
Fig. 10. Comparison of the compaction curves for kaolinite, and
kaolinite + carbon black.

3.2. Formation of Alumina and SiC Phases

3.2.1. Carbothermal Reduction Experiments

Although there has been a general agreement about the gas–solid reactions involved in the carbothermic reduction of mullite or silica, widely different results have been presented in the literature about the temperature and time required for the formation of SiC. Also, the physical state of the reactants was thought to affect the temperature of formation of SiC.[72,77] Moreover, the carbothermic reduction process of SiO_2 and/or mullite has been studied only during pressure–less heating and no attempt has been made to study the role of applied pressure on this reaction during heating of kaolinite–carbon mixture.

For the above reasons, a series of sintering and hot–pressing experiments were performed at various temperatures in the range 1275° to $1810^\circ C$ and over different periods of time. The amount of carbon that was mixed with clay was varied and different reactants were tried for sintering. For hot–pressing experiments different pressure schedules were also tried. The product phases were analysed qualitatively by X–ray diffraction analysis. The various experiments that were performed and their details are summarized in Table III and IV.

In the sintering experiments, all samples have a porous coating, white in colour, on all surfaces that were exposed to atmosphere during sintering. The coating was found to be Al_2O_3. This could be due to the dissociation of mullite with the formation and loss of SiO vapour by reaction (5) leaving behind the stable Al_2O_3. The loss of SiO

Table III. Summary of carbothermic reduction reactions performed under atmospheric pressure.

Expt.#	Reactants	Temp(°C)	Time (min)	Products	Comments
39	SiO_2 + 2C	1510	14	α–cristobalite + C + SiC(traces)	
40	SiO_2 + C	1800	30	α–SiC	
80A	$Al_2O_3 \cdot 2SiO_2 \cdot 2H_2O$ + 2C	1400	120	Mullite + C + α–Al_2O_3(little) + SiC(traces) + α–cristobalite(little)	reduction possible but very slow
81A	$Al_2O_3 \cdot 2SiO_2 \cdot 2H_2O$ + 2C	1460	120	SiC + α–Al_2O_3 + mullite(little)	reduction not complete
52A	Mullite + SiO_2 + 3C	1525	120	SiC + α–Al_2O_3 + C	
52	$Al_2O_3 \cdot 2SiO_2 \cdot 2H_2O$ + SiO_2(10wt%) + 2C(19wt% excess)	1525	120	SiC + α–Al_2O_3 + C + mullite + quartz + α–cristobalite(traces)	reduction not complete
47A	$Al_2O_3 \cdot 2SiO_2 \cdot 2H_2O$ + 2C(28wt% excess)	1655	130	SiC + α–Al_2O_3 + C	
47B	SiC + α–Al_2O_3 + C(12wt%)	1655	130	SiC + α–Al_2O_3 + C	α–Al_2O_3 not reduced
46A	Mullite + SiO_2 + 3C	1805	30	SiC + α–Al_2O_3 + C	Reaction is faster
46B	$Al_2O_3 \cdot 2SiO_2 \cdot 2H_2O$ + 2C(17wt% excess)	1805	30	SiC + α–Al_2O_3 + C	Reaction is faster

Table IV. Summary of carbothermal reduction reactions performed under a pressure of 20 MPa(except #114 and #115 where pr.=30–50 MPa). Pressure applied at the beginning of the soaking period (except for #115).

Expt.#	Reactants	Temp(° C)	Time (min)	Products	Comments
49	$Al_2O_3 \cdot 2SiO_2 \cdot 2H_2O$ + 2C(22.5wt% excess)	1273	15	Mullite + C	No cristobalite
82	$Al_2O_3 \cdot 2SiO_2 \cdot 2H_2O$ + 2C	1460	63	Mullite + α-cristobalite + SiC(traces)	
45	$Al_2O_3 \cdot 2SiO_2 \cdot 2H_2O$ + 2C(17wt% excess)	1550	18.5	Mullite + C	
83	$Al_2O_3 \cdot 2SiO_2 \cdot 2H_2O$ + 2C	1550	61	Mullite + α-Al_2O_3(traces) + SiC(traces)	
84	clay + SiO_2(10wt%) + C(stoi.)	1550	62	Mullite + α-cristobalite + α-Al_2O_3(traces) + SiC(traces)	
73	$Al_2O_3 \cdot 2SiO_2 \cdot 2H_2O$ + 2C	1600	10	Mullite + C	
57	$Al_2O_3 \cdot 2SiO_2 \cdot 2H_2O$ + 2C(22.5wt% excess)	1650	13	Mullite + SiC(traces) + α-Al_2O_3(traces)	
48	clay + SiO_2(10wt%) + C(18.6wt% ex.)	1620	90	SiC + α-Al_2O_3 + C	
85	$Al_2O_3 \cdot 2SiO_2 \cdot 2H_2O$ + 2C	1620	90	SiC + α-Al_2O_3 + C(traces) + mullite(traces)	
114*	$Al_2O_3 \cdot 2SiO_2 \cdot 2H_2O$ + 2C	1805	3	Mullite + C	Pr. applied at
		1660	10		room temp.
115	$Al_2O_3 \cdot 2SiO_2 \cdot 2H_2O$ + 2C	1810	33	SiC + α-Al_2O_3	

* Pressure of 30MPa applied at room temperature, heated to 1805° C soaked for 3 min, temperature decreased to 1660° C and pressure of 50MPa applied, soaked for 10 min.

vapour was also reported previously by various workers.[61,66,72]

The Al_2O_3 surface coating was not observed on the hot-pressed specimens indicating that the closed system, as it exists in a die, prevented the SiO vapour from escaping, and this might have prevented the dissociation of mullite.

From Tables III and IV it can be seen that

— Silica is preferentially reduced during the carbothermic reduction of mullite or kaolinite upto a temperature of 1805°C (Expt. # 46A & B of Table III)

— There is no effect of pressure on this preferential reduction of silica (Expt. # 115 of Table IV)

— Reduction of silica started very slowly at 1400°C, became faster at 1460°C and completed at 1520°C within 2 hours (Expt. # 80A, 81A and 52A of Table III). At higher temperatures the reduction rate became much faster (Expt. # 46A & B of Table III)

— There is a clear indication that an induction period is present for the nucleation of alumina, even at higher temperatures. (Expt. # 82, 73 and 57 of Table IV; #39, 80A of Table III)

— There was not much effect of pressure on the reaction rate when applied at the beginning of the soaking period.

— The carbothermal reduction process did not seem to start even at 1805°C under an applied pressure of 30MPa, applied at the beginning of the heating process (Expt. # 114 of Table IV). This suggests that pressure had significant effect on the initial reaction of the carbothermal reduction process. This would be discussed further in a later section.

3.2.2. Kinetics of the carbothermic Reduction of Kaolinite

The temperature range investigated was 1590° to 1660°C, during which the reaction rate was found to be moderate, but below 1590°C the rate was very slow.

3.2.1.1. Reaction Zone

Figure 11 shows the photographs and a schematic diagram of incompletely reacted pellets which have two distinct zones, a darker central region completely surrounded by a lighter cylindrical zone. It was established by XRD that the outer zone was a composite of Al_2O_3 and SiC, whereas the inner region was primarily mullite, carbon and traces of Al_2O_3 and SiC. It is possible that some undetected amorphous silica was also present in the mullite zone. The reaction thus appears to proceed inward from the outer edges of the pellet. In the process of the formation of Al_2O_3 and SiC both CO and SiO gas must diffuse out of the pellet.

Figure 12 shows the effect of temperature on the reaction of kaolinite–carbon black pellets. Bechtold and Cutler[61] showed that this effect was not due to a heat–transfer–limited process but the reaction kinetics are controlled by a thermally activated process. The figure also shows that there may be an "induction period" for the reaction which decreased with the temperature. This induction period observed for many solid/gas reactions may be connected in this study with the required nucleation of Al_2O_3.

26min   40min   60min   90min
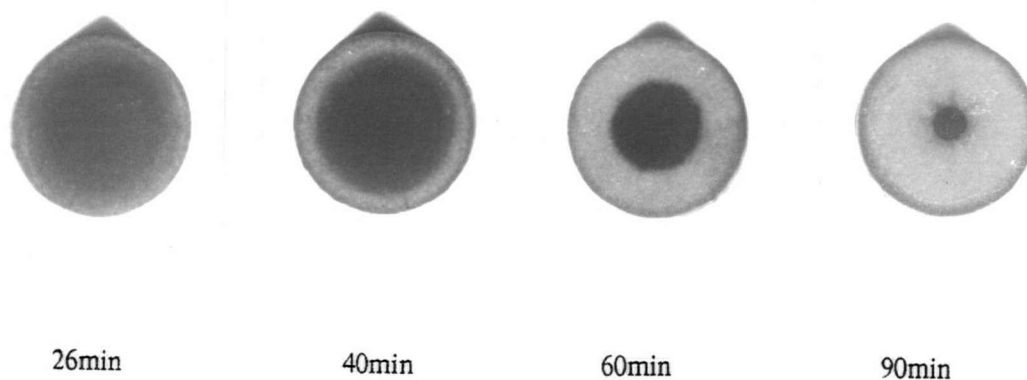
Fig. 11(a) Pellets show the inner contracting mullite–silica–C region and the outer expanding Al_2O_3 – SiC region, with time. (Hot–pressing temp was $1620°C$ and Pr. 20MPa)

hot - pressing direction

SiC + Alumina

Mullite + C

direction of reaction interface

R

L
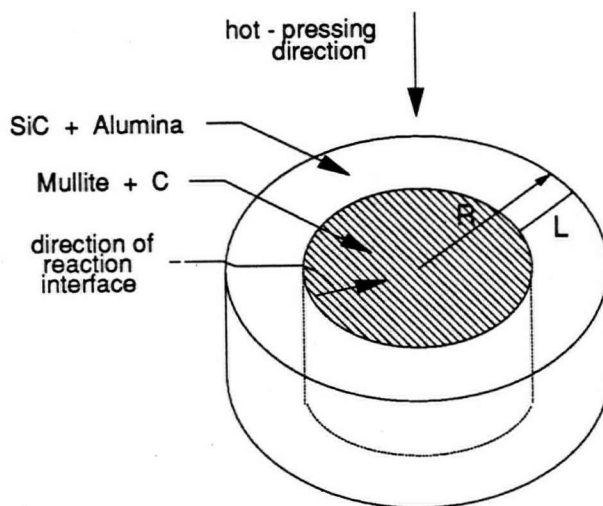
Contracting Cylindrical Model

$$(1 - a)^{1/2} = 1 - Kt/R$$

where

a = reacted fraction

$$= 1 - (1 - Kt/R)^2$$

where

K = interfacial velocity

t = time in minutes

and L = K t

Fig. 11(b) An illustration of the reaction interface movement seen in the pellets above.
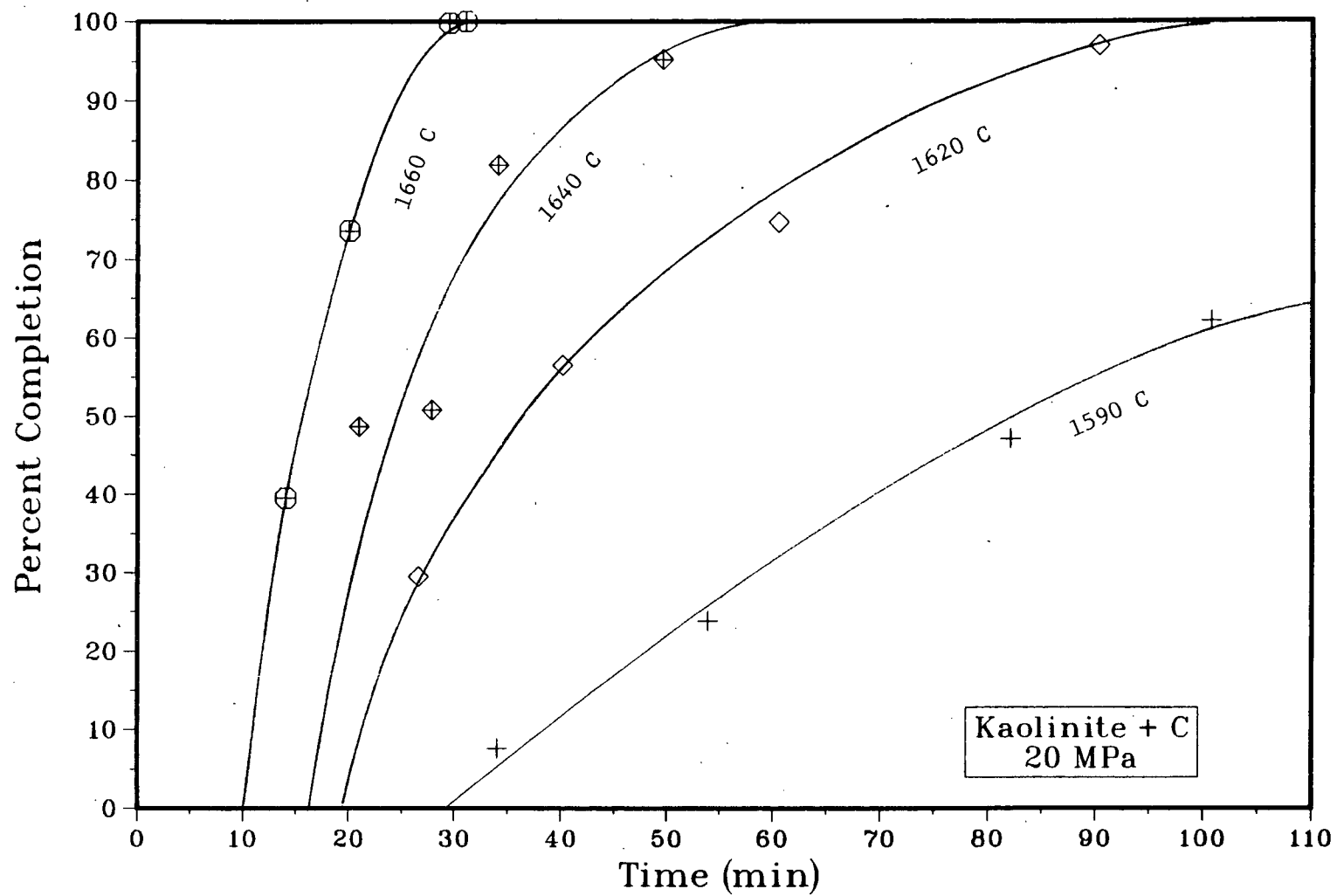
Fig. 12. Effect of temperature on reaction rate.

3.2.1.2. Reaction Kinetics

The carbothermic reduction of clay involves the formation of Al_2O_3 and SiC phases and the evolution of CO gas. The kinetics of the process may then be derived typically by studying the rate of formation of Al_2O_3 and SiC or from the rate of evolution of CO gas by the reaction. The latter choice

$$SiO \ (g) \ + \ 2C \ = \ SiC \ + \ CO \ (g) \qquad \qquad .... \ 7$$
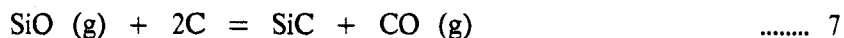
lends itself to noting the weight loss of the reaction mixture as a function of time, as reported previously by some of the earlier workers.[61,66,78] In the present study, however, the rate of formation of SiC and Al_2O_3 was followed as a function of time at various temperatures. This method was used mainly for two reasons. i) It was not possible to measure the weight loss or to evaluate the amount of CO evolved during the hot-pressing of the clay-carbon black mixture. ii) The reaction interface (as shown in Fig. 11) was very sharp, co-centered with the rest of the pellet thereby allowing accurate determination of its position as a funtion of time.

The kinetic data obtained at temperatures 1590°, 1620°, 1640° and 1660°C, shown in Fig. 13 were found to follow the contracting cylinder model. The model described in Fig. 11(b) can be represented by the relation

$$(1 \ - \ a)^{1/2} \ = \ 1 \ - \ Kt/R \qquad \qquad .... \ 8$$

where a = the fraction of the composite formed

K = interfacial velocity towards the centre

t = time in minutes
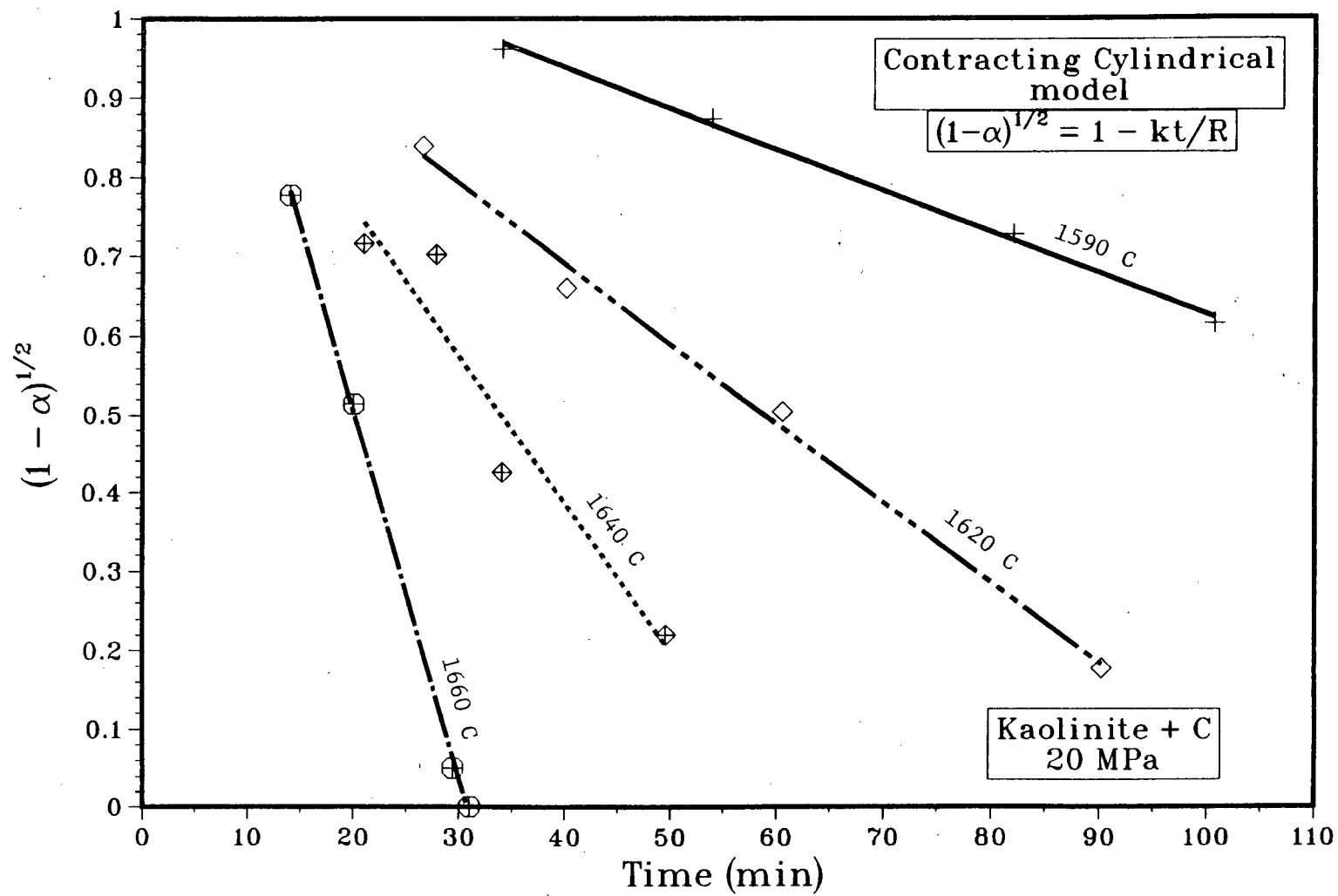
Fig. 13. Kinetic data of the formation of alumina–silicon carbide vs contracting cylinder model.

and   R = radius of the pellet

The plot of $(1-a)^{1/2}$ vs t, is linear, in agreement with the *contracting cylinder model.*

3.2.1.3. Activation Energy

The activation energy for the carbothermic reduction of kaolinite was determined by plotting the slopes of the lines in Fig. 13 as shown in Fig. 14. From the slope of this plot and using the Arrhenius equation

$$K = Ae^{-E/RT}$$

.... 9

the activation energy E was calculated. It is 922 KJ/mole.

3.3. Density Measurements

The density measurements of some of the selected specimens are presented in Table V. The densities obtained, in general, were very low. The measurements were based on the theoretical density and amount of the phases present in the pellet.
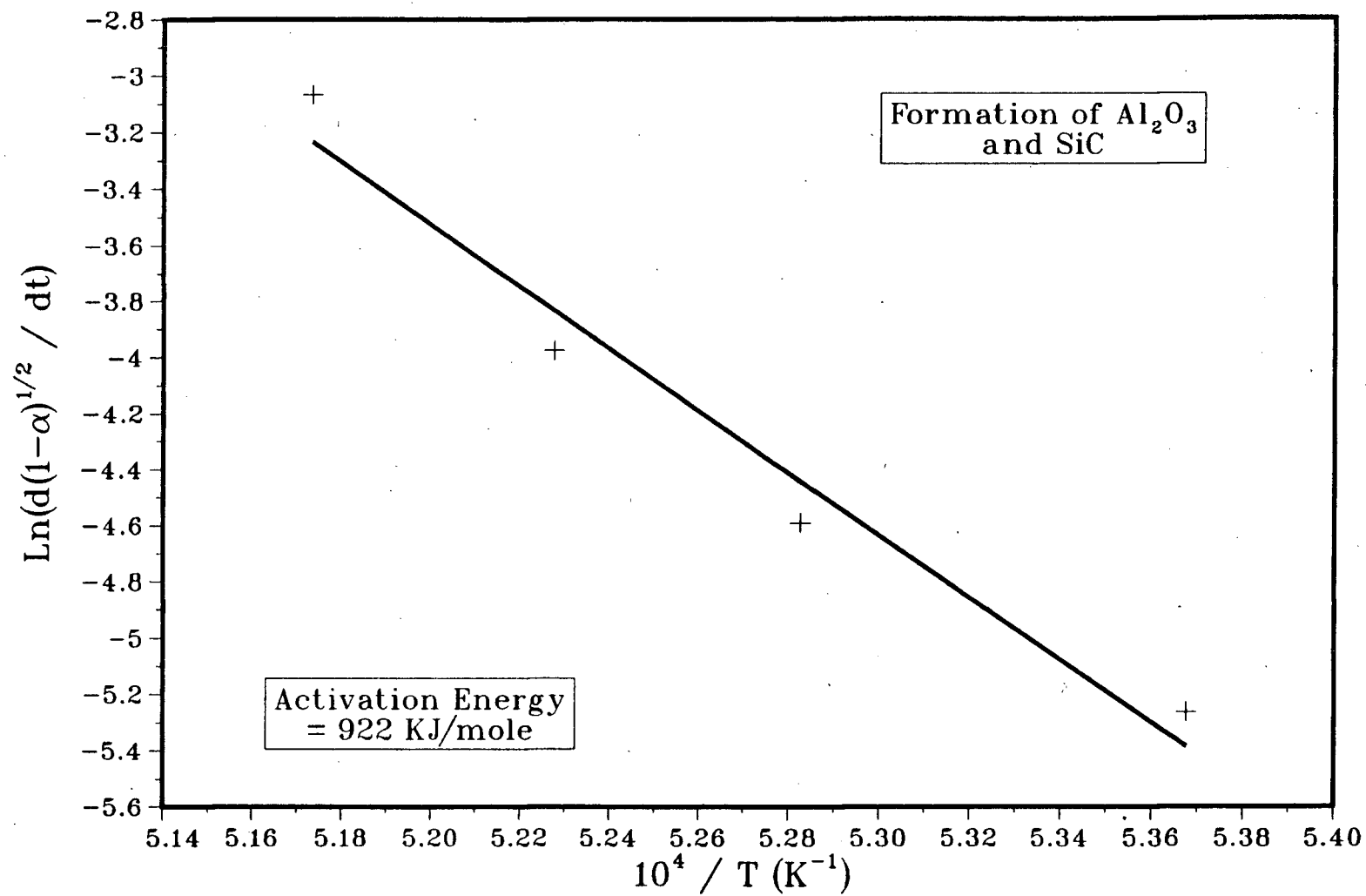
Fig. 14. Arrhenius plot to calculate the activation energy of the formation of alumina and silicon carbide.

Table V. DENSITY MEASUREMENTS OF SOME SELECTED SPECIMENS.

EXP. #	TEMP (C)	PRESS. (MPa)	% APP. POROSITY	% Th. DENSITY	PHASES PRESENT
58	1200	20	35.67	56.1	MULLITE + SiO_2 + C(22.5 wt% excess)
59	1300	20	29.15	62.8	"
60	1400	20	22.24	69.2	"
61	1500	20	18.18	73.7	"
62	1600	20	24.30	72.2	"
77	1200	20	34.06	56.0	MULLITE + SiO_2 + C
78	1300	20	27.37	62.8	"
75	1400	20	18.40	70.6	"
70	1600	20	22.06	75.1	"
114	1810	45	2.02	94.0	"
110	1640	20	46.43	51.4	SiC + Alpha-ALUMINA
99	1660	20	47.03	51.7	"
113	1780	40	34.30	64.3	"
115	1800	40	32.41	66.9	"

3.4. Microstructure

3.4.1. SEM Analysis —

The Scanning Electron Microscopy (SEM) was used to look at the morphology of the hot–pressed specimens of kaolinite + carbon. The Hitachi S–570 Scanning Electron Microscope attached with the Kevex EDX Analyser was used for the SEM study. The voltage used was 20KV. The specimen preparation was relatively simple. The specimen surface was carbon coated for the EDX analyses and gold coated for taking high magnification/resolution photomicrographs.

At low magnifications some surface details could be seen on the photomicrographs. The individual grains could not be identified phases could not be analysed using the EDX analysis. EDX analysis showed both the Al and Si Kα peaks all over the specimen that contained the SiC and Al_2O_3 phases. X-ray maps were generated scanning for Al and Si individually but no information could be gained from them as both the elements were spread thoughout the micrograph. Due to this difficulty SEM analysis at low magnification was not pursued further. The photomicrographs of the samples taken at high magnifications are shown in Fig. 15 and 16. 15(a) shows, at 6000 X, magnification the surface features of a sample containing mullite + SiO_2 + C and 15(b) shows that of an Al_2O_3-SiC composite. The mullite sample was hot-pressed at 1600°C and 20MPa whereas the Al_2O_3-SiC sample was hot-pressed at 1660°C and 20MPa. For samples hot-pressed at 1800°C and 40MPa the photomicrographs at magnification 50K are shown in Fig. 16(a&b);(a) corresponds to (mullite + SiO_2 + C) and (b) corresponds to (Al_2O_3 + SiC). From these micrographs at 50K X the features of the individual grains were clear but the phase identification could not be done, as the EDX analysis was not possible in that set up.

3.4.2. TEM Analysis

Microstructural observations by Transmission Electron Microscopy (TEM) were accomplished by bright field (BF) and selected area electron diffraction (SAD) on samples prepared by disk grinding, dimpling, and ion milling at an angle of 20°. Dark field (DF) imaging in the diffuse region of diffraction space was also used for the observations. The Hitachi H-800 Electron Microscope with a computer developed by ORTEC systems of Oregon was used for the TEM study. The voltage used was 200 KV.

Fig. 15(a) SEM micrograph of mullite + SiO_2 + C hot pressed at $1600°C$ and 20MPa for 10min (bar = 2.5μm).
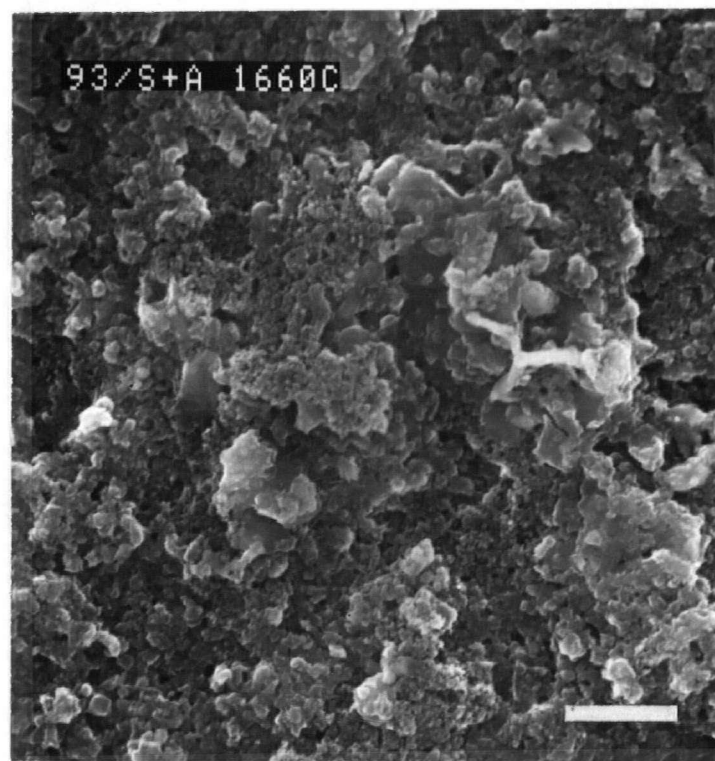
(b) SEM micrograph of the composite Al_2O_3 − SiC hot-pressed at $1660°C$ and 20MPa for 28min (bar = 2.5μm).
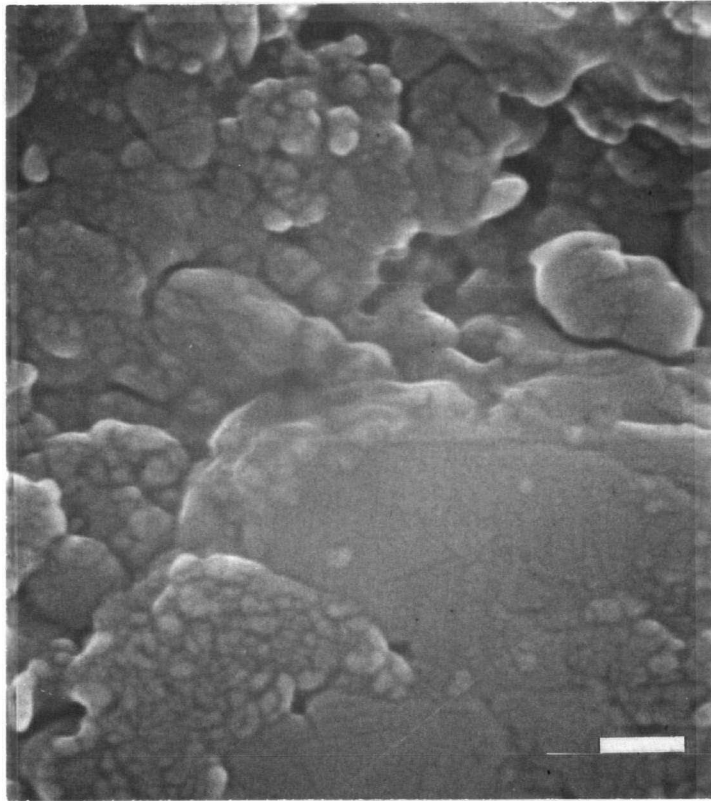
Fig. 16(a) SEM micrograph of mullite + SiO_2 + C hot-pressed at $1800°C$ and 40MPa for 3min bar = 0.2μm.
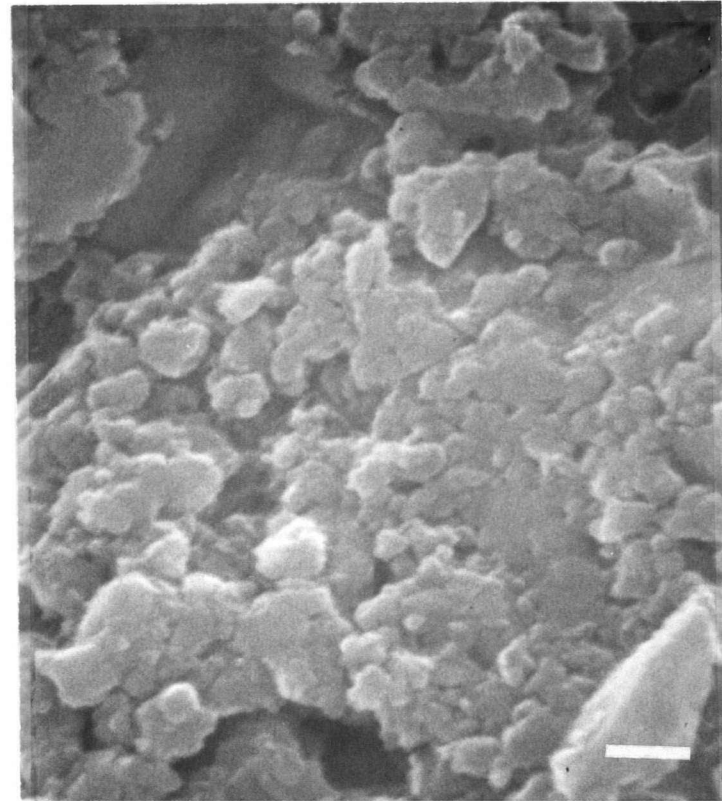
(b) SEM micrograph of the composite Al_2O_3 – SiC hot-pressed at $1800°C$ and 40MPa for 33min bar = 0.2μm.

3.4.2.1. Analysis using ion milled specimens.

The specimen preparation was found to be the most critical and difficult step in the whole analysis. Several specimens had to be made before obtaining an usable specimen for TEM. The first specimen used in the analysis was that of a composite, Al_2O_3–SiC, obtained by hot–pressing a mixture of kaolinite + carbon black at $1800°C$ and 40MPa. The TEM micrographs of this specimen are shown in Fig.17 (a to f); (a) shows the BF image of the areas of the specimen; (b) shows the Bright Field(BF) image of the same area of (a) but with the specimen tilted slightly; (c) shows a DF image of the phase marked "A"(or "B"); (d) is the diffraction pattern corresponding to (c); (e) shows a Dark Field(DF) image of the phase marked "C"; and (f) shows the diffraction pattern corresponding to (e).

As the size of the crystals in the specimen was smaller than the selected area diffraction spot(objective aperture), it was felt that microdiffraction would be useful in obtaining single crystal patterns. Figure 18(a) shows a photomicrograph of an area of interest in which at "A" and "B" microdiffraction patterns were obtained. They are shown in Figs. 18(b) and (c). As the favourable conditions for microdiffraction were difficult to achieve good photographs of the diffraction pattern could not be obtained. At "A" and "B" the black spots seen were that of the carbon deposit formed by the electron beam.

As full information could not be obtained by the poor microdiffraction photographs it was decided that different X–ray spectra could be generated by energy dispersive microanalysis (EDX) to verify the above results. The various grains shown in Fig. 18(a) were scanned (in the spot mode) for X–ray spectra and only Ti $K\alpha$ peak was

Fig. 17(a) BF image showing the different areas of Al_2O_3 – SiC specimen (bar = $0.2\,\mu$m).
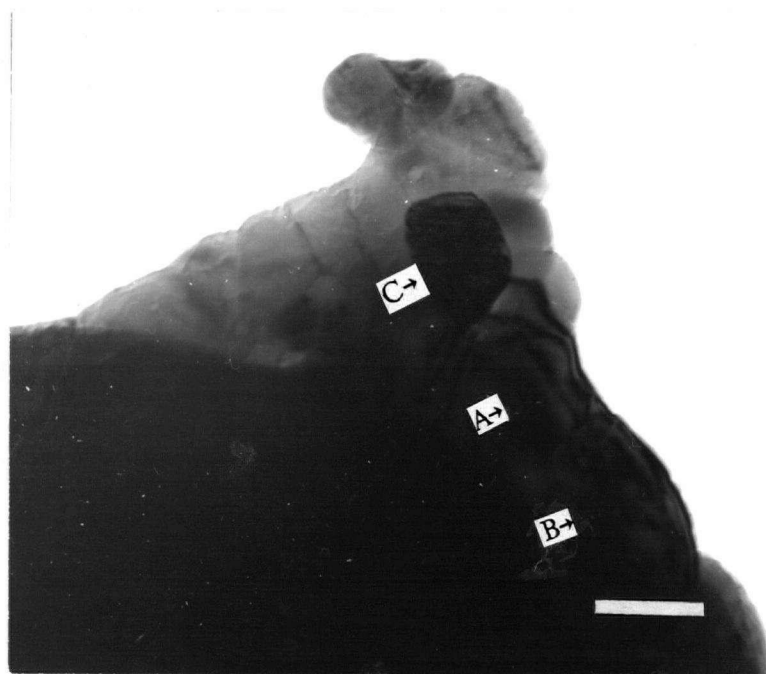
(b) BF image of the area in (a) when the specimen is tilted slightly (bar = $0.2\,\mu$m).
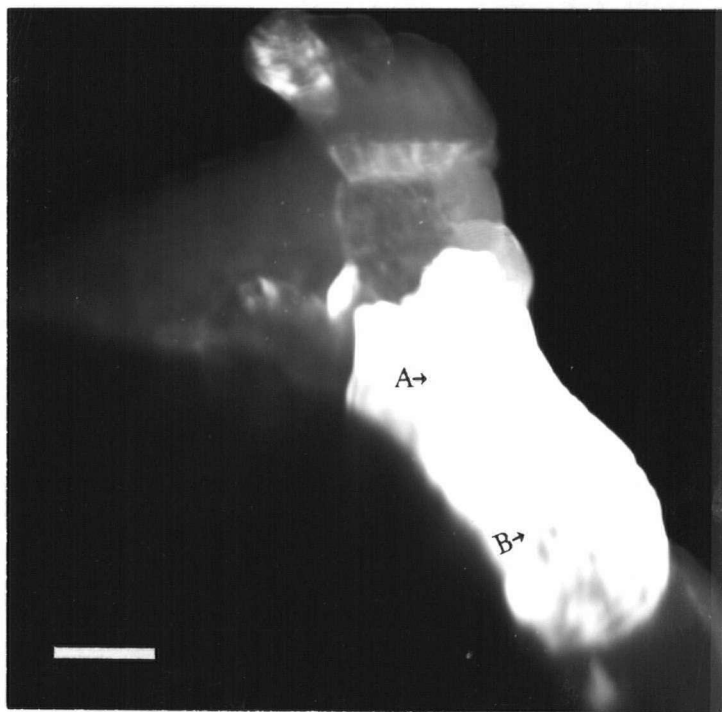
Fig. 17(c) DF image showing crystals "A"
and "B" (bar = $0.2\,\mu$m).

(d) Superimposed diffraction patterns
of "A" and "B" of (c).

Fig. 17(e) DF image showing crystal "C"
(bar = 0.2μm).

(f) Diffraction pattern of the crystal of (e).
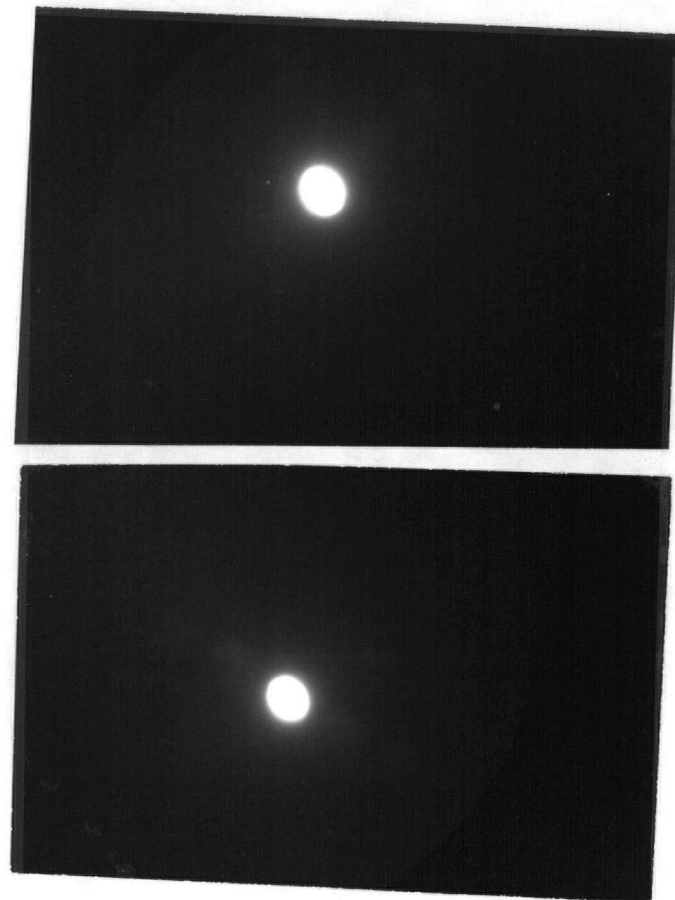
Fig. 18(a). An area of interest in Al_2O_3 – SiC specimen" (bar = 0.4μm).   (b) Microdiffraction pattern at "A" of (a).

(c) Microdiffraction pattern at "B" of (a).

indicated in the spectra one of which is shown in Fig. 19. The fact that titanium was the only element to be identified through out the area that was ion milled was very surprising. To verify the concentration gradients of the elements, if any, present in the specimen three different X-ray spectra were acquired at three different locations starting from the perforation towards the rim of the specimen. The areas in which EDX was done were photographed on the SEM mode of the STEM and are shown in Fig. 19(a) along with the corresponding X-ray spectrum. Fig. 19(e) also shows the pyramids generated as a result of the preferential sputtering throughout the area of the photograph, indicating a lot of damage to the microstructural features of the specimen. For the area shown in Fig. 19(a) which was ion milled for about 60 hours, a diffraction pattern was taken which is shown in Fig. 20.

3.4.2.2. Analysis using mechanically microthinned specimens.

When the ion milled specimens were found to contain microstructural damage and heavy concentrations of titanium throughout the ion milled area, it was decided that the mechanical microthinning be adopted for making the TEM specimens. There are a few reports[76,79,80] in the literature about the mechanical microthinning of ceramic specimens for TEM analysis. However, the tools recommended to be used for the purpose of microthinning a ceramic specimen are special and are not available for the present study. For this reason a different method was devised for the purpose of microthinning a TEM specimen. This consisted of mounting a specimen with the help of mounting wax on a small glass plate and grinding it on a glass slab with abrasive liquid. When the specimen thickness was of the order of 20μm then the position of holding it onto the glass slab was changed such that only one edge of the specimen was touching. In this
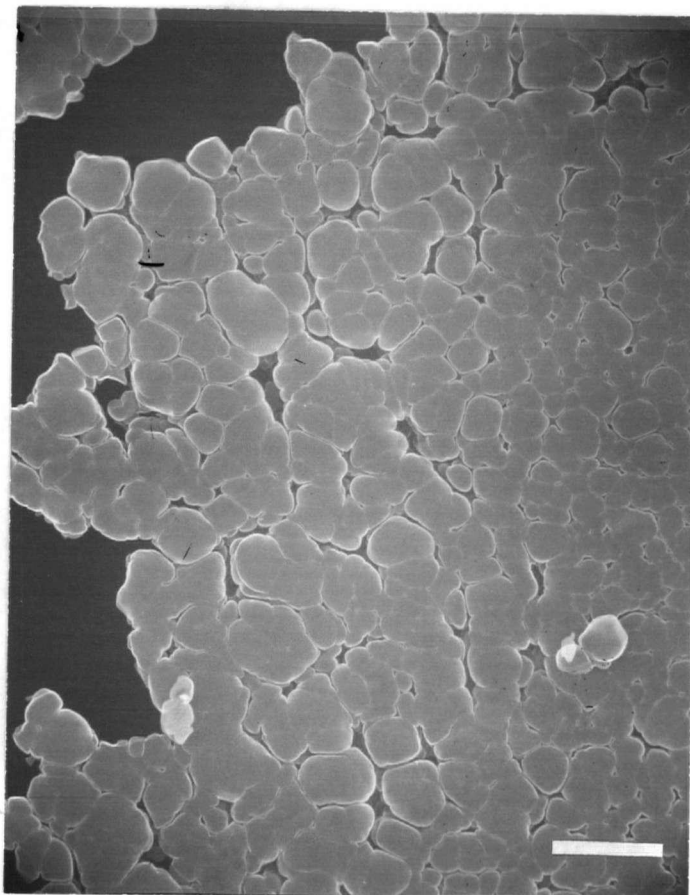
Fig. 19(a). Edge of the perforation in the Al_2O_3 – SiC specimen (bar = 2.5 μm).
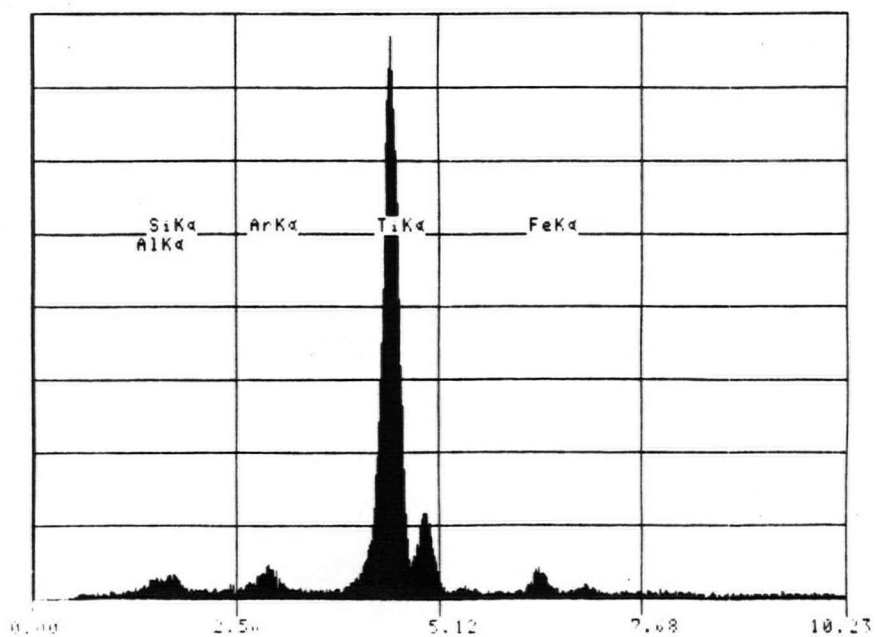
(b) X-ray spectrum observed on any grain in (a).

Fig. 19 (c) An area half the way from the perforation
towards the edge of the specimen (bar = 20 μm).
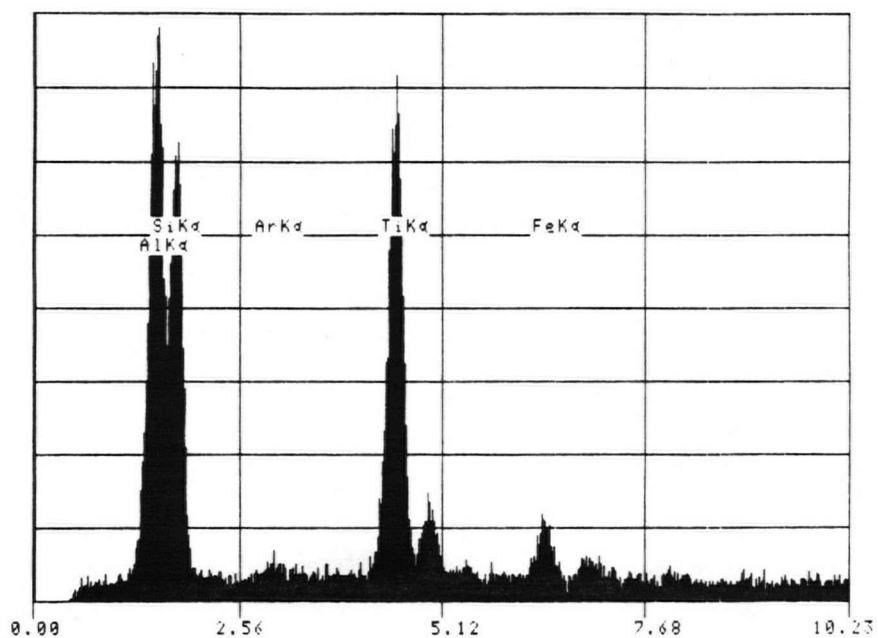
(d) The X-ray spectrum corresponding to the centre of (c).

Fig. 1(e) An area near the edge of the specimen (bar = 20 μm).
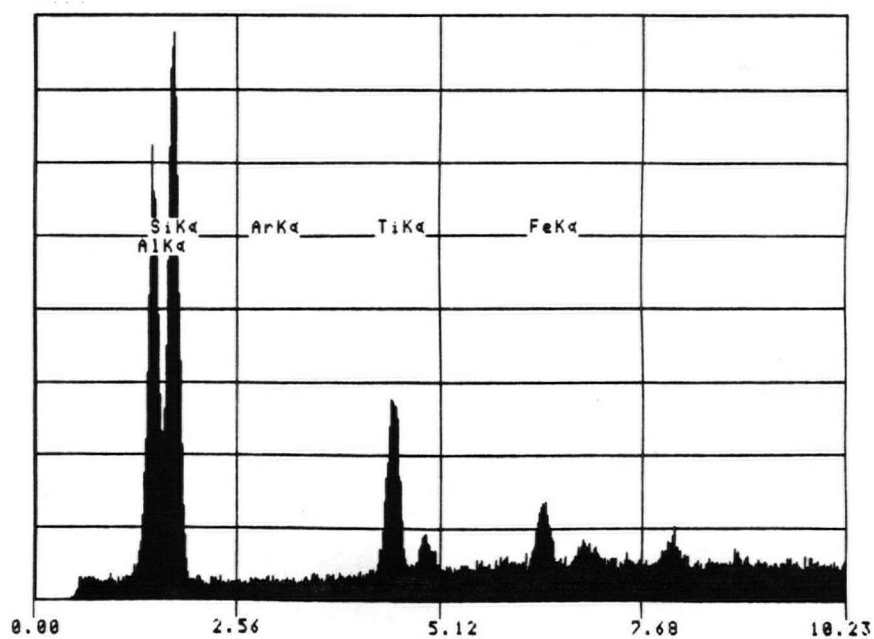
(f) The X-ray spectrum corresponding to the centre of (e).
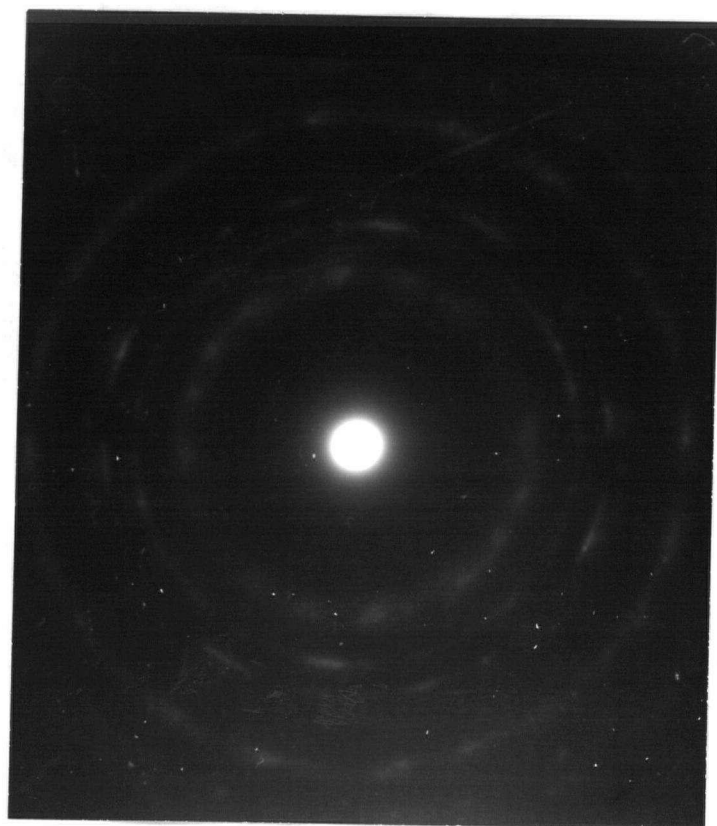
Fig. 20. SAD of the area shown in Fig. 19(a).

position the specimen was further thinned to the point where the thin end of the specimen would just disappear in the next grinding cycle. Grinding was done slowly and with care lest the specimen would not be good for TEM analysis. The mounting wax was dissolved in acetone and the specimen removed into a beaker of acetone. The specimen was always handled very gently until it was set up between the copper grids and into the TEM specimen holder. The method described was successful in obtaining reasonably good specimens thin enough for TEM analysis.

a) Analysis of mullite + SiO_2 + C by TEM.

A specimen obtained by hot-pressing a mixture of kaolinite + carbon at $1600^{\circ}C$ and 20MPa for 10 min as mechanically microthinned and analysed by TEM. Figure 21 shows a photomicrograph of the general distribution of the phases present along with the X-ray spectrum taken at "A". The area looking very transparent in the micrograph was canada balsam which was used to mount the specimen on the glass plate. A small fraction of the canada balsam was not dissolved in acetone when cleaned and this was holding the thinner areas of the specimen without falling apart. Figure 22 shows a photomicrograph of an area with clusters of rounded particles, and the X-ray spectrum taken on one of these particles. The diffraction pattern observed in this area (not shown here) has concentric, broad and diffuse rings, which are typical of amorphous phases.

b) Analysis of Al_2O_3-SiC specimen by TEM.

A specimen obtained by hot-pressing a mixture of kaolinite + carbon at $1800^{\circ}C$ and 40MPa for 33min (specimen # 115) was mechanically microthinned and

Fig. 21(a). STEM micrograph of mullite + SiO$_2$ + C showing the general nature of the phases present (bar = 2μm).
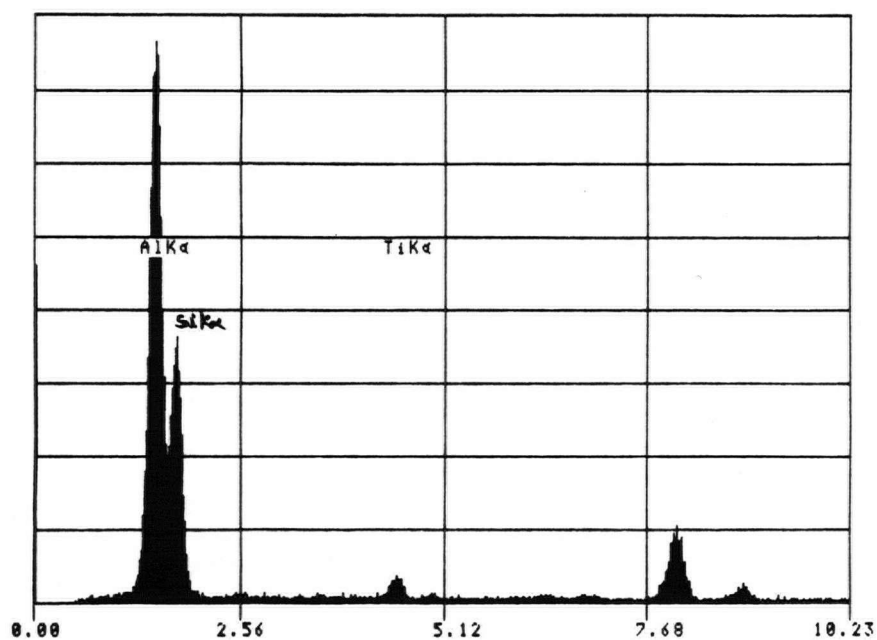
(b) The X-ray spectrum at "A" of (a).
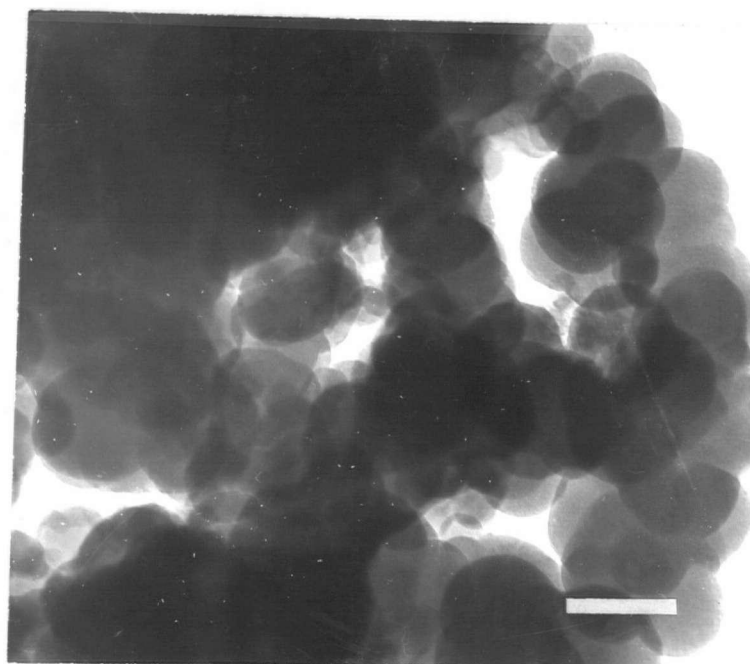
Fig. 22(a). BF image of mullite + SiO_2 + C showing an area of rounded particles (bar = $0.4\mu m$).
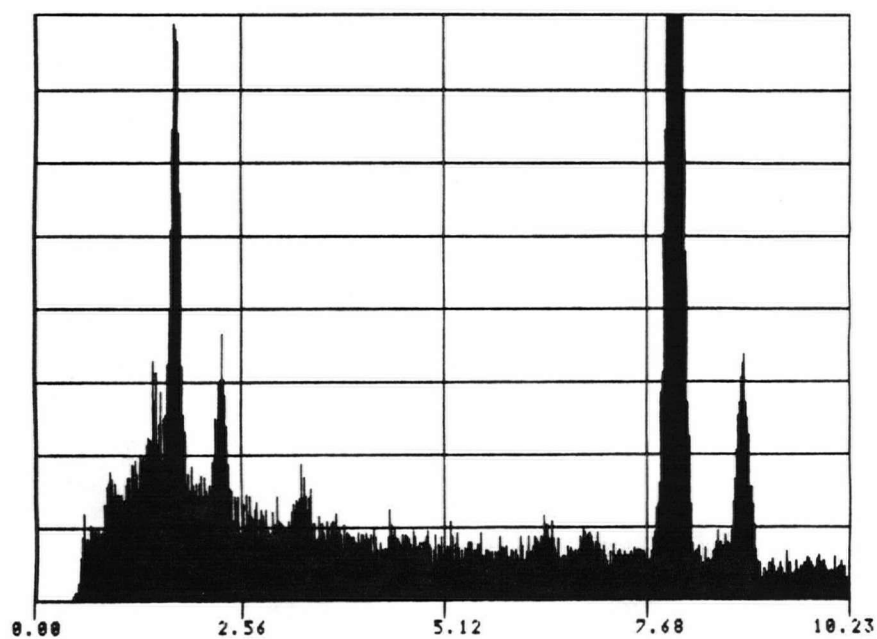
(b) The X-ray spectrum observed on one of the rounded particles of (a).

analysed by TEM, and a series of photomicrographs were taken to describe the microstructure.

Figure 23 shows the different areas of the specimen. Figure 24 shows an area of interest along with the Selected Area Diffraction (SAD) patterns taken at "A" and "B". Figure 24(b) shows the hexagonal net-work pattern taken at "A" where as Fig. 24(c) shows the cubic net-work pattern taken at "B". Figure 25 shows another area of interest and the corresponding SAD pattern (hexagonal net-work in shape) taken at "C". A typical microstructure is shown in Fig. 26 and Fig. 27 in which hexagonal platelets of silicon carbide can be seen in various sizes.

Following the TEM procedures in a TEM/STEM microscope using a probe size of $\simeq$ 20nm, the different X-ray spectra by EDX were acquired from this sample. Figure 28(a) shows a photomicrograph of the microstructure of Al_2O_3 – SiC composite with the major impurity TiO_2. The various phases identified on the EDX were marked on the micrograph and the corresponding X-ray spectra are shown on Figures 28(b to f). It was noted that Ti existed in higher concentrations at some places within the microstructure. In order to find its distribution an X-ray mapping for Ti was done on the area shown in Fig. 29. The corresponding Ti X-ray map is shown in Fig. 30. One other place where Ti was found in higher concentrations was around a hole. One such area is shown in Fig. 31. At point "A" in Fig. 31 an X-ray spectrum was obtained which is shown in Fig. 31(b). The X-ray spectrum shows that only Ti is present at that point.
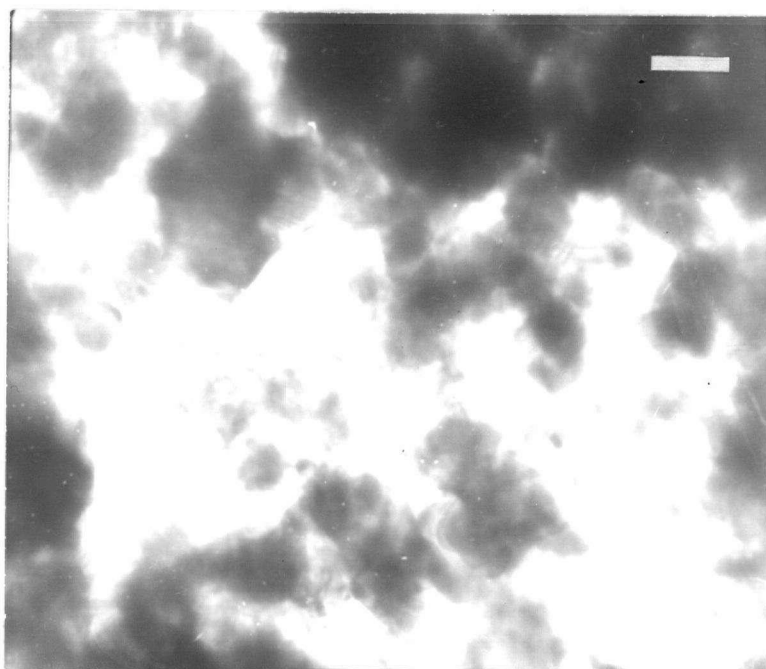
Fig. 23. TEM micrograph of Al_2O_3 – SiC specimen showing the general nature of
the phases present (bar = $0.2\,\mu$m).
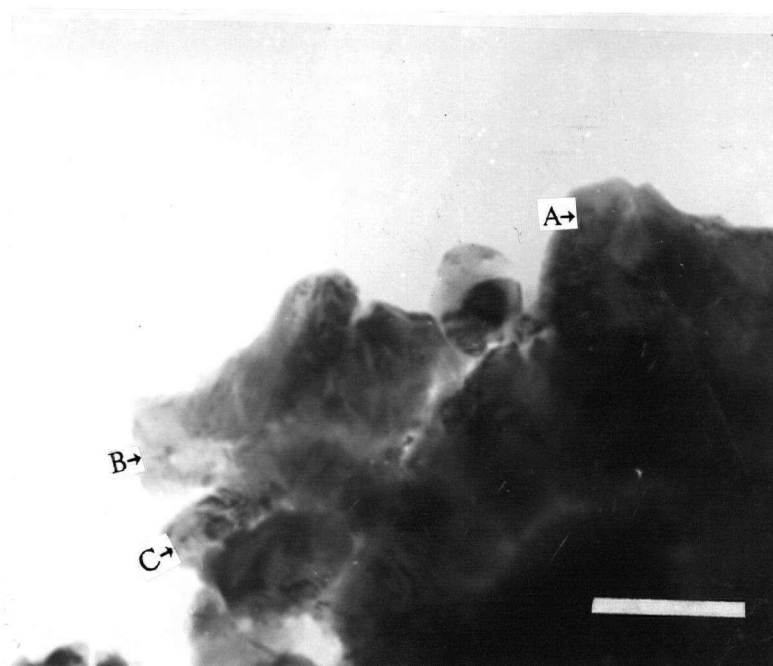
Fig. 24(a). BF image of Al_2O_3 – SiC specimen showing an area of interest (bar =
$0.2\,\mu$m).

Fig. 24 (b) SAD at "A" of (a).

Fig. 24(c). SAD at "B" of (a).
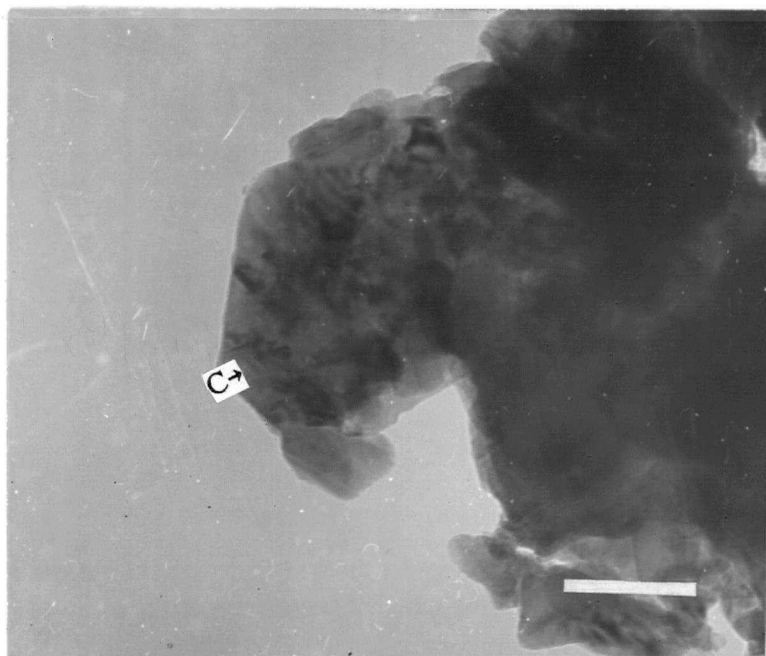
Fig. 25(a). BF image of an area of interest in Al_2O_3 – SiC specimen (bar = 0.2μm).

(b) SAD at "C" of (a).
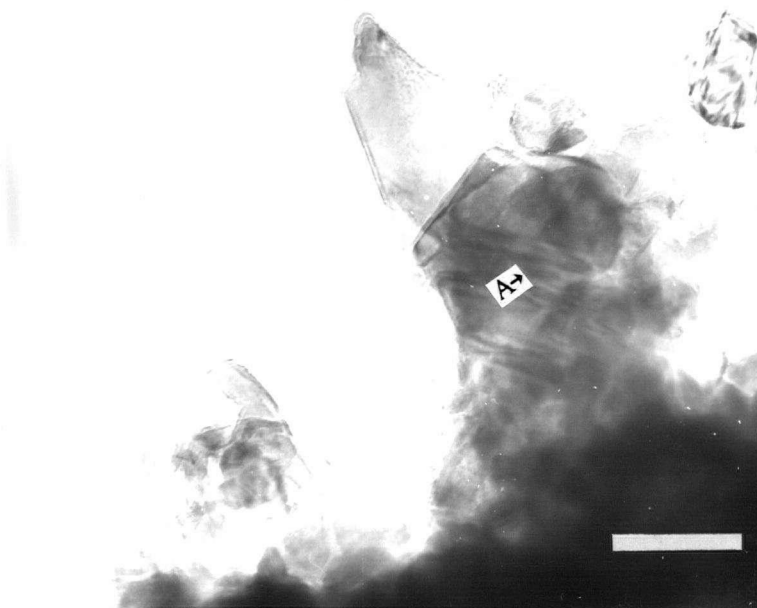
Fig. 26. BF image of Al_2O_3 – SiC specimen showing some of the structural details of the specimen (bar = 0.2μm).
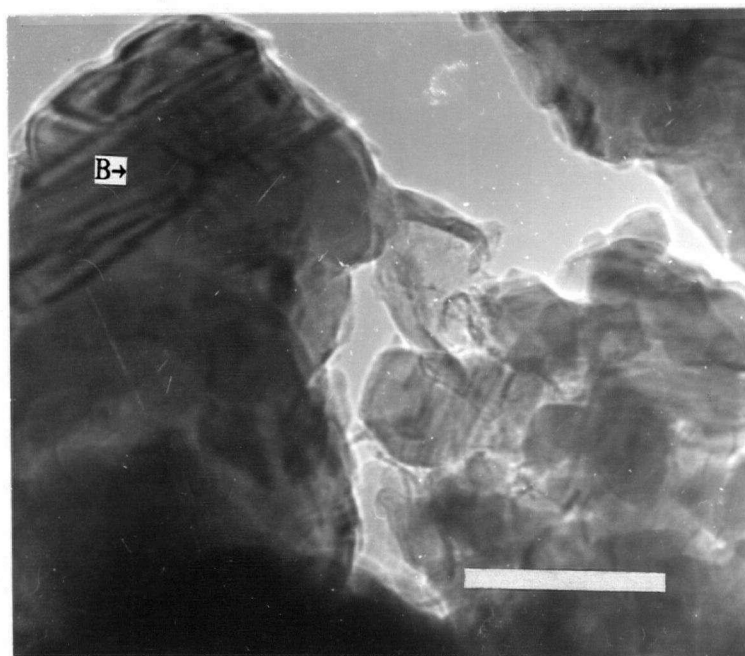
Fig. 27. BF image of Al_2O_3 – SiC specimen showing the typical microstructure (bar = 0.2μm).
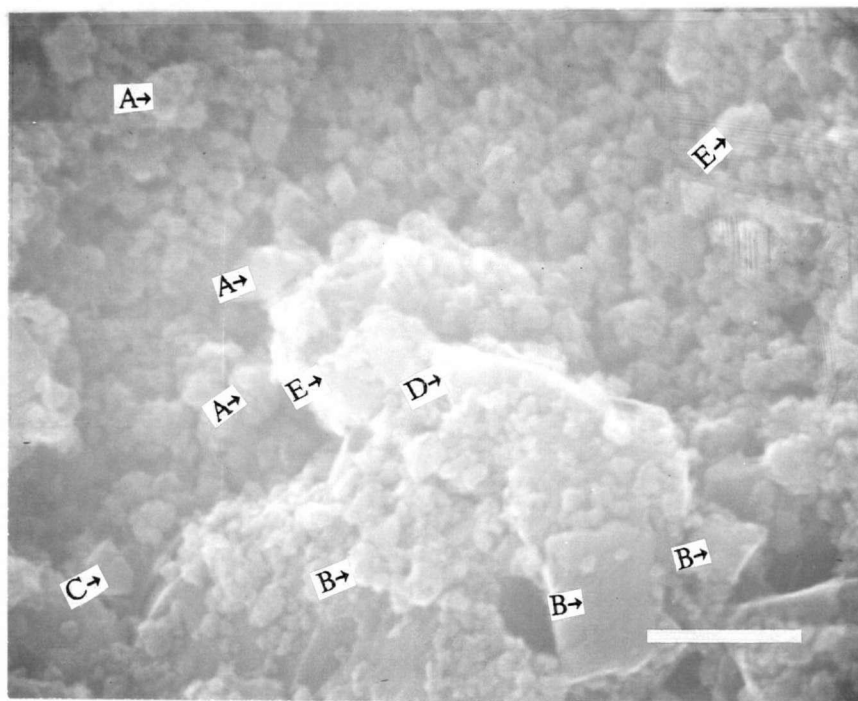
Fig. 28(a). STEM micrograph of $Al_2O_3 - SiC$ specimen showing a typical phase distribution (bar = $0.2\mu m$).
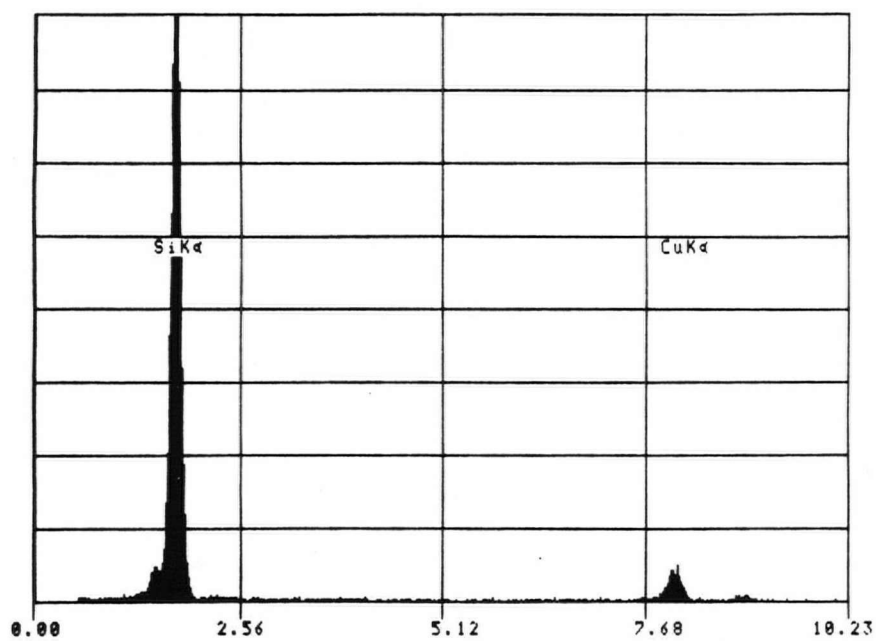
(b) The X-ray spectrum at "A" of (a).
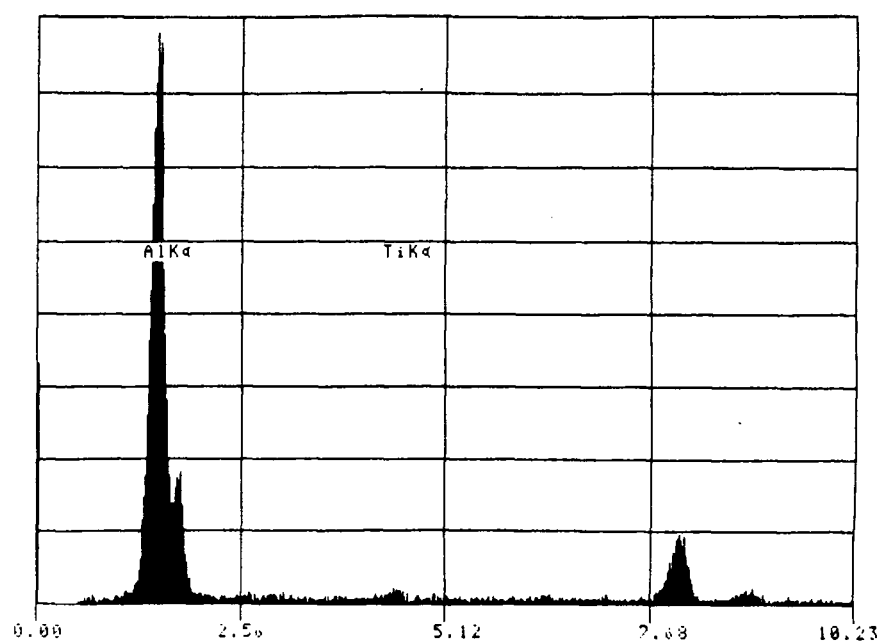
Fig. 28(c) The X-ray spectrum at "B" of (a).
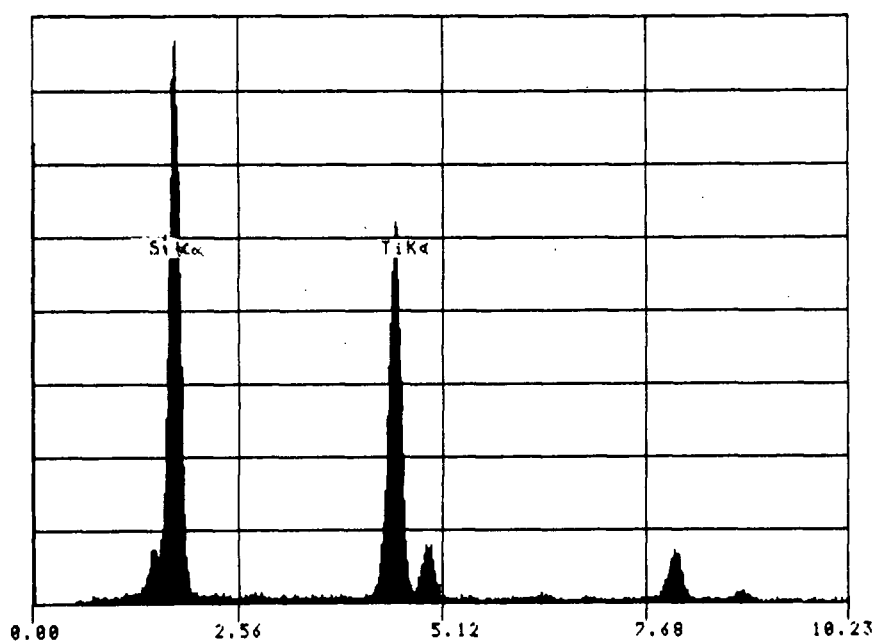
Fig. 28 (d). The X-ray spectrum at "C" of (a).
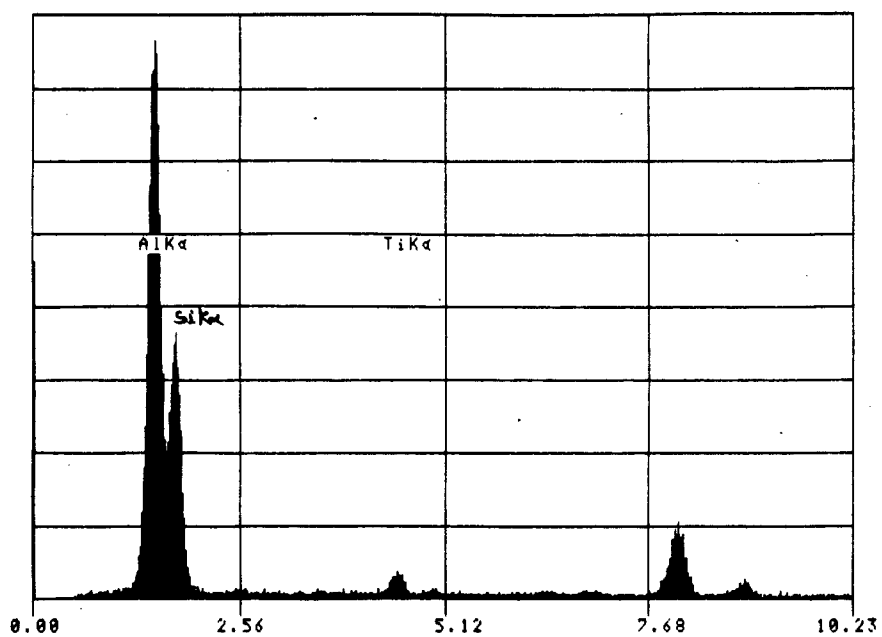
Fig. 28(e) The X-ray spectrum at "D" of (a).
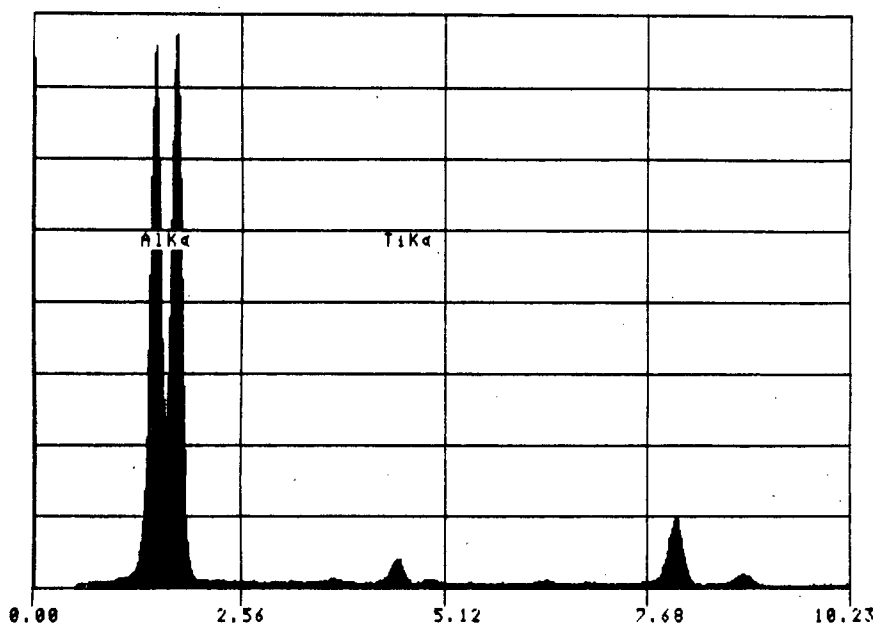
Fig. 28(f) The X-ray spectrum at "E" of (a).
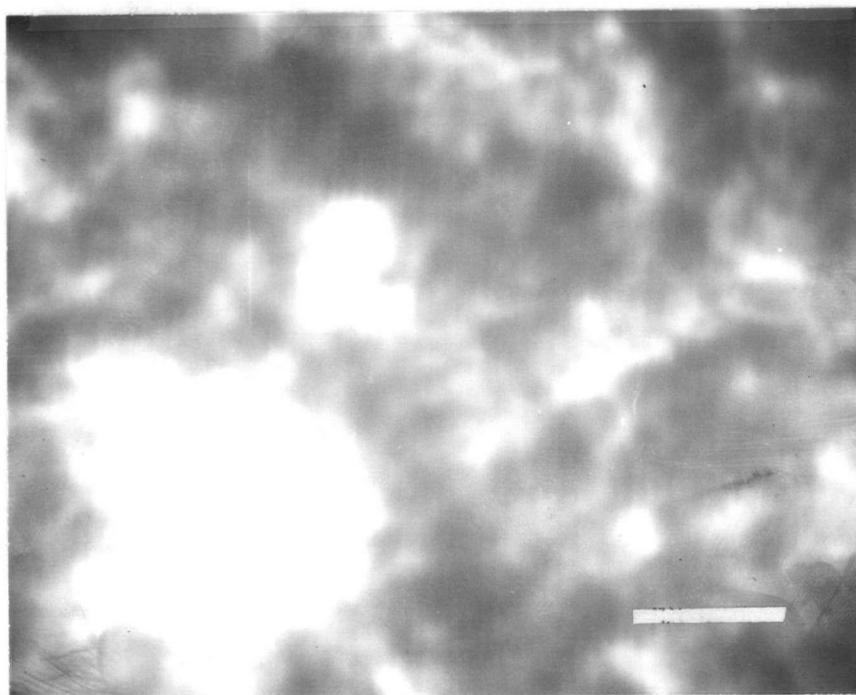
Fig. 29 .. STEM micrograph of spcimen #115 showing the areas of Ti impurity concentrations bar = 0.4μm.

Fig. 30 The X-ray map of Ti on the area shown in (a).
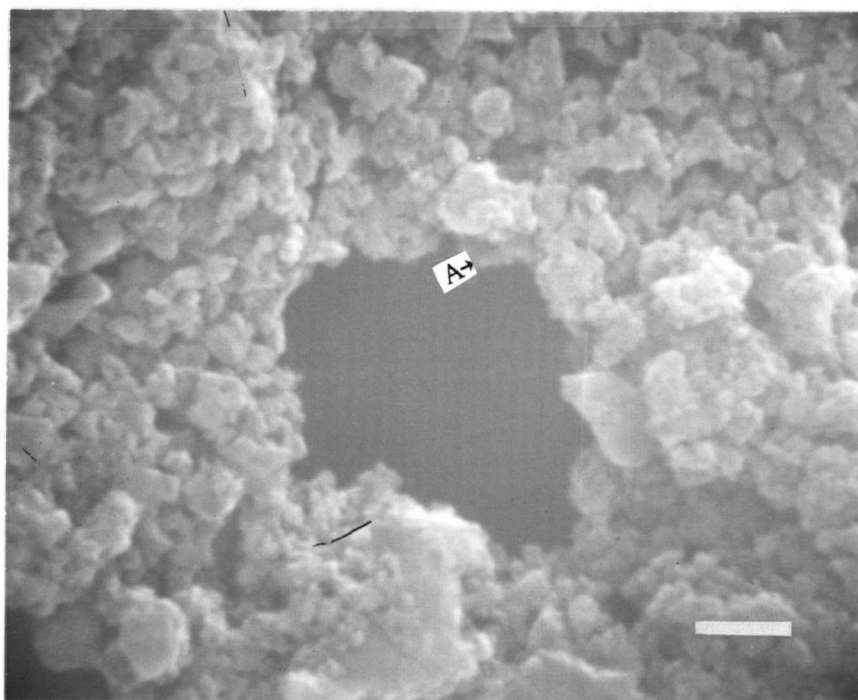
Fig. 31(a). STEM micrograph of Al_2O_3 – SiC specimen showing an area around a hole of high Ti concentration (bar $=$ 1μm).
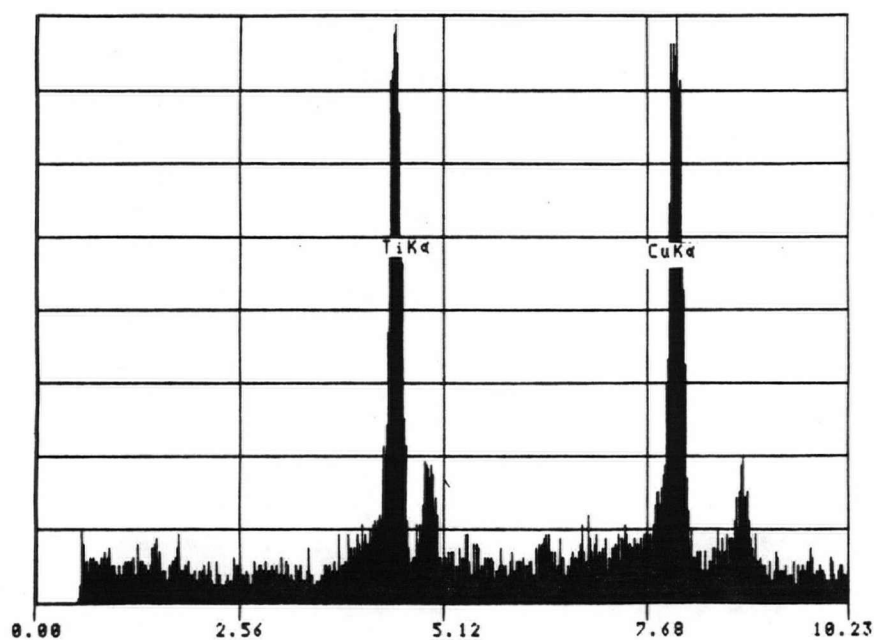
Fig. 31(b) The X-ray spectrum at "A" of (a).

3.5. Isothermal compaction behaviour of kaolinite-carbon black mixture

3.5.1. Isothermal compaction curves

Figures 32 and 33 show a series of isothermal compaction curves ($\Delta L/L_o$ Vs time) obtained at different temperatures above $1200°C$. Figure 32 represents compaction curves for a kaolinite + 28(wt%) C mixture whereas Figure 33 represents a kaolinite + 34(wt%) C mixture. The applied pressure (σ_{ref}) used at all temperatures was the same and was 20MPa.

The temperature range $1200°$ to $1800°C$ was selected since carbothermal reduction of kaolinite takes place only in this temperature range and not below $1200°C$. Moreover, the compaction data for the lower two ranges of temperature at which enhanced compaction was encountered are already available in the literature[73,74] for pure kaolinite.

These isothermal experiments under a constant pressure were performed using the heating and loading conditions described in section 2.4.2.. The linear dimensional change was recorded as a function of time and was corrected for elastic strain, resulted from the removal of the load at the end of the compaction experiments and noting the magnitude of the elastic "spring back".

To determine the reproducibility of the compaction curves all the experiments were repeated and the data obtained were plotted as symbols superimposed on the compaction curves of the first set of experiments in Figures 34 and 35.
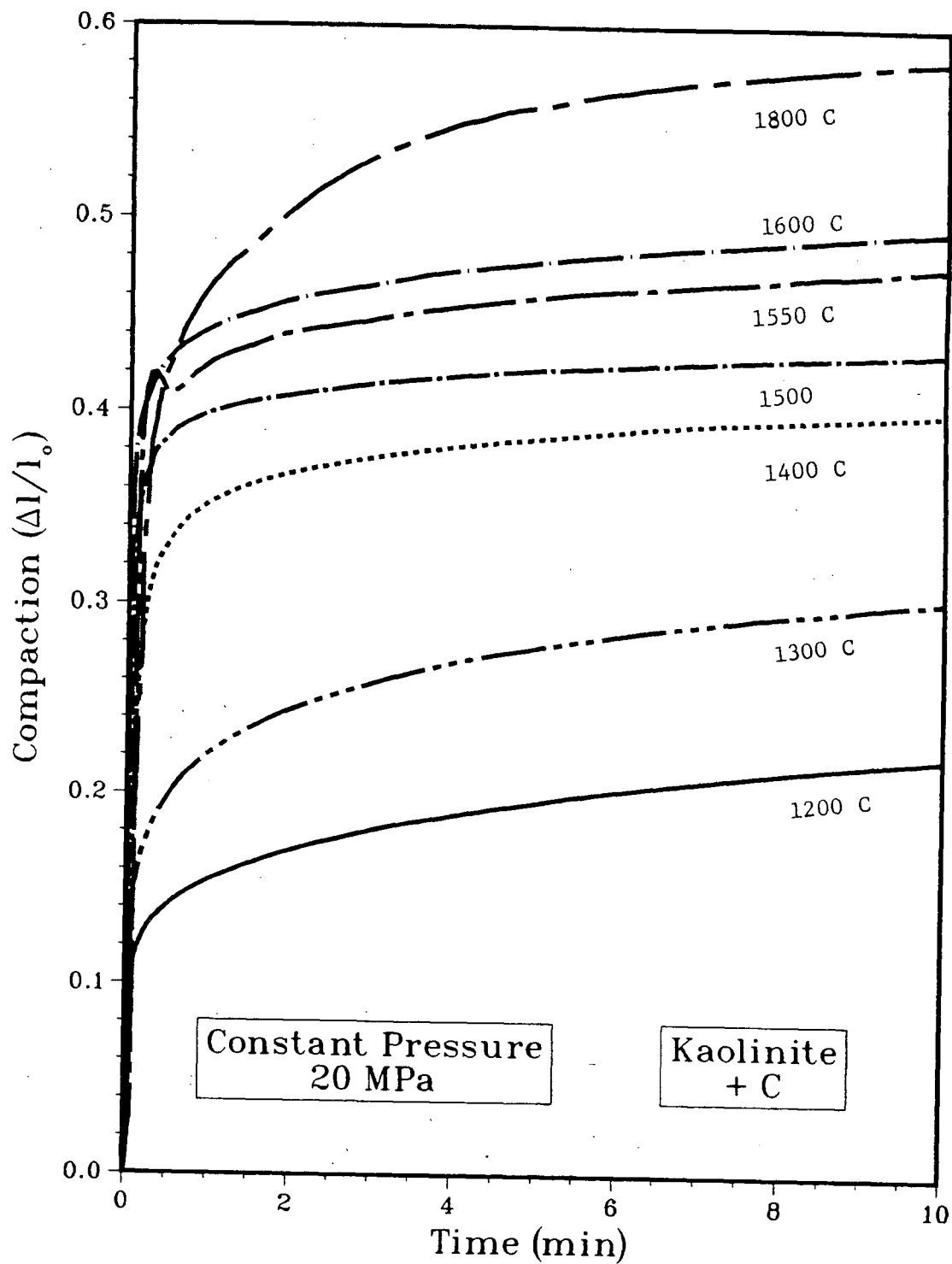
Fig. 32. Isothermal compaction curves for kaolinite + carbon black in the temperature range 1200°–1800°C. C is present in molar equivalents of SiO_2.
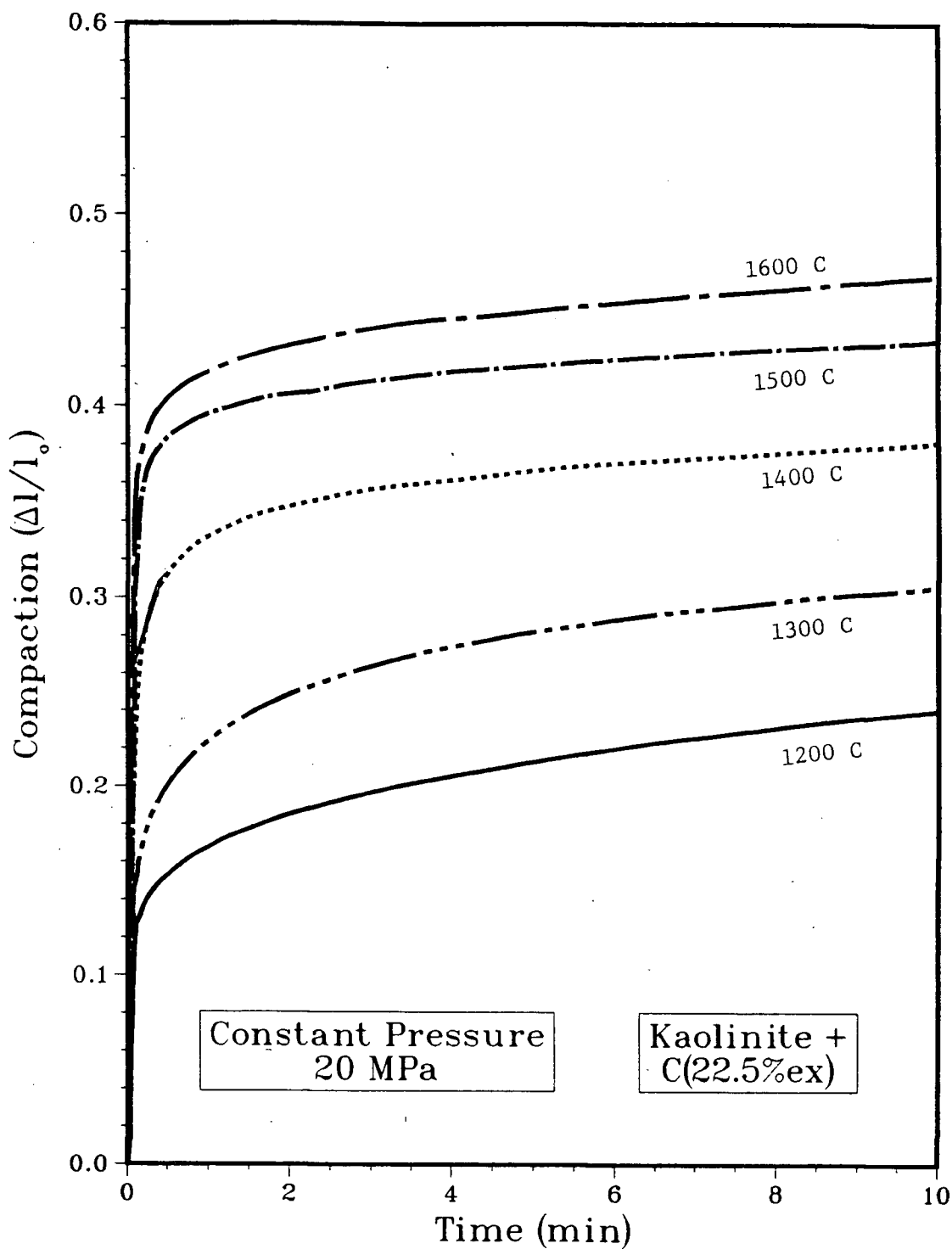
Fig. 33. Isothermal compaction curves for kaolinite + carbon black (excess) in the temperature range 1200° – 1800° C. 22.5wt% C is present in addition to the molar equivalents of SiO_2.
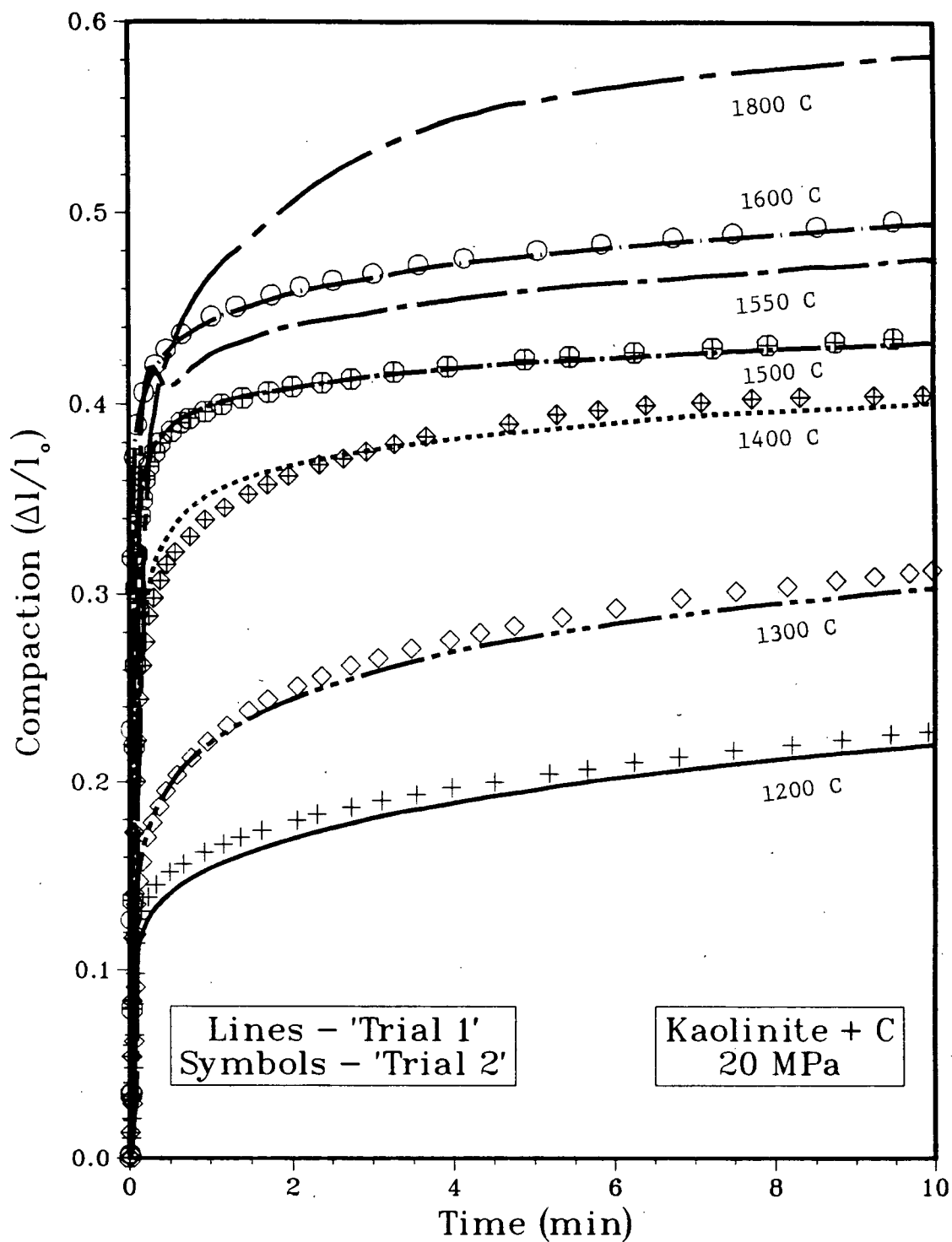
Fig. 34. Isothermal compaction curves obtained in two different trials for kaolinite + C compared for reproducibility.
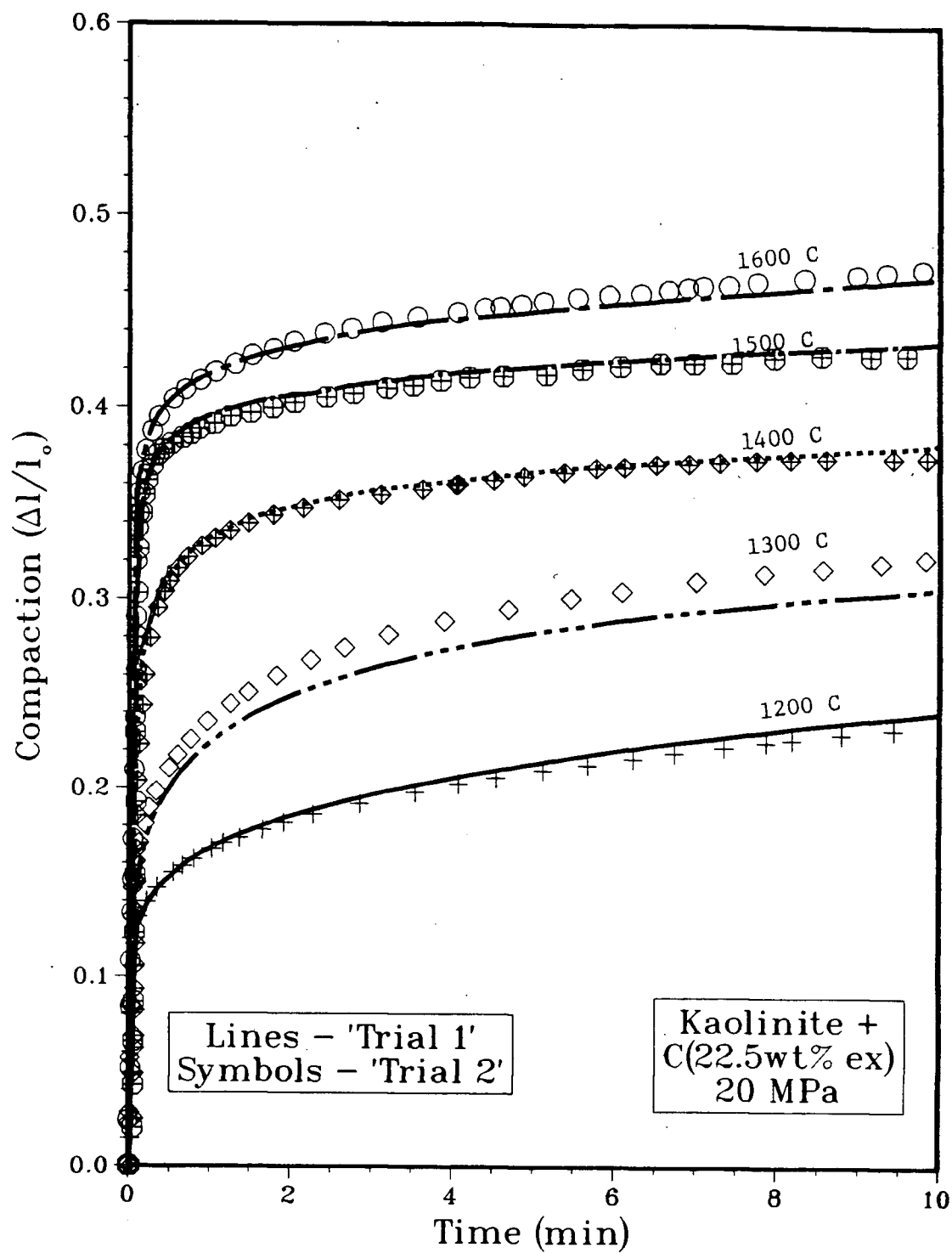
Fig. 35. Isothermal compaction curves obtained in two different trials for kaolinite + C(excess) compared for reproducibility.

The close proximity between the points and the lines (within the experimental error) show that the compaction curves are very reproducible.

3.5.2. *Mathematical modelling and determination of the coefficients*

Data for each isothermal compation curve were fitted to a mathematical model which can describe the strain behaviour of the compaction process. Earlier, attempts were made to fit the present data to a semi-log plot corresponding to the viscous-phase hot-pressing model and a log-log plot corresponding to the liquid-phase sintering model but were found not successful. However, Bradbeer[76] found that data similar to the present set of data could be represented by an equation of the form

$$\epsilon \ = \ \Delta L/L_0 \ = \ K(1 \ - \ Ae^{-at} \ - \ Be^{-\beta t}) \qquad\qquad ....\ 9$$

where K, A, a, B and β are constants which can be uniquely determined by using the experimental strain-time data, where

$\Delta L/L_0 \ (= \ \epsilon)$ is the strain (compaction)

t is the time in minutes

$K \ = \ (\Delta L/L_0)_{t=\infty}$, i.e., the final compaction

A and B are constants for which the following condition must be satisfied.

at time, t = 0,

$(\Delta L/L_0)_{t=0} \ = \ 0$

or A + B = 1 $\qquad\qquad ....\ 10$

Equation (9) has been found to adequately represent the data for the present set of compaction. In order to determine the coefficients of Eqn. 9, Bradbeer plotted

Ln($d\epsilon/dt$) Vs time and used the slope and intercept of the resulting plot. In the present case, a computer program using a curve fitting routine, NL2SNO[67] calculated the values of the equation coefficients K, A, a, B and β. The program is listed as appendix A. The routine NL2SNO whichuses the means to accomplish a least squares fit and represents the state of the art in robustness, is very sophisticated and is free of internal arithmetic problems.

The computer program takes in a set of parameters (5 in number) that are roughly related to K, the final compaction and other coefficients and uses the experimental data points to generate the values of the coefficients K, A, a, B and β. The parameters act just as starters of the computational process and their choice does not affect the determined values of K, A, a, B and β. This in fact, shows the uniqueness of the solution for the coefficients. A second solution for the coefficients can however, be obtained by altering the giving and not giving the constraint A + B = 1 (Eqn. 10) in the main program. Both the solution sets of the coefficients K, A, a, B and β were obtained and the set giving a better fit to the experimental values was selected, though only little difference was often found between the solution sets.

Figures 36 and 37, show the experimental data superimposed on the theoretical compaction curves for all the selected temperatures. The model describes the data accurately. The mathematical expressions that represent the theoretical curves are also shown in the figures. It is possible that the very nature of the computer program which fitted the mathematical equations, with the experimental data, produced such a good agreement.
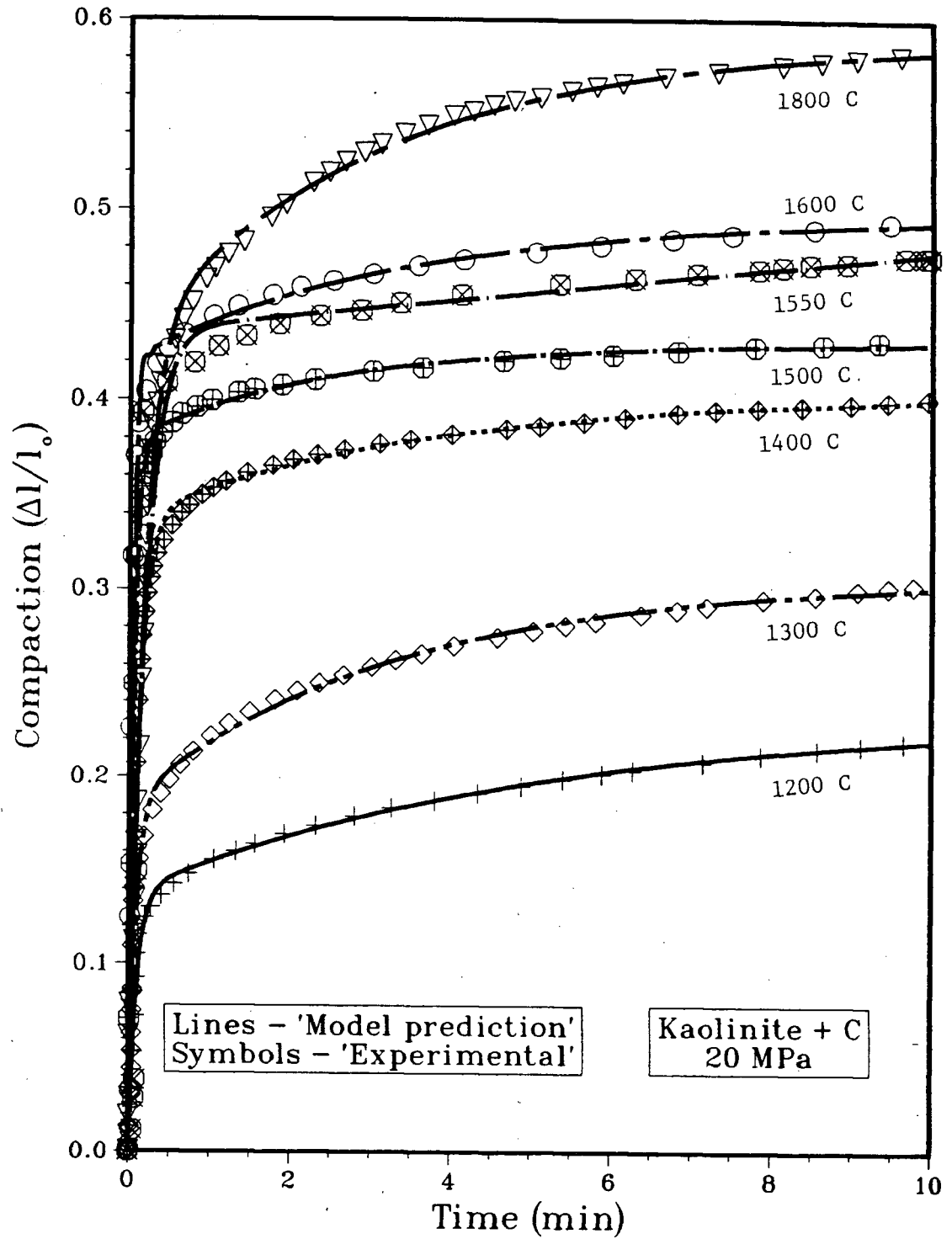
Fig. 36. Experimental data on the isothermal compaction curves of kaolinite + C superimposed on the mathematical prediction shows a good fit.
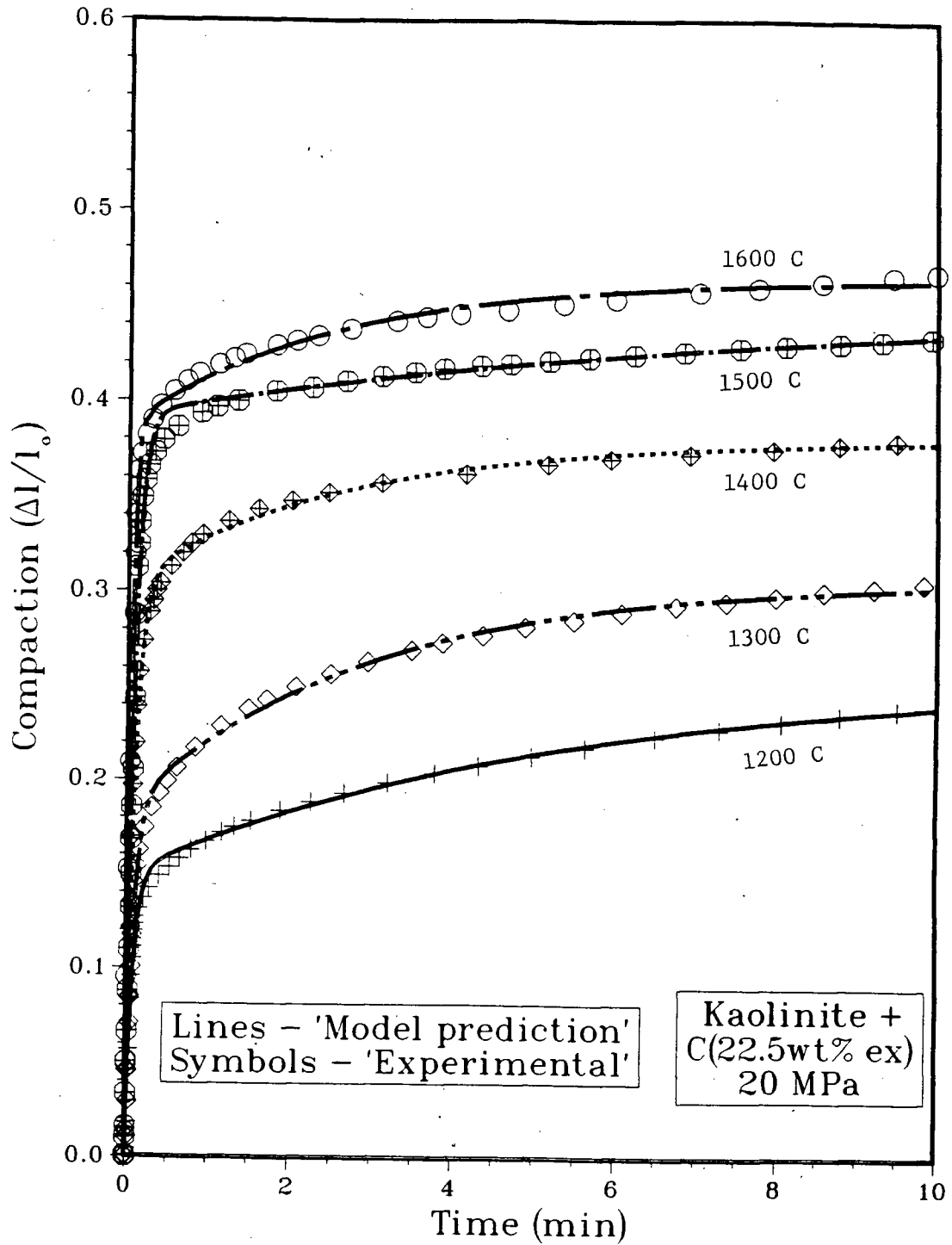
Fig. 37. Experimental data on the isothermal compaction curves of kaolinite + C(excess) superimposed on the mathematical prediction shows a good fit.

4. DISCUSSION

4.1. Behaviour of Kaolinite – Carbon Black Mixture During Reactive Hot–Pressing

The kaolinite, a naturally occuring mineral is complex in terms of its high temperature behaviour and particularly under pressure. Addition of carbon black to it might contribute to the complexity during reactive hot–pressing, especially in the temperature range when it is undergoing transformation and is reactive.

Figure 9 shows the successive transformations of both pure kaolinite and that of a mixture of carbon black and kaolinite. The compaction associated with each transformation can be easily identified. The successive phase transformations are

a) Kaolinite to metakaolinite at around $650^{\circ}C$

b) Metakaolinite to spinel/γ–alumina and lower mullite at about $960^{\circ}C$

c) Formation of secondary mullite above $1200^{\circ}C$.

It would be proper to select the temperature range for each transformation and study the isothermal compaction behaviour of kaolinite + carbon black mixture so that the effect of carbon during each transformation of kaolinite can be known.

However, it can be seen in Fig. 10 that during the second stage of the transformation the slopes of the compaction curves are the same for both kaolinites with and without carbon. Only the amount of compaction has decreased considerably. Hence it can be concluded that carbon acts just as an inert filler and doesn't have any effect on the phase transformation or on the products. Moreover, Chaklader[73] had studied the

92

isothermal compaction behaviour of pure kaolinite during the transformation of metakaolinite→ spinel, whose results are shown in Fig. 38.
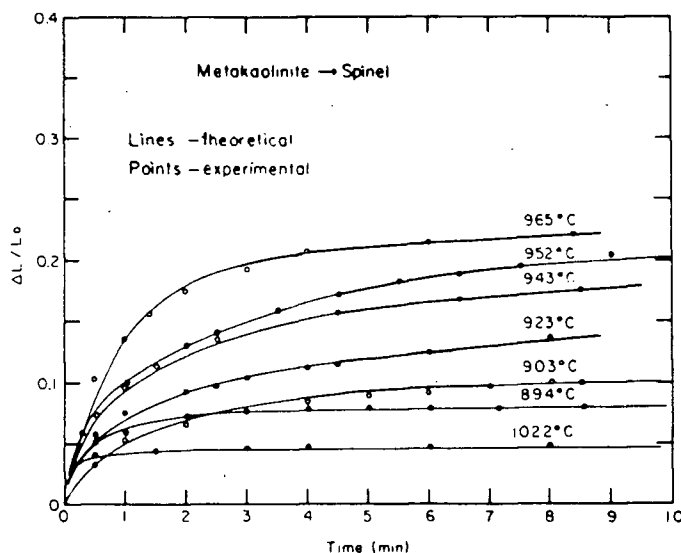
Fig. 38. Isothermal compaction curves during metakaolin
to spinel transformation (after A.C.D.Chaklader[73]).

So it was felt that no new insight could be gained by performing the isothermal compaction experiments in the temperature range of both the first and the second stage transformations.

Comparing the compaction curves in the third transformation range (Fig. 10) it can be seen that for the kaolinite with carbon the slope has decreased from that of kaolinite alone. This was in the temperature range 1200 – 1400°C. Above this temperature range, however, the compaction in kaolinite has completely stopped whereas compaction continued in the case of kaolinite with carbon black until the maximum experimental temperature. This suggests that carbon becomes chemically active in the presence of kaolinite above ≃1200°C and so this region 1200° – 1800°C was thought to be interesting to study and was selected for the isothermal compaction experiments.

Moreover, in the temperature region above 1400°C, the carbothermal reduction of mullite and silica with the formation of SiC and Al_2O_3 phases take place. And it is one of main objectives of the project to analyse this temperature region.

Unlike the other two phase transformations the transformation of spinel/γ-alumina to mullite seems to be sluggish and seems to start at about 1200°C which carries on until about 1400°C where the transformation is complete. It is interesting to compare Figure 38 with Figure 32. In Fig. 38 where Chaklader plotted the isothermal compaction curves in the temperature region 894° – 1022°C, the compaction curve at 1022°C shows the least compaction of all. The reason he gave for that behaviour was that the metakaolinite → spinel transformation ended at about 970°C and above that temperature (say 1022°C) the transformation plasticity is not present in the system any more. He also did not study the transformation plasticity above 1022°C

In this study, the transformation plasticity during spinel to mullite conversion was also studied. In Fig. 32 compaction studies in the temperature range 1200 – 1800°C show that there is a slow and steady transformation occuring during 1200 – 1400°C, as expected, above which there is a slow reaction, can be identified by the apparently slow compaction behaviour.

The reaction above 1400°C could be the carbothermal reduction of silica and mullite whose rate becomes faster at higher temperatures. The data in Table III and IV confirm this kind of reaction. The particular reaction that is significant at this temperature is[68]

$$SiO_2 \; + \; C \; \longrightarrow \; SiO \; + \; CO \qquad\qquad .... \; 8$$
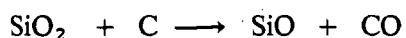
The loss of some SiO gas and CO gas from the system would account for the observed compaction encountered with the kaolinite – carbon black mixtures above $1400°C$. From Fig. 10 it may be seen that this type of compaction is more prominent in a mixture with less carbon (28wt%). This is because with higer concentrations of carbon, it acted as an inert filler, whereas stoichiometric concentration of carbon produced higher reaction rate.[68] In order to focus more attention and to seek a clear explanation, a visco elastic model is considered in the last section.

4.2. Feasibility of Producing an Alumina – SiC Ceramic Composite by Hot–Pressing a mixture of Kaolinite + C

The main objective of this project is to verify the feasibility of producing a composite ceramic consisting of Al_2O_3 and SiC phases. This has to be done in terms of the thermodynamics, kinetics, microstructural aspects and other factors such as densification.

4.2.1. Formation of SiC and Al_2O_3 phases – influence of various parameters

4.2.1.1. Stable Al_2O_3 phase

Though there have been a number of reports on the carbothermal reduction of silica, the reports on mullite are scarce. From the present results (listed in Table III and IV) it has been verified that the reduction of mullite leads to the preferential reduction of its silica content. The temperature range verified was $1400° - 1810°C$ and even at $1810°C$ the Al_2O_3 phase was very stable and showed no reduction even under pressure. Earlier, it was suggested by Bechtold and Cutler[61] that the reduction of Al_2O_3 would

begin above 1505°C, which is found to be not true. In experiment # 47B excess C(12wt%) was added to the Al_2O_3 and SiC phases that were earlier formed and resintered the mixture at 1655°C for 130 mins. This was done to see whether Al_2O_3 can be reduced once the reduction of SiO_2 is over. However, the results have conclusively shown that alumina was not reduced. Thus there is an indication that a stable Al_2O_3 phase can be obtained along with the reduced phase of SiO_2 even at temperatures > 1650°C. The stability of Al_2O_3 at higher temperatures is essential in order to be able to sinter the composite ceramic to near theoritical densities.

4.2.1.2. Stable SiC phase

It was mentioned that the SiO_2 content of kaolinite(or mullite) gets reduced and reacts in preference to alumina. However, the reduction of silica could result in the formation of Si (crystalline or amorphous), SiO (vapour that escapes) or SiC, according to the following reactions

$$SiO_2(s) + 2C(s) \longrightarrow Si(l) + 2CO(g)^{61} \qquad \text{........ 11}$$

$$3Al_2O_3 \cdot 2SiO_2(s) + 2CO(g) = 3Al_2O_3 + 2SiO + 2CO_2{}^{81} \qquad \text{........ 12}$$

$$SiO_2(s) + 3C(s) \longrightarrow SiC(s) + 2CO(g) \qquad \text{........ 13}$$
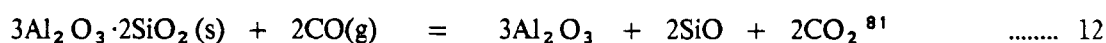
Equation 13 can be considered as a combined reaction of the various reaction steps leading to the formation of SiC. In fact, Kronert and Buhl[81] who studied the reduction of various mullite types and mullite refractories in CO atmosphere in the temperature range 1100° – 1600°C, found that the reaction products were alumina, gaseous silicon monoxide and carbon dioxide of which the later two escaped from the system. They

suggested Eqn. 12 as the prevalent reaction between mullite and CO gas.

Also Bentsen et al.[66] very recently, found that in the temperature range 1660 to 1730°C the weight loss during the mullite reduction process was considerably higher than that predicted by Eqn. (4). They attributed the higher weight loss to the SiO vapour which escaped the system without coming into contact with carbon because of the coarser silica particles.

The formation of liquid silicon through Eqn. 11 was ruled out by various workers on the basis of thermodynamic as well as kinetic studies.[61,68]

Considering the above facts it is essential that SiO vapour should somehow be trapped in the system for it to react with carbon to form silicon carbide. In their study Kronert et al., did not have any carbon that was mixed with the mullite to attract the escaping SiO vapour. Their study also makes it clear that SiO vapour reacting with carbon through Eqn. 7(on page 100) is responsible to the formation of SiC and not the CO gas.

In the present case, the hot-pressed specimens did not indicate any loss of SiO_2 as SiO vapour for there was no alumina rich layer that was formed on the surface of the specimen. This was confirmed by XRD. This could be due to the two reasons,

a) carbon in the form of very fine carbon black was used which was wet mixed with kaolin in an alcohol medium. Thus carbon was in intimate mixture with mullite (or silica) and reacted effectively with the CO_2 gas evolved by Eqn. 5(on page 99) from its

surface through Eqn. 6. And Eqn. 6(on page 100) lowers the CO_2 pressure thus favouring an increase in SiO pressure (of Eqn. 5).

b) During hot-pressing the only escape route for SiO vapour is through the edge of the cylindrical specimens and thus hard to escape without reacting with the carbon present in the system.

During sintering the later constraint was not present as SiO vapour could escape easily form the exposed surface of the specimen. As a result, on all the sintered specimens a surface layer of white, soft, silica free alumina layer was seen. This kind of behaviour was observed by Bentsen et al.,[66] on their mullite grains. Below this thin Al_2O_3 layer the material from a fully reacted specimen was found to be a composite of $\alpha-Al_2O_3$ and SiC by XRD analyses.

From these results it may be suggested that the carbothermal reduction of mullite or silica can lead to form a stable SiC phase by having an intimate mixture of kaolin and carbon and by the suitable selection of other parameters some of which will be discussed in the next section.

4.2.1.3. Influence of various parameters on the formation of silicon carbide

The mechanism for the reduction of silica or mullite involves a chain reaction involving gas – solid reactions. Both silica and carbon particles (surfaces) are involved. The most likely reaction sequence for the reduction process mentioned is written here again, for convenience.
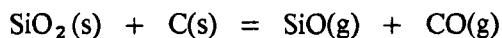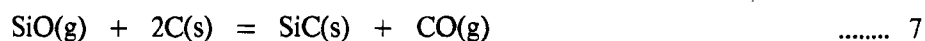
$$SiO_2(s) \; + \; C(s) \; = \; SiO(g) \; + \; CO(g) \qquad\qquad .... \; 8$$

$$SiO_2(s) + CO(g) = SiO(g) + CO_2(g) \qquad \text{....... 5}$$

$$CO_2(g) + C(s) = 2CO(g) \qquad \text{........ 6}$$

$$SiO(g) + 2C(s) = SiC(s) + CO(g) \qquad \text{........ 7}$$

The initial CO gas for Reaction (5) can be obtained from reaction at the solid–solid contacts between carbon and silica particles.[68]

a) Effect of particle size

Since these reactions 5–8 proceed through a gas–solid reaction route, surface areas of the reactants play an important role.

For this reason the particle size of both mullite/silica and carbon are important and the smaller the size the shorter the path for diffusion of CO molecules to SiO_2 surface and SiO molecules to carbon surface and thus higher the rate of reaction.[68,84]

In the present experiments the particle size of the kaolinite was less than $1\mu m$ and that of carbon black was much smaller than $1\mu m$. However, the particle sizes of mullite and silica formed after the phase transformations of kaolinite are perhaps more relevant than that of kaolinite.

Using the photomicrographs of the hot–pressed material mullite + SiO_2 + C (Figs.21(a) and 22(a)) the size of the mullite crystals and amorphous silica particles were determined. The hot–pressing conditions for this material were $1600°C$ and 20MPa. From

Figure 21(a) it was found that the mullite crystallite size ranges from 0.2 to 0.3μm (see A in the figure). From Figure 22(a) it was found that the particle size of the amorphous silica was typically of 0.5μm. In a recent publication it was reported by Sarikaya and Aksay,[82] who studied the formation of mullite in metakaolinite through high-resolution TEM, that the crystal size of mullites falls in the range 0.1 to 0.2μm. The temperature, they heat treated before the analysis for the grain size of mullite was also 1600°C, as at was in the present case. Thus the value of $0.2 - 0.3\mu$m for mullite crystal size obtained in this study agrees with previous observations.

Thus the system kaolinite + carbon, after the successive phase transformations of kaolinite, produces a system with very fine grains of mullite, SiO_2 and carbon. This kind of system having very large surface area values of the reactants would be very favourable for the formation of Al_2O_3 and SiC phases through the gas – solid reactions.

b) Effect of external pressure

The reaction scheme, 5-8 for the carbothermal reduction of mullite and silica involve gaseous products and hence, the rate and products formed are highly pressure dependent. As external pressure on the powder compact can alter the partial pressures of the various gaseous species in the system, even it can affect the rate and products of the reactions.

In order to study the effect of external pressure on the carbothermal reduction process of mullite and silica an experiment (#114 of Table IV) was performed. Before going into the details of this experiment it is worthwhile to consider the equilibrium

pressures of the gaseous species in reactions 5-7.

Figure 39 (of ref. 72) shows the equilibrium pressures of SiO and/or CO_2 for various reactions of interest and it can be seen that below 1900°C, of all conceivable reactions, reaction (5) gives higher SiO and CO_2 pressures and thus becomes the most likely primary reaction. The carbon dioxide will next react with carbon (reaction 6) whereby the CO_2 pressure is lowered to less than 10^{-4} atm so that the reaction may be sustained.

The last reaction in the sequence is reaction (7) whose Ellingham diagram (from ref 72) is shown in Fig. 40(a). The standard free energy change for the reaction is negative and essentially invariant with temperature. The values of the ratio p_{co}/p_{sio} (derived using the Vant Hoff isotherm)[72] plotted against temperature are shown in Fig. 40(b).

For reaction (7) to occur, p_{co}/p_{sio} must be less than the equilibrium ratio or should fall into the unhatched area. Now considering the SiO pressure (Fig. 28) produced by reaction (5) under the conditions P_{CO} = 1 atm and P_{SiO} = P_{CO_2}, the ratio p_{co}/p_{sio} would be higher up in the hatched region, or in other words, reaction (7) cannot take place.

However, the CO_2 pressure from reaction (5) can be lowered by immediate contact with carbon (reaction 7) and thus SiO pressure from reactin (6) can increase correspondingly making it feasible to form SiC through reaction (8). In terms of the CO pressure it may be worth noting that the equilibrium p_{co}/p_{sio} ratio is fairly high being
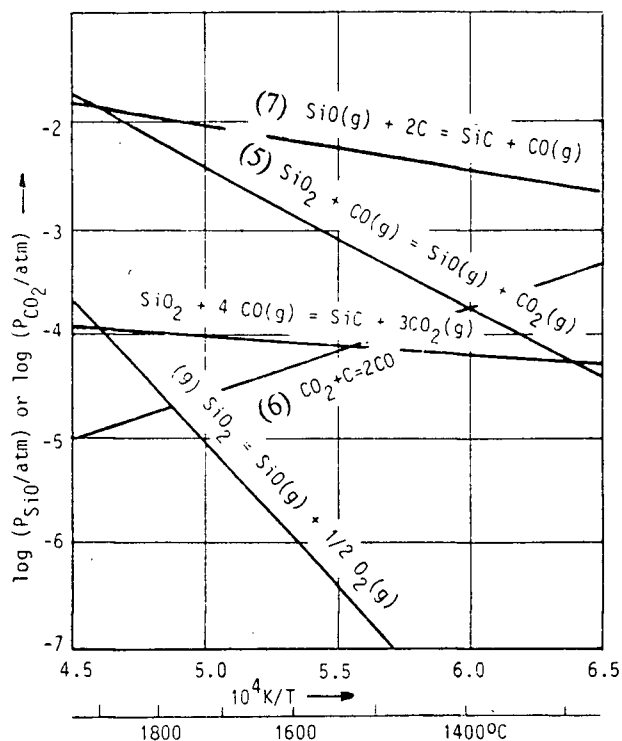
Fig. 39. Equilibrium pressures of SiO and /or CO_2 for various reactions of interest for the kinetics of the reaction between carbon and silica. Reactions (5), (6) and (7) are calculated with $P_{CO} = 1$ atm, reaction (5) with the additional restriction $P_{sio} = P_{co}$. For reaction (a), $P_{sio} = 2P_{O_2}$
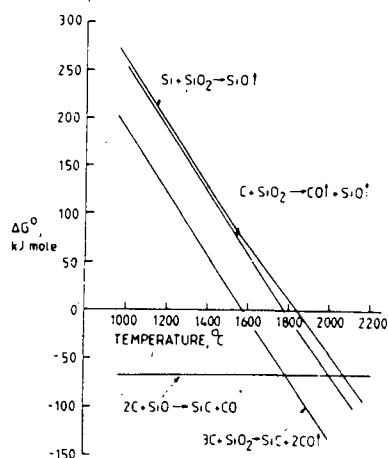
Fig. 40(a). Variation of free energy with temperature for reactions in the Si–O–C system.
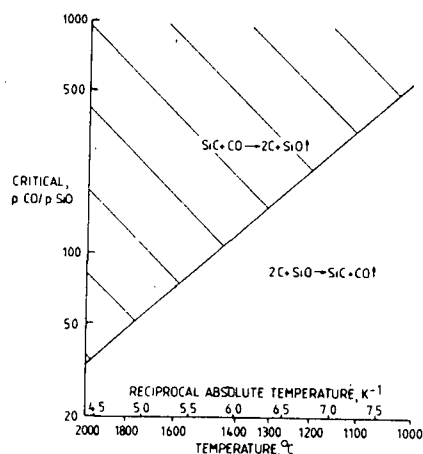
Fig. 40(b). Variation of equilibrium p_{co}/p_{sio} for $2C + SiO \rightarrow SiC + CO$.

about 75 at $1600°C$. Thus SiC formation is favoured even when the removal of CO is poor.

Now looking at the experiment (#114) in which the kaolinite + carbon black mixture was heated from room temperature to $1805°C$ under a pressure of 30MPa, held for 3 mins; them temperature lowered to $1660°C$ and pressure increased to 50MPa, soaked for 10 mins — one would expect the near completion of the reduction of mullite and silica in the pellet. In fact except for a trace of SiC + Al_2O_3 layer on the edge of the pellet, the hot-pressed pellet was found to be a 95% dense mullite + C (plus amorphous silica not detected by X-ray analysis) ceramic. This result suggests that high external pressure severely retards the rate controlling reactions.

4.2.2. Kinetics of the formation of SiC

4.2.2.1. Reaction rate

Figure 12 shows the effect of temperature on the formation of SiC. In general, the rate of reaction was strongly temperature dependent and increased rapidly with temperature. Though the reduction of SiO_2 or mullite with carbon is endothermic, Bechtold and Cutler[61] found that it is not a heat-transfer-limited process. It is possible that the reaction rate is controlled by a thermally activated process.

The reduction of mullite must be a heterogeneous reaction and involves i) an interdiffusion of the gaseous SiO and CO_2 outwards and CO inwards through the pores of the alumina layer and ii) reaction at the phase boundaries, CO with SiO_2, CO_2 with

carbon and SiO with carbon.

Kronert and Buhl[81] suggested that both gas transport by diffusion as well as phase boundary reactions could be rate controlling. Lee, Miller and Cutler[83] concluded that the reactions between SiO_2 and CO and between CO_2 and carbon might be rate controlling. Bentsen et al.,[66] in their recent study, however, found that the reaction with CO on the silica surface was not rate controlling (as the rate did not increase with the CO pressure). They suggested that gas diffusion and some other slow step outside the mullite grains could be rate controlling.

In the present case the kinetic data of the formation of SiC + Al_2O_3 phases followed a contracting cylinder model. This suggests that gas diffusion may be rate controlling in mullite reduction.

It was established (in section 4.2.1.3.b) that the rate controlling step was sensitive to external pressure and the rate was retarded with pressure. Gas diffusion should be definitely affected with external pressure in a hot–pressing die, as it is a closed system. Thus gas diffusivity may significantly decrease with increasing external pressure and vice versa. This suggests that gas transport is most likely the rate controlling mechanism.

4.2.2.2. Activation energy

The activation energy calculated based on the contracting cylinder model and using the Arrhenius equation $K = Ae^{-E/RT}$ was found to be 922 KJ/mole. The only report in the literature on the activation energy of the carbothermal reduction of kaolinite

was that of Bechtold and Cutler[61] who obtained a value of 322 KJ/mole. Their calculation was based, however, on the weight loss of the kaolinite + C mixture as a result of CO gas escape during heating. The present estimation was based on the rate at which the reaction interface was penetrating the mullite/silica + C zone. So these values may not be directly comparable.

Bechtold and Cutler have compared their activation energy value with the values that were reported on the carbothermal reduction of silica. The reports on the activation energy of the reduction of silica with carbon are many and the values vary in a wide range between 490KJ/mole[77] and 569 KJ/mole.[83] It may be noted that the kinetics involved in the reduction of kaolinite with carbon would be different from the kinetics involved in the reduction of silica. Kaolinite at the reduction temperature contains a mixture of mullite and silica (some amorphous and some crystalline) and each phase should have different kinetics of reaction with carbon. In a recent study, Bentsen et al.,[66] have compared the relative kinetics of the reduction of mullite and silica with carbon and based on the weight loss rates found that silica reacted faster than mullite by a factor of 2.0 to 2.5. This was ascribed partly to the lower activity of silica in the mullite and partly to the extra resistance for gaseous diffusion through the porous alumina layer formed on the mullite grains.

Thus in the reduction of kaolinite with carbon the kinetics of the process would be rather dictated by the relative amounts of mullite and silica present at the reduction temperature and the overall activation energy would lie somewhere in between the values for mullite alone and silica alone. This would be the same whether the kinetics are followed from the wt. loss rate measurements or from the reaction interface penetration

rate, as in both the cases, both the mullite and silica phases that are intimately mixed contribute to the reaction kinetics.

4.3. Microstructure

The microstructure should be considered as the key to the quality of advanced ceramics since the physical, particularly, the mechanical properties of an advanced ceramic product depend on their microstructure. The presence of grain boundaries and the study of the effect of grain size on a property are of major importance in most polycrystalline materials. The effect of porosity, together with that of the grain boundaries, is of considerable importance to the material properties. In the case of particulate composite ceramics, the properties depend upon the microstructural aspects of the second phase inclusion and as well on their interaction with the matrix phase.

4.3.1. Use of Scanning Electron Microscopy.

Scanning electron microscopy was used because it can reveal the structure of a porous body and the three dimensional grain (or crystallite) morphology. In Figures 15 and 16 the change in the morphology of mullite$-SiO_2-C$ and Al_2O_3-SiC composite can be noted as the hot$-$pressing temperature increased. Large voids (2 to 4μm) as well as small pores (0.15$-$0.2μm) are present in mullite $+ SiO_2 + C$ sample hotpressed at $1600°C$ and 20MPa. With increase in hot$-$pressing temperature to $1800°C$ and pressure of 40MPa, the porosity drastically decreased with the disappearence of large voids. There was an increase in the grain size.

In the case of Al_2O_3-SiC composite at $1660°C$, the structure is more porous than that of mullite and most of the grains have micropores $(0.02\mu m$ in them (Figure 15b). The particles are much finer than those of mullite $+ SiO_2 + C$ and are very conglomerated. There are also larger crystallites often flaky which are surrounded by finer conglomerates. This type of structure for the composite sample may be attributed to the gas–solid reactions prevalent during the formation of the phases of Al_2O_3 and SiC. When the hot–pressing temperature was increased to $1800°C$ a less porous structure is obtained (Figure 16b). This observation is in agreement with the density results (Table V). The crystallites are rounded and more agglomerated, indicating a significant degree of diffusion–controlled interaction between crystallites. The rounded grain morphology observed by TEM on the same sample (Figure 24a) is in agreement with the above observation.

4.3.2. Use of Transmission Electron Microscopy

4.3.2.1. Importance of TEM in Ceramics

Transmission Electron Microscopic studies have made a considerable impact in Ceramics particularly in the last 10–15 years. Some of the reasons for this development are: 1) The problem of preparing samples thin enough for electron transmission has been alieviated by advances in techniques, e.g., ion beam thinning[84] and mechanical microthinning.[76,79] 2) High voltage electron microscopes with their greater beam penetrating power were introduced. 3) Adequate theories have become available for the interpretation of images and diffraction effects thereby making it possible to carry out properly the quantitative microscopy of ceramics which generally have complex structures. In the present study, TEM was found to be very useful in studying the grain

morphology and in estimating the grain size. Other techniques were found to be not very useful because of the very small grain size.

4.3.2.2. Difficulty with Ion Milling

It was surprising that only Ti was detected (Figure 19(b)) throughout the area that was ion milled (Figure 19(a)). It has been reported[76] that long ion milling could introduce several artifacts and also preferentially sputter some of the elements present in the material thereby affecting the morphology and the chemical composition of the specimen surface. The two big shell like particles "A" and "B" in Figure 19(c) could be the artifacts introduced by ion milling. Titanium was found in high concentrations in the X-ray spot analysis on the two particles. The pyramids observed in small numbers in Figure 19(c) and, in large numbers in Figure 19(e) must be due to the preferential sputtering of the lighter element Al that took place. The milling time used to thin down the specimen to perforation, in the present case, was 60 hrs which was long enough for surface contamination.

However, it was not understood how Ti was the only element present in the ion milled area (Figures 19(a) and (b)). The total content of the Ti impurity in the raw material (kaolinite) was only 0.6 wt% or less which makes it impossible to form a continuous structure even if none of the Ti was removed during the ion milling operation. The fact that Ti was detected in very high concentrations even at the edge of the specimen (Figure 19(e) and (f)) suggests that there was an external source of Ti present inside the ion mill chamber which could have deposited on the specimen surface. It was reported[85] that impurities might originate from the specimen, specimen platform

and clamping plates, vacuum system and other components. Also it was reported that the contamination might take the form of discrete particles or continuous films and comprises many of the compositional and microstructural analyses. In the present case, the contamination took the form of discrete particles that are very uniform in size and seen in Figure 19(a). The explanation for the presence of very high Ti impurity in the specimen can not be given without further investigation.

4.3.2.3. Use of Mechanical Microthinning for TEM Ceramic Specimen Preparation

Mechanical microthinning can be effectively used to prepare thin enough specimens useful for TEM without damaging the structural integrity or the chemical composition of the specimen. As for example, the X-ray spectra taken on the area in Figure 21 showed both, Al and Si peaks indicating the presence of mullite and silica, and showed Ti in minute amounts. Thus the original composition remained unchanged by mechanical microthinning which may suggest that even brittle and friable materials can be microthinned. Sometimes the technique of coating or impregnating wax or Canada Balsam into the pores of the brittle specimen and then grinding it to the required thickness may be used.

There was no presence of a transparent phase in the micrographs in Figures 23 and 24(a) indicating that all the mounting wax was dissolved in acetone while cleaning. Even without the wax film the specimen was strong to hold itself and thin enough for TEM. The EDX analysis on the area in Figure 23 showed no major impurity. Thus the mechanical microthinning provides an useful method to prepare ceramic specimens for TEM, particularly, when the ion milling causes structural damage and chemical change.

4.3.2.4. Phase Distribution Prior to the Carbothermal Reduction Process

Prior to the carbothermal reduction process the reaction mixture was found to contain a mixture of mulllite and carbon as analysed by the X-ray analysis. This is confirmed in the STEM micrograph (Figure 21) where mullite is seen as a dark phase distributed uniformly through out the microstructure. Figures 22(a) and (b) show the presence of an amorphous phase in the mullite specimen (noting the diffused concentric ring shaped diffraction pattern). This suggests that silica was present as an amorphous phase confirming the results of the X-ray analyses in which no crystalline forms of silica were found. The average size of the mullite crystals, calculated from Figure 9 falls in the range 0.25 - $0.3 \mu m$. The size of the silica particles as measured from Figure 22(a) is typically $0.5 \mu m$.

4.3.2.5. Phase Distribution After the Carbothermal Reduction Process

Assuming that the TEM micrographs in Figures 17-18 represent the actual microstructure of the Al_2O_3-SiC composite and not that of the titanium impurity the following observations can be made.

"A" and "B" of the BF image in Figure 17(b) represent two crystals of the same phase and their SAD's are seen superimposed in Figure 17(d). The structural details of the edges of "A" and "B" (pointed with arrows) came into view when the specimen was tilted slightly from the position in (a) to that in (b). These edges resemble the characteristically faceted appearance of $\beta-SiC$ which contains occasional planar faults.[86] The "C" in BF image (Figure 17a) correspond to "C's" in the other BF image (Figure 17b) and in the DF images (Figures 17c and 17e). The average grain size of the sample

as measured from "C" is 0.17μm.

The diffraction pattern in Figure 20 corresponds typically to a single phase multicrystalline material. This suggests that all the grains seen in Figure 19(a) have the same phase and possibly TiO_2. The grain size of the Al_2O_3-SiC composite as measured from Figure 24(a) is 0.25 - 0.3μm. The size of the silica particles, measured from Figure 22(a) is typically 0.4μm. Larger, as well as smaller grains are seen in Figure 27. Their grain size range from 0.1 to 0.35μm. In a sintered α-SiC the grain size was reported[87] as $\simeq$ 1μm. Thus the carbothermal reduction of kaolinite with carbon black can produce a composite ceramic with a very fine grain size.

Some microstructural features observed are graphite inclusions as shown at 'C' in Figure 24(a). It may be understood that the black areas within the hexagonal platelet in Figure 25 are indications of the intragranular carbon. The lines seen on "A" of Figure 26 and on "B" of Figure 27 are due to grooving caused during grinding.

As seen in Figures 26 and 27 the typical microstructure consists of hexagonal platelets stacked on each other and with little grain boundary phase. The aspect ratio seems to be large with the thickness value of a platelet being only a fraction of its width value. Short fibers or whiskers are not observed in the microstructure.

In the STEM micrograph (Figure 28) it may be seen that Al_2O_3 phase consists of large grains compared to SiC grains. At some places both Al_2O_3 and SiC are present in very fine sizes and so the spot X-ray generated showed both the Al $K\alpha$ and Si $K\alpha$ peaks. At some places (e.g., at D) it could be the unreacted mullite as seen

from the peaks intensities of Al Kα and Si Kα.

It is very interesting to note that the Ti impurity exists at higher concentrations at some places. There might be some preferred regions such as grain boundaries, where this phase was concentrated, but the exact reason for the kind of Ti distribution observed in its map(Figure 30(b)) is not understood.

Thorough knowledge of diffraction patterns is necessary to interpret the results of SAD. As was the case in Figure 17(d), two or three diffraction patterns of different crystals might interact or superimpose in a systematic way thereby complicating the SAD's. It may be pointed out that regarding the TEM analysis in the present study only a first attempt has been made to analyse the microstructure.

4.4. Effect of the Carbothermal Reduction on the densification of alumina-SiC composite

Density is often a limiting factor in the case of ceramics in achieving the full potential of their mechanical properties. Unfortunately, it is difficult to fabricate ceramics with theoretical density, particularly, those that are covalently bonded such as SiC, Si_3N_4 and B_4C and others. In general, high temperatures and high pressures are used along with the densification aids in order to achieve high densities in the covalent bonded ceramics.

Table V shows that the density of the specimens containing mullite, amorphous silica and carbon (stoi. or excess proportions) as the final phases, increased with temperature with the exception at 1600°C. It reached a maximum value of 94% of

theoritical at 1800°C. A very interesting fact that can be seen from the table is that when mullite and carbon react to form α-alumina and silicon carbide the material becomes considerably more porous and loses density by one third. For example a 75% dense specimen (#70) containing mullite, SiO_2 and C reduced to only 51% dense, when the composition was changed to Al_2O_3 and SiC (#110).

These observations are supported by the SEM micrographs of these materials (Figures 15 and 16). At 1600°C the material mullite + SiO_2 + C is seen porous (Figure 15a) with large voids and small pores. At 1800°C the same material is seen in Figure 15(b) almost as a continuous phase with the disappearence of voids and many pores. After the carbothermal reduction, the material mullite + SiO_2 + C has become considerably more porous with the introduction of micropores within the grains. This is seen in Figure 15(b) and 16(b) at temperatures 1660° and 1800°C, respectively. This explains the decrease in the density values for Al_2O_3-SiC composite. However, even in the case of Al_2O_3-SiC composite the density improved with temperature.

From the above observations it becomes clear that the application of higher pressures on the material mullite + SiO_2 + C after its carbothermal reduction, and high temperatures can improve the density of the composite ceramic. This at best can be done by taking the specimen to the hot-pressing temperature under a moderate pressure ($\simeq$ 20MPa), allowing it to convert to Al_2O_3-SiC composite, and then applying higher pressures (40MPa and above). Two experiments #113 and #115 were performed using the above procedure. As a result, about 30% increase in the density was attained by hot-pressing at 1800°C and at 40MPa (final density 67%).

4.5. The Viscoelastic model for R.H.P. of kaolinite + Carbon Black

As stated in section 4.1., data obtained from isothermal compaction curves could be used as an aid in understanding the behaviour of kaolinite + carbon black mixture during and after the formation of mullite. While the compaction data as shown in Figs. 32 and 33, appear to be somewhat complex in nature, an attempt has been made to relate the data to a simple viscoelastic system. It is also possible to fit the compaction data to higher order polynomial,[88] using a computer, but such an equation would not lend itself to the development of a viscoelastic model.

4.5.1. The dynamic system

If a mathematical model is to suitably describe reactive hot-pressing, it must be dynamic, that is time varying to any given input (stress, strain, voltage etc.). The simplest dynamic system which could possibly be related to R.H.P. of kaolinite + C is a second order system whose response to a unit step input can be described by an equation of the form.[89]

$$\epsilon = K(1 - Ae^{-at} - Be^{-\beta t}) \qquad \text{........ 9}$$

It has been shown in section 3.5 that R.H.P. of kaolinite + C can be expressed by an equation of the form in (9).

As the data was obtained as a function of time by heating the powder to a given temperature and applying a constant stress (or pressure), it can be said that the system is responding as described by Eqn. 9 to an input which can be considered a unit

step input.[67] This is explained schematically in Fig. 41 and mathematically in appendix B.

INPUT (stress)   OUTPUT (strain)

$$\sigma = \sigma_0 U_{-1}(t)$$ $$\epsilon = K(1 - A e^{-\alpha t} - B e^{-\beta t})$$
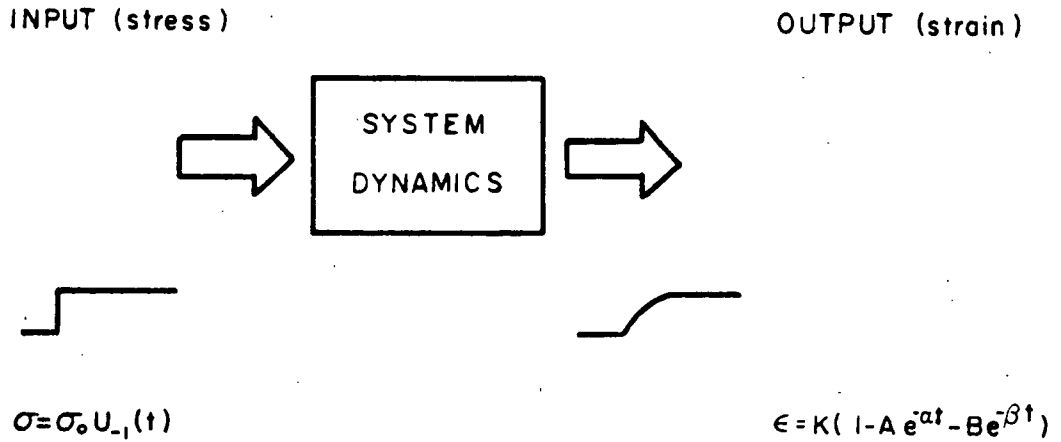
Fig. 41. Schematic representation of "system dynamics" relating output (strain) to input (stress).

The output (strain) can be effectively described by a second order differential equation. Such an equation is derived in appendix B and is shown below.

$$\frac{d^2 \epsilon}{dt^2} + (\alpha + \beta) \frac{d\epsilon}{dt} + \alpha\beta\epsilon = K(A\alpha + B\beta) \frac{d\sigma}{dt} + K\alpha\beta\sigma \qquad \text{........ 14}$$

4.5.2. The Mechanical Analog

A mechanical model based on linear devices like springs and dashpots can be developed, in which the constants α, β, A and B (of eqs. 9 & 14) can be expressed in terms of the mechanical constants of these devices. A spring is an ideal device for which the stress is directly proportional to the stress, while a dashpot is a hypothetical device

which is strain rate sensitive (Fig. 42).

SPRING (STRAIN SENSITIVE)   **DASHPOT (STRAIN RATE) SENSITIVE**

$$\sigma = M\epsilon$$ $$\sigma = \eta \frac{d\epsilon}{dt}$$

M (ELASTIC SHEAR MODULUS) η **(NEWTONIAN VISCOSITY)**

Fig. 42. Defining the spring (a strain sensitive device) and dashpot
(a strain rate sensitive device).

The final viscoelastic model[76] that was found to have a response similar to

Eqn. 14, is shown in Figure 43, and the equivalent differential equation for its response

is given by Eqn. 15.

$$\frac{d^2\epsilon}{dt} + \left[\frac{\eta_2(M_1 + M_2) + M_2\eta_1}{\eta_1\eta_2}\right]\frac{d\epsilon}{dt} + \left[\frac{M_1 M_2}{\eta_1\eta_2}\right]\epsilon = \left[\frac{1}{\eta_2}\right]\frac{d\sigma}{dt} + \left[\frac{M_1 + M_2}{\eta_1\eta_2}\right]\sigma \quad \cdots\cdots 15$$
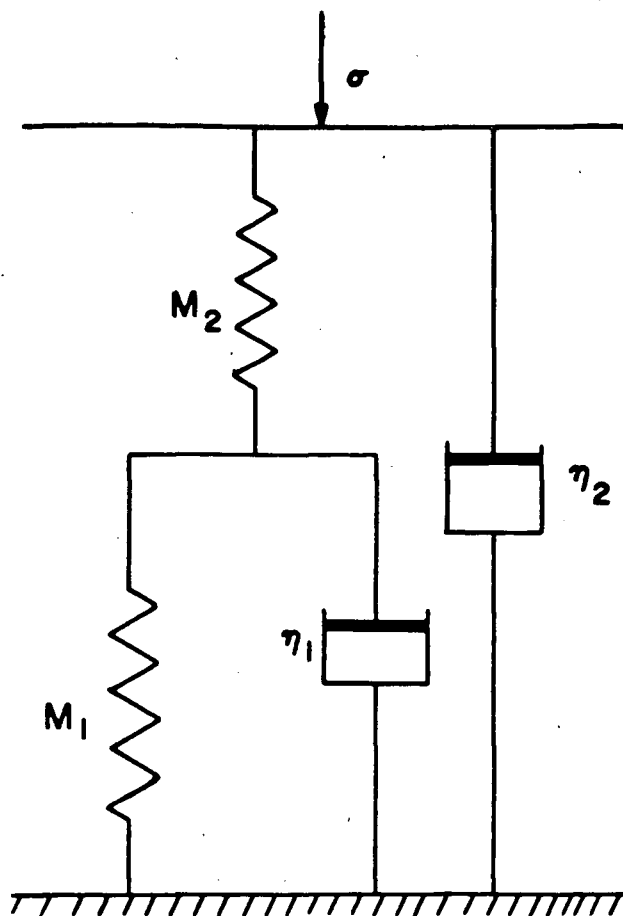
Fig. 43. Interactive–double–Kelvin Unit.

By comparing Eqns. 14 and 15, one obtains the following relationships.

$$\eta_2 = \frac{K}{A\alpha + B\beta}$$

$$M_2 = \eta_2[\alpha + \beta - K\alpha\beta\eta_2]$$

$$\eta_1 = \frac{M_2}{[\alpha + \beta - \frac{M_2}{\eta_2} - \frac{\alpha\beta\eta_2}{M_2}]}$$

$$M_1 = \frac{\eta_1\eta_2\alpha\beta}{M_2}$$

$$\cdots 16$$

4.5.3. Significance of Mechanical Parameters M_1, η_1, M_2 and η_2

The values of mechanical parameters M_1, η_1, M_2 and η_2 were calculated by substituting the computed values of K, A, a, B and β of the experimental curves in Eqn. 16. Their values for both the kaolinite + C and Kaolinite + C(22.5wt% excess) mixtures are listed in Tables VI and VII and are shown as a function of temperature in Figures 44 and 45.

It is quite evident from the figures that one of the elastic elements (M_1) and one of the viscous components (η_1) are temperature sensitive whereas the other two are not. Thus, these two components can be assigned to the behaviour of the system mullite – silica – carbon during reactive hot–pressing. Some clear observations from Figures 44 and 45 are:

a) In the temperature range 1500° – 1600°C the values of viscosity component (η_1) for kaolinite with stoichiometric C increased rapidly, reached the maximum, and then dropped to the original value. This happens at the expense of the elastic component (M_1) which behaves just opposite to η_1).

b) In the case of kaolinite with 22.5wt% excess carbon the same type of behaviour is observed except that there is a leftward shift of 50°C in the case of the viscous component η_1. The high viscosity component for the system implies that the system is resistant to flow or compaction and vice versa.

TABLE VI. VALUES OF MECHANICAL PARAMETERS FOR
KAOLINITE + CARBON BLACK

EXP #	M1	ETA1	M2	ETA2	TEMP(C)
77T	10.8811	54.8470	7.0702	0.7250	1200
78T	13.2595	39.7477	4.3196	3.0873	1300
79	15.7782	55.8761	2.9339	0.3295	1400
74T	21.3238	51.8603	2.6052	0.3400	1500
83T	2.3787	250.8121	2.0698	0.3724	1550
73	14.8200	48.8143	2.3290	0.4684	1600
115	7.0520	21.5518	2.2326	0.3794	1800

TABLE VII. VALUES OF MECHANICAL PARAMETERS FOR
KAOLINITE + CARBON BLACK(EXCESS)

EXP #	M1	ETA1	M2	ETA2	TEMP(C)
65T	11.9609	60.1754	5.7909	3.5976	1200
63T	16.0734	42.1642	4.0822	3.5948	1300
66T	41.4935	103.4149	2.8012	3.3300	1400
64	21.3155	148.1791	2.4915	1.5128	1500
67	21.4575	51.8231	2.3900	1.3611	1600
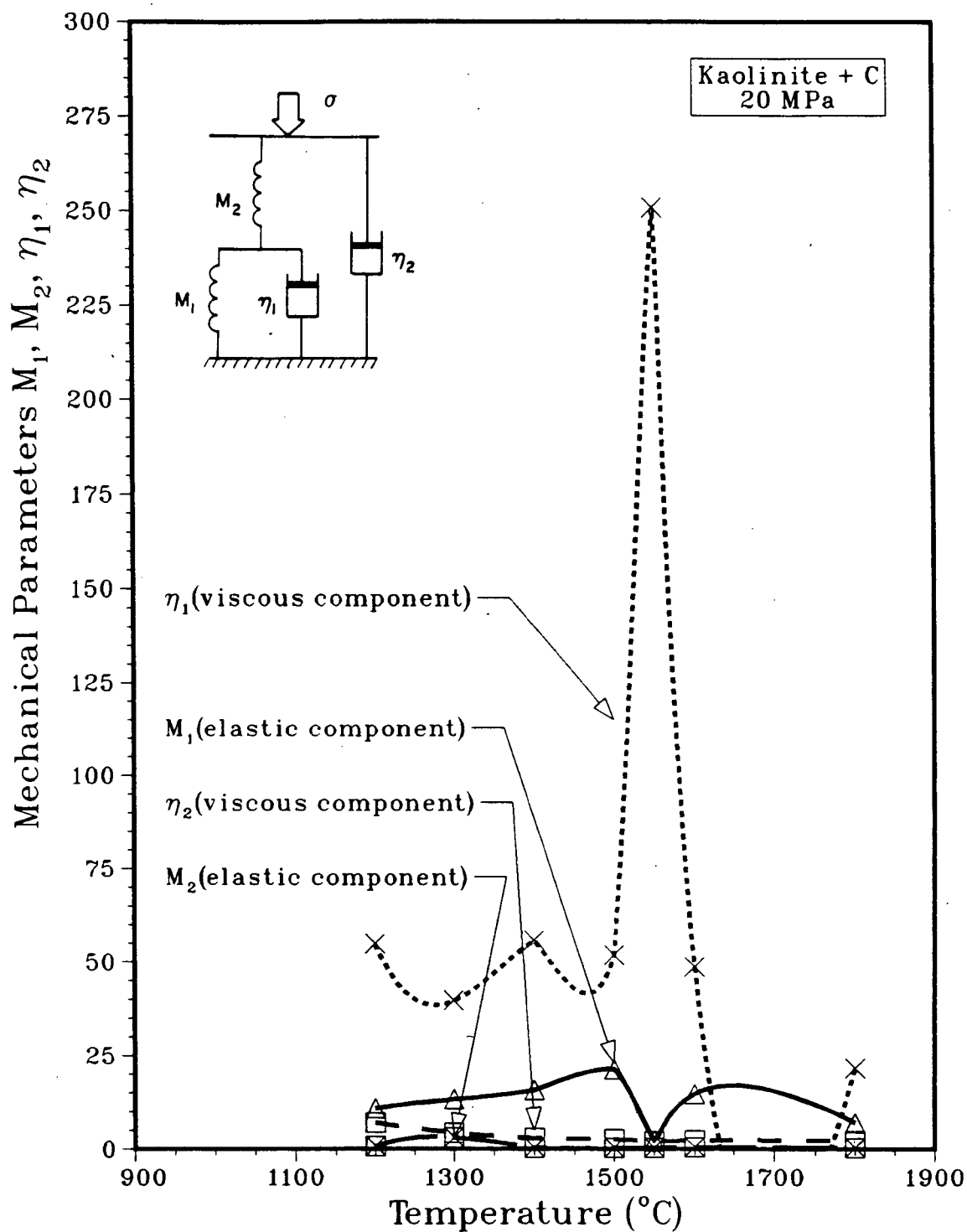
Fig. 44. The values of mechanical parameters η_1, η_2, M_1, M_2 as a function of temperature for kaolinite + carbon black.
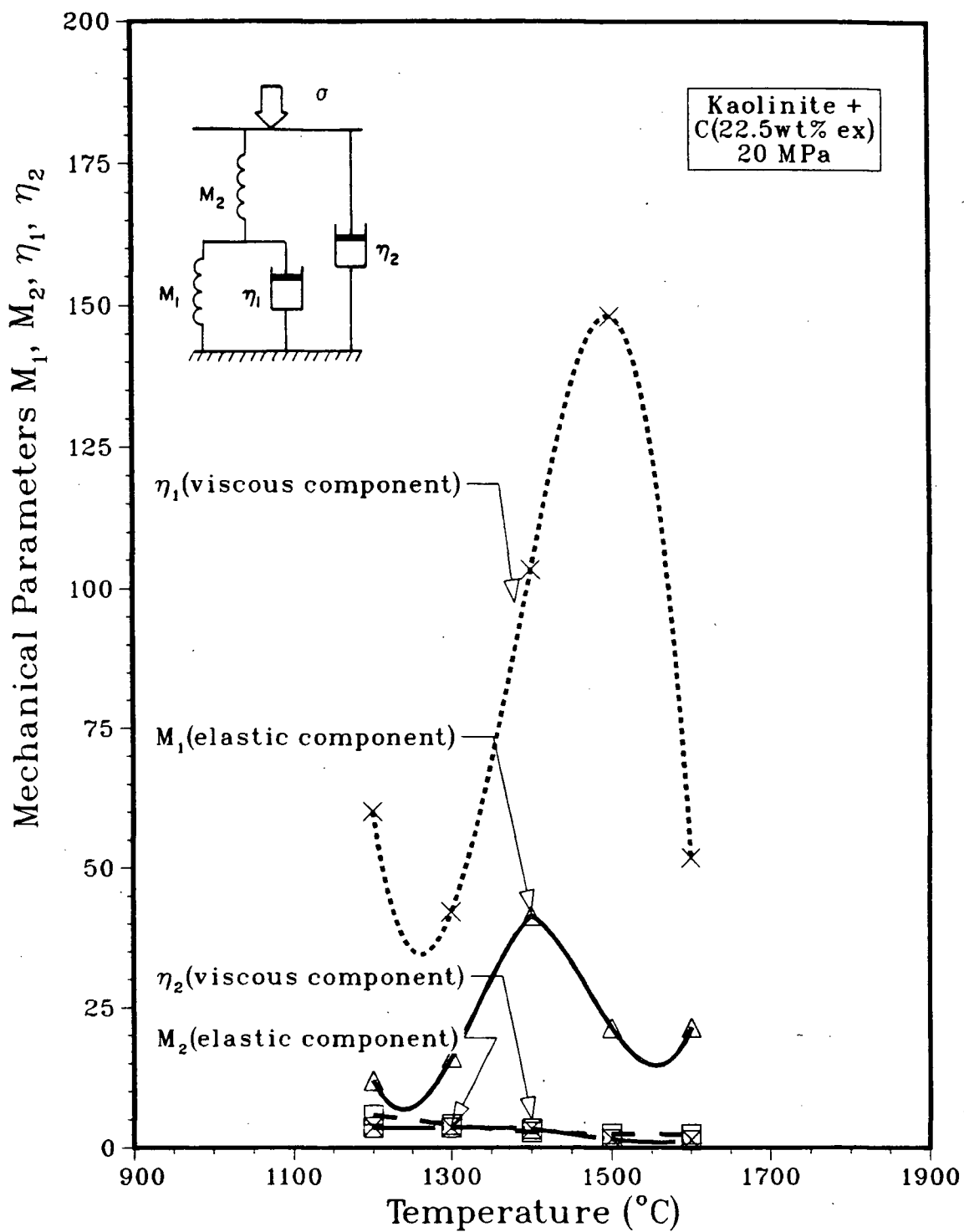
Fig. 45. The values of mechanical parameters η_1, η_2, M_1, M_2 as a function of temperature for kaolinite + carbon black(excess).

component η_1. The high viscosity component for the system implies that the system is resistant to flow or compaction and vice versa.

The correlation between the pseudo–plasticity observed during reaction hot–pressing in the kaolinite–carbon system above 1500 (Fig. 10, p45) and also during isothermal compaction experiments (Fig. 32, p84) and the reaction between mullite and carbon leading to the formation of Al_2O_3 and SiC can be explained as follows.

The final mullitization reaction is almost complete, when the temperature of $1500°C$ is reached. This is known from the kinetics of kaolinite transformations to mullite and this is also reflected in the compaction curve of pure kaolinite. It can be seen in Fig. 10 (p45), that compaction ceased when the transformation was completed in pure kaolinite.

However, a new reaction, which is the dissociation of mullite and formation of SiC, took over in the kaolinite–carbon system above $1500°C$. The sharp decrease in the value of the viscous component η_1 above $1550°C$, which implies more plasticity in the system, can be directly related to the following reactions, which resulted in the formation of Al_2O_3 and SiC.

$$3Al_2O_3 \cdot 2SiO_2 \ + \ 6C \ \longrightarrow \ 3Al_2O_3 \ + \ 2SiC \ + \ 4CO \qquad \text{........4}$$
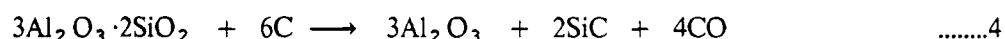
The above reaction must involve in some form of breakdown of rigid mullite structure, which produced the pseudo–plasticity observed during reactive hot pressing above $1550°C$. Between 1550 and $1750°C$, the value of η_1 is almost zero (Fig. 44) indicating that the system has lost its rigidity or structural integrity which produced compaction above

1550°C. There are indications that the value of η_1 tends to increase at or above 1800°C, implying that the reactions which produced the transient plasticity in the system were completed at $\simeq$ 1800°C.

As the specimens were heated under atmospheric pressure before the application of any pressure, the carbothermal reduction of mullite starts at around 1550°C. Klinger et al.,[77] and Poch and Dietzel[90] found that SiC starts to form at 1530°C when a mixture of silica and C is heated. Baumann[91] observed that the formation started at 1500°C. Thus in the range 1500° – 1550°C the phases Al_2O_3 and SiC start forming from the carbothermal reduction of mullite as well as silica.

However, the rate of formation of Al_2O_3 and SiC below 1550°C is slow with a long induction period for the nucleation of Al_2O_3. This is well supported from the present experiments ($\#$ 45, 83 and 84 of Table IV)

From the above considerations, it may be understood that the sluggish formation of SiC and Al_2O_3 at lower temperatures may offer some resistance to flow in the system which situation is altered at higher temperatures because of the improved reaction rate.

4.6. Scope for Future Study

The present study was confined to producing an Al_2O_3–SiC ceramic composite and to the study of the compaction behaviour and kinetics involved during the carbothermal reduction of kaolinite. It did not extend to densifying the composite ceramic

to near theoritical density or to testing its mechanical properties. With the success in the first step, in producing a composite ceramic there is a scope for future study in this subject.

Some specific areas are identified as follows and which may be worth investigating.

a) It was mentioned that Fe catalyzed the SiC formation reaction during the pyrolysis of rice hulls[56,92] and during the carbothermal reduction of kaolinite.[61] It was also mentioned that its catalytic effect decreased with increasing temperature.[56] However, it would be worth investigating whether addition of Fe improves the rate of formation of the Al_2O_3–SiC composite.

b) It was found that the composite ceramic became considerably porous during the carbothermal reduction process due to the gas–solid reactions that were involved. As a result the composite formed directly from the precursors (kaolinite and carbon black) was not very dense. Further experiments should be done to produce the composite powder of Al_2O_3 and SiC under atmospheric pressure and then to fabricate the composite ceramic to near theoritical densities by hot–pressing the milled powder. Densification aids may or may not be added.

c) In the present study a closed system was used for the carbothermal reduction process to take place. Future experiments should be done to study the various rate controlling mechanisms including the rate of the chemical reaction.

d) Mechanical properties of these composites should also be investigated, as a funtion of compositions, heat treatment etc.

5. CONCLUSIONS

The carbon additives acted as an inert filler and reduced the overall compaction during the reactive hot-pressing of kaolinite + carbon black mixtures. Carbon becomes reactive only above 1350°C where it affects the compaction behaviour of kaolinite, due to reduction of mullite by carbon.

The carbothermal reduction of mullite leads to the preferential reduction of SiO_2 and nucleation of alumina. Alumina is stable until 1800°C and does not get reduced even with excess carbon below that temperature.

The reduction of mullite and silica proceeds through a gaseous intermediate SiO and starts very slowly at 1450°C. The rate of reaction increases with temperature and the kinetics follow a contracting cylinder model because of the geometry of the specimens. There is an induction period observed for the nucleation of alumina. The rate of reaction is controlled by a thermally activated process for which the activation energy was found to be 922 KJ/mole.

The composite ceramic produced has a very fine grained microstructure which itself made the identification of the individual phases extremely difficult. The grain size was of the order of 0.2μm and the particles were of platelet form. The phases Al_2O_3 and SiC are intimately mixed throughout the microstructure. The major impurity in the composite was found to be titanium, which at locations was present in higher concentrations.

Contrary to what was predicted by Bechtold and Cutler[61] the SiC-whisker formation was not encountered in the present study. However, the fine grained microstructure should provide the composite ceramic with good mechanical properties.

Thus, it is feasible to produce a particulate composite of Al_2O_3 and SiC by hot-pressing cheap precursors, kaolinite and carbon black. Pure raw materials, wet mixing, high hot-pressing temperature in the range $1800° - 1850°C$, and high pressures 40 to 50MPa applied at the beginning of the soaking period would be very favourable to produce a dense $Al_2O_3 - SiC$ composite ceramic.

Empirically, a viscoelastic model can be used to interpret the complex isothermal compaction data of the kaolinite + C mixtures. The interactive-double-Kelvin unit was found to fit the data and only one elastic component (M_1) and one viscous component (η_1) were found to be temperature sensitive. The temperature dependence of η_1 and M_1 are correlated with transformation plasticity encountered during the dissociation of mullite by carbon, leading to the formation of Al_2O_3 and SiC.

REFERENCES

1. "The Promise of Ceramics," *Adv. Mat. and Processes,* 131[1] 44–50 (1987).

2. Hiroaki Yanagida, "Industrial and Cultural Revolution through High–Tech Ceramics," *Adv. Cer. Mat.,"* 2[1] 31–33, 38 (1987).

3. A.G.Evans and B.J.Dagleish, "Some Aspects of the High Temperature Performance of Ceramics and Ceramic Composites," *Cer. Eng. Sci. Proc.,* [9–10] 1073–94 (1986).

4. A.G.Evans and R.M.Cannon, in "Mechanical properties and Phase Transformations in Engineering Materials", *P–409, AIME Publication* (1986).

5. A.G.Evans, "Structural Reliability: A Processing Dependent Phenomenon," *J. Am. Ceram. Soc.,* 65[3] 127–37 (1982).

6. J.W.Edington, D.J.Rowcliffe and J.L. Hensel, "Powder Metallurgical Review 8: The Mechanical Properties of Silicon Nitride and Silicon Carbide, Part II. Engineering Properties," *Powder Met.Int.,* 7[3] 136–147 (1975).

7. "Ceramics on a Seesaw," *Adv.Mater.Proc.inc.Met.Prog.,* 131[5] 62–63 (1987).

8. L.J.Schioler and J.J.Stiglich, Jr., "Ceramic Matrix Composites: A Literature Review," *Am. Ceram. Soc. Bull.,* 65[2] 289–292 (1986).

9. R.A.J. Sambell, D.H.Bowen, and D.C.Phillips, "Carbon Fiber Composites with Ceramic and Glass Matrices, Part I. Discontinuous Fibers," *J. Mater. Sci.,* 7[7] 663–75 (1972).

10. R.A.J.Sambell, A.Briggs, D.C.Phillips, and D.H.Bowen, "Carbon Fiber Composites with Ceramic and Glass Matrices, Part 2–Continuous Fibers," *J. Mater. Sci.,* 7[7] 676–81 (1972).

11. S.Yajima, K.Okamura, J.Hayashi, and M.Omori, "Synthesis and Continuous SiC Fibers with High Tensile Strength," *J. Am. Ceram. Soc.,* 59[7–8] 324–27 (1986).

12. J.Brennan and K.Prewo, "Silicon Carbide Fiber Reinforced Glass–Ceramic Matrix Composites Exhibiting High Strength and Toughness," *J. Mater. Sci.,* 17, 2371–83 (1982).

13. Tai–il Mah, M.G.Mendiratta, A.P.Katz and K.S.Mazdiyasni, "Recent Developments in Fiber–Reinforced High Temperature Ceramic Composites," *Am. Ceram. Soc. Bull.,* 66[2] 304 –308, 317 (1987).

14. B.Bender, D.Shadwell, C.Bulik, L.Incorvaki,and D.Lewis III, "Effect of Fiber Coating and Composite Processing on Properties of Zirconia Based Matrix SiC Fiber Composites," *Am. Ceram. Soc. Bull.,* 65[2] 363–69 (1986).

15. A.J.Caputo, W.J.Laekey, and D.P.Stinton, "Development of New, Faster Process for the Fabrication of Ceramic Fiber–Reinforced Ceramic Composites by Chemical

Vapour Infiltration," *Cer. Eng. Sci. Proc.,* 6[7-8] 694-706 (1985).

16. J.V.Milewski, F.D.Gac, J.J.Petrovic, "Production and Characterization of Beta-Silicon Carbide and Alpha-Silicon Nitride Whiskers for Ceramic Matrix Composites," *Los Alamos National Laboratory Report* LA-9650-MS, UC-25, Feb.1983.

17. S.T.Buljan, J.Gary Baldoni and M.L.Huekabee," Al_2O_3-SiC-whisker Composites," *Am. Ceram. Soc. Bull.,* 66[2] 347-52 (1987).

18. M.A.Janney, "Mechanical Properties and Oxidation Behaviour of a Hot-Pressed SiC-15 vol%-TiB_2 Composite," *J. Am. Ceram. Soc.,* [2] 322-24 (1987).

19. C.H.McMurtry, W.D.G.Boecker, S.G.Seshadri and J.S.Zanghi, "Microstructure and Material Properties of SiC-TiB_2 Particle Composites, *Am. Ceram. Soc. Bull.,* 66[2] 325-9 (1987).

20. G.C.Wei, P.F.Beeher, "Improvements in Mechanical Properties in SiC by the Addition of TiC Particles," *J. Am. Ceram. Soc.,* 67[8] 571-4 (1984).

21. J.G.Baldoni, M.L.Huckabee and S.T.Buljan, "Mechanical Properties and Wear Resistance of Silicon Nitride-Titanium Carbide Composites, in *Tailoring Multiphase and Composite Ceramics,* Mat. Sci. Res. Vol.20, pp.329-45. Ed. R.E.Tressler, G.L.Messing, C.G.Pantano and R.E.Newnham, Plenum Press, New York.

22. R.W.Rice, "Ceramic Matrix Composite Toughening Mechanisms: An Update," *Cer. Eng. Sci. Proc.,* 6[7-8] 589-607 (1985).

23. N.Claussen, "Stress Induced Transformation of the Tetragonal ZrO_2 Particles in Ceramic Matrices, " *J. Am. Ceram. Soc.,* 61[1-2] 85-86 (1970).

24. P.F.Beeher and G.C.Wei, "Toughening Behaviour in SiC Whisker-Reinforced Alumina," *J. Am. Ceram. Soc.,* 67[12] C-267-C-269 (1984).

25. David B.Marshall and John E.Ritter, "Reliability of Advanced Structural Ceramics and Ceramic Matrix Composites - A Review," *Am. Ceram. Soc. Bull.,* 66[2] 309-317 (1987).

26. K.T.Faber, "Toughening of Ceramic Materials by Crack Deflection Processes, "Ph.D. Thesis, University of California, Berkeley.

27. A.G.Evans and K.T.Faber, "Crack-Growth Resistance of Microcracking Brittle Materials," *J. Am. Ceram. Soc.,* 67[4] 255-60 (1984).

28. T.Kosmac, J.S.Wallace and N.Claussen, "Influence of MgO Additions on the Microstructure and Mechanical properties of Al_2O_3-ZrO_2 Composites," *J. Am. Ceram. Soc.,* 65[5] C-66 - C-67 (1982).

29. F.Cambier, C.Baudin De La Lastra, P.Pilate and A.Leriche, "Formation of Microstructural Defects in Mullite-Zirconia and Mullite-AluminaZirconia Composites obtained by Reaction-Sintering of Mixed Powders" *Br.Ceram.Trans.J.* 83, 196-200,

1984.

30. Paul F.Becher and George C.Wei, "Toughening Behaviour in SiC-Whisker-Reinforced Alumina," *J. Am. Ceram. Soc.,* 67[12] C-267-C-269 (1984).

31. A.H.Chokshi and J.R.Porter, "Creep Deformation of an Alumina Matrix Composite Reinforced with SiC Whiskers," *J. Am. Ceram. Soc.,* 68[6] C-144-C-145 (1985).

32. Karl M.Prewo, J.J.Brennan, and G.K.Layden, "Fiber Reinforced Glasses and Glass-Ceramics for High Performance Applications" *Am. Ceram. Soc. Bull.,* 65[2] 305-313, 322 (1986).

33. David P.Stinton, A.J. Caputo and R.A.Lowden, "Synthesis of Fiber Reinforced SiC Composites by Chemical Vapour Infiltrtation" *Am. Ceram. Soc. Bull.,* 65[2] 347-350 (1986).

34. J.Cornie, Y.M.Chiang, D.R. Uhlmann, A.Mortensen, and J.M.Collins "Processing of Metal and Ceramic Matric Composites" *Am. Ceram. Soc. Bull.,* 65[2] 293-304 (1986).

35. H.Toshio, N.Koichi, N.Atsushi and N.Tetsuo, "Heat-Resistant Alumina-Silicon Carbide Composite and its Manufacture" Jpn. Kokai Tokkyo Koho JP 61/174165 A2[86/174165], 5 Aug 1986, 5pp.

36. George C.Wei and Paul F.Beeher, "Development of SiC Whisker Reinforced Ceramics" *Am. Ceram. Soc. Bull.,* 64[2] 298-304 (1985).

37. Terry N.Tiego and Paul F.Becher, "Sintered Al_2O_3-SiC Whisker Composites" *Am. Ceram. Soc. Bull.,* 66[2] 339-42 (1987).

38. Laurel M. Shepparrd, "Ceramics at the 'Cutting Edge'" *Adv. Mater. Proc. inc. Met. Prog.,* 132[2] 73-79 (1987).

39. Rodger D.Blake and Thomas T.Meek, "Microwave Processed Composite Materials" *J. Mater. Sci. Lett. 5* 1097-1098 (1986).

40. Hidehiko Tanaka, Peter Greil and Guntar Petzow, "Sintering and Srength of Silicon Nitride-Silicon Carbide Composites" *Int. J. High Tech. Ceram 1* (1985) 107-18.

41. R.Lundberg, L.Kahlman, R.Pompe and R.Carlsson, "SiC-Whisker Reinforced Silicon Nitride Composites" *Am. Ceram. Soc. Bull.,* 66[2] 330-33 (1987).

42. C.O.McHugh, T.J.Whalen and M.Humenik Jr., "Dispersion Strengthened Aluminum Oxide" *J. Am. Ceram. Soc.,* 49[9] 486-491 (1966).

43. D.T.Rankin, J.J.Stiglich, D.R.Petrak and R.Ruh, "Hot Pressing and Mechanical Properties of Al_2O_3 with a Mo Dispersed Phase" *J. Am. Ceram. Soc.,* 54[6] 277-281 (1971).

44. L.A.Simpson and A.Wasylyshin, "Fracture Energy of Aluminum Oxide Containing Mo

Fibers" *J. Am. Ceram. Soc.*, 54[1] 56–57 (1971).

45. D.J.Lloyd and K.Tangri, "Acoustic Emission from Al_2O_3–Mo Fibre Composites" *J. Mater. Sci.*, 9 pp. 482–486 (1974).

46. R.P.Wahi and B.Ilschner, "Fracture Behaviour of Composites based on Al_2O_3–TiC," *J. Mater. Sci.*, 15 875–885 (1980).

47. T.Zamebetakis, J.L.Guille, B.Willer and M.Daire," Mechanical Properties of Pressure–Sintered Al_2O_3–ZrC Composites," *J. Mater. Sci.*, 22 1135–1140 (1987).

48. D.P.H.Hasselman, P.F.Becher and K.S.Mazdiyasni, "Analysis of the Resistance of High–E, Low–E Brittle Composites to Failure by Thermal Shock," *Z.Werkstofftech*, 11 (3)., 82–92 (1980).

49. N.Claussen, "Fracture Toughness of Al_2O_3 with an Unstablized ZrO_2 Dispersed Phase," *J. Am. Ceram. Soc.*, 59 [1–2] 49–51 (1976).

50. N.Claussen, R.L.Cox and J.S.Wallace, "Slow Growth of Microcracks Evidence for One Type of ZrO_2 Toughening," *J. Am. Ceram. Soc.*, 65[11] C–190–C–191 (1981).

51. N.Claussen, J.Steeb and R.F.Pabst, "Effect of Induced Microcracking on the Fracture Toughness of Ceramics," *Am. Ceram. Soc. Bull.*, 56[6] 559–62 (1977).

52. T.N.Tiegs and P.F.Becher, "Whisker Reinforced Ceramic Composites," in Tailoring Multiphase and Composite Ceramics, Mat. Sci. Res. Vol.20, pp.639–48 Edited by R.E.Tressler, G.L.Messing, C.G.Pantano and R.E.Newnham. Plenum Press, New York, 1985.

53. P.F.Becher, T.N.Teigs, J.C.Ogle and W.H.Warwich, "Toughening of Ceramics by Whisker Reinforcement," pp.61–73 in Fracture Mechanics of Ceramics, Vol.7. Edited by R.C.Bradt, A.G.Evans, D.P.H.Hasselman and F.F.Lange, Plenum Press, New York, 1986.

54. J.R.Porter, F.F.Lange and A.H.Chokshi, "Processing and Creep Performance of SiC–Whisker–Reinforced Al_2O_3 " *Am. Ceram. Soc. Bull.*, 66[2] 343–47 (1987).

55. M.G.Jenkins, A.S.Kobayashi, K.W.White and R.C.Bradt, "Crack Initiation and Arrest in a SiC Whisker/Al_2O_3 Matrix Composite," *J. Am. Ceram. Soc.*, 70[6] 393–95 (1987).

56. J.Lee and I.B.Culter, "Formation of Silicon Carbide from Rice Hulls." *Am. Ceram. Soc. Bull.*, 54[2] 195–98 (1975).

57. S.R.Nutt, "Defects in Silicon Carbide Whiskers," *J. Am. Ceram. Soc.*, 67[6] 428–31 (1984).

58. P.D.Shalek, J.J.Petrovic, G.F.Hurley and F.D.Gac, "Hot–Pressed SiC Whisker/Si_3N_4 Matrix Composites," *Am. Ceram. Soc. Bull.*, 65[2] 351–56 (1986).

59. J.Homeny, W.L.Vaughn and M.K.Ferber, "Processing and Mechanical Properties of SiC−Whisker−Al_2O_3−Matrix Composites," *Am. Ceram. Soc. Bull.,* 67[2] 333−38 (1987).

60. J.V.Milewski, J.L.Sandstrom and W.S.Brown, "Production of Silicon Carbide from Rice Hulls, " pp.634−39 in Silicon Carbide − 1973, Proceedings of the Third International Conference on Silicon Carbide, Edited by R.C.Marshall, J.W.Faust Jr. and C.E.Ryan, University of South Carolina Press, Collumbia, SC, 1973.

61. B.C.Bechtold and I.B.Culter, "Reaction of Clay and Carbon to Form and Separate Al_2O_3 and SiC," *J. Am. Ceram. Soc.,* 63[5−6] 271−75 (1980).

62. J.G.Lee and I.B.Culter, "Sinterable Sailon Powder by Reaction of Clay with Carbon and Nitrogen, *Am. Ceram. Soc. Bull.,* 58[9] 869−71 (1979).

63. F.K.VanDyen, R.Metselaar and C.A.M.Siskens, "Reaction−Rate−Limiting Steps in Carbothermal Reduction Processes,' *J. Am. Ceram. Soc.,* 68[1] 16−19 (1985).

64. I.Higgins and A.Hendry, "Production of β'−Sailon of Carbothermal Reduction of Kaolinite," Br.Ceram.Trans.J., 85[5] 161−66 (1986).

65. I.W.M.Brown, K.J.D.Mackenzie, M.E.Bowden and R.H.Meinhold, "Outstanding Problems in the Kaolinite−Mullite Reaction Sequence Investigated by ^{29}Si and ^{27}Al Solid−State Nuclear Magnetic Resonance: II, High−Temperature Transformations of Metakaolinite," *J. Am. Ceram. Soc.,* 68[6] 298−301 (1985).

66. Siri Bentsen, Svein Jorgensen, Kjell Wiik and Ketil Motzfeldt, "Reactions Between Carbon and the Oxides Mullite and Silica," Mater.Sci. Monogr., 28A, 621−26 (1985).

67. Carolyn Moore, "UBC Curve," UBC Computing Centre Documentation, 1984.

68. J.L.Blumenthal, M.J.Santy and E.A.Burns, "Kinetic Studies of High−Temperature Carbon−Silica Reactions in Charred Silica−Reinforced Phenolic Resins," AIAA Journal, V4, 1053−7 (1966).

69. N.L.Bowen and J.W.Greig, "The System Al_2O_3−SiO_2" *J. Am. Ceram. Soc.,* 7[4] 238−54 (1924).; corrections, ibid., [5] 410.

70. R.R.West and T.J.Gray, "Reactions in Silica−Alumina Mixtures," *J. Am. Ceram. Soc.,* 41[4] 132−36 (1958).

71. F.Onike, G.D.Martin and A.C.Dunham, "Time−Temperature−Transformation Curves for Kaolinite," Mater. Sci. Forum, 7, 73−82 (1986).

72. P.Kennedy and B.North, "The Production of Fine Silicon Carbide Powder by the Reaction of Gaseous Silicon Monoxide with Particulate Carbon," Spl. Ceramics Vol. pp.1−15.

73. A.C.D.Chaklader, "Transformation Plasticity and Hot Pressing," in Deformation of Ceramic Materials, Ed. R.C.Bradt and R.E.Tressler, Plenum Publishing Corp., NY

1975.

74. A.C.D.Chaklader and R.C.Cook, "Kinetics of Reactive Hot-Pressing of Clays and Hydroxides, *Am. Ceram. Soc. Bull.,* 47[8] 712-16 (1968).

75. R.R.West, "High-Temperature Reactions in Domestic Ceramic Clays," *Am. Ceram. Soc. Bull.,* 37[6] 262-68 (1958).

76. C.P.Haltom, "Mechanical Prethinning and Thinning of Unique Materials for TEM," Proceedings of the 43rd Annual Meeting of the Electron Microscopy Society of America, pp.180-81 (1985).

77. R.S.Bradbeer, "Reactive Hot Pressing of Boehmite $(a-Al_2O_3.H_2O).,$" M.S. Thesis Report, University of British Columbia, 1965.

78. N.Klinger, E.L.Strauss and K.L.Komarek, "Reactions Between Silica and Graphite," *J. Am. Ceram. Soc.,* 49[7] 369-75 (1966).

79. H.K.Plummer,Jr. and S.S.Shinozaki, "Mechanical Microthinning: An Alternative to Chemical or Ion-Beam Thinning for TEM Specimen Preparation," Proceedings of the 43rd Annual Meeting of the Electron Microscopy Society of America, pp.398-99 (1985).

80. H.K.Plummer Jr. and S.S.Shinozaki, "Mechanical Microthinning for TEM Specimen Preparation," Proceedings of the 43rd Annual Meeting of the Electron Microscopy Society of America, pp.178-79 (1985).

81. W.Kronert and H.Buhl, "The Influence of Various Gaseous Atmospheres on Refractories of the $Al_2O_3-SiO_2-$System, Part I and Part II," Interceram 27[2] 68-72 and 140-146 (1978).

82. M.Sarikaya and I.A.Aksay, "High-Resolution TEM Studies of Mullite Formation in Metakaolinite," Proc. 44th Annual Meeting of the Electron Microscopy Society of America, pp.466-67. Ed. G.W.Bailey, San Francisco Press, Inc, 1986.

83. J.G.Lee, P.D.Miller and I.B.Cutler, "Carbothermal Reduction of Silica," in 'Reactivity of Solids', pp.707-11. Ed. J.Wood, O.Lindqvist, C.Helgesson and N.G.Vannerberg, Plenum Press 1976.

84. S.E.Khalafalla and L.A.Hass, "Kinetics of Carbothermal Reduction of Quartz under Vacuum," *J. Am. Ceram. Soc.,* 55[8] 414-17 (1972).

85. A.T.Fisher and P.Angelini, "Preparation of Backthinned Ceramic Specimens," Proceedings of the 43rd Annual Meeting of the Electron Microscopy Society of America, pp.182-83 (1985).

86. S.Shinozaki and K.R.Kinsman, "Influence of Structure on Morphology In Polycrystalline Silicon Carbide," pp.60-70 in Ceramic Microstructures '76. Ed. R.M.Fulrath and J.A.Pask. Westview Press, Boulder, Colarado, 1977.

87. C.H.Yang, T.E.Mitchell and R.A.Youngman, "High-Resolution Microscopy of Silicon Carbide," Proceedings of the 43rd Annual Meeting of the Electron Microscopy Society of America, pp.474-75 (1985).

88. A.C.D.Chaklader and M.G.K.Grant, "Fluid Phase Densification and Reactive Hot-pressing of Alumina," Agglomeration 85, pp.665-73, (1985)., C.E.Capes (ed.)., Toronto, Canada, The Iron and Steel Society Inc.

89. J.H.Goldberg, "Automatic Controls: Principles of System Dynamics," Allyn and Bacon Inc., (1969).

90. W.Poch and A.Dietzel, "Formation of Silicon Carbide from Silicon Dioxide and Carbon," Ber.Deut.Keram.Ges., 39[8] 413-26 (1962).

91. H.N.Baumann, Jr. "Relationship of Alpha and Beta Silicon Carbide," J.Electrochem.Soc., 99[3] 109-14 (1952).

92. N.A.L.Mansour and S.B.Hanna, "Silicon Carbide and Nitride from Rice Hulls II. Effect of Iron on the Formation of Silicon Carbide," Trans. and J. of the British Ceramic Society, 78[6] 132-6 (1979).

PROGRAM TO CALCULATE THE MATHEMATICAL COEFFICIENTS OF THE MODEL THAT FITS THE ISOTHERMAL COMPACTION CURVES OBTAINED FOR KAOLINITE + C. IT USES THE CURVE FITTING ROUTINE NL2SNO, WHICH USES THE MEANS TO ACCOMPLISH A LEAST SQUARES FIT. THE PROGRAM ALSO CALCULATES THE PARAMETERS OF THE MECHANICAL ANALOG OF THE MODEL.

```
      PROGRAM MMODEL

      IMPLICIT REAL*8(A-H,O-Z)
      DIMENSION P(5),Q(5),IV(67),V(1000),XX(120),YY(120)
      DIMENSION YYD(120), ALGY(120)
      DIMENSION IX(60)
      EXTERNAL CALCR
      COMMON X(60),Y(60)

      DO 12 I=1,60
      READ(5,11) X(I),Y(I),IX(I)
11    FORMAT(F7.3, 3X, F7.5, 3X, I1)
      N=I
      IF(IX(I)-1)12,20,12
12    CONTINUE
20    M=5
      P(1)=.46554D0
      P(2)=.0802D0
      P(3)=.907D0
      P(4)=.4038D0
      P(5)=7.D0
      IV(1)=0

      DO 13 J=1,5
      Q(J) = P(J)
13    CONTINUE

      CALL NL2SNO(N,M,P,CALCR,IV,V,IPARM,RPARM,FPARM)
      DINC=.1D0
      XX(1)=0.D0
      DO 30 I=2,101
30    XX(I)=XX(I-1)+DINC
      DO 31 I=1,101
      YY(I)=STRAIN(P,XX(I))
      YYD(I)=EPSDOT(P,XX(I))
31    ALGY(I)=DLOG(YYD(I))
```

```
      AK=P(1)
      A=P(2)/AK
      A1=P(3)
      B=1-A
      B1=P(5)


      TB  = P(4)/P(1)
      E2  = 1/(AK * (A * A1 + B * B1))
      RM2 = E2 * (A1 + B1 - AK * A1 * B1 * E2)
      E1  = RM2/(A1+B1-RM2/E2-A1*B1*E2/RM2)
      RM1 = A1 * B1 * E1 * E2/RM2

      WRITE(6,40)
 40   FORMAT(T34,'SAMPLE: 83',//)
      WRITE(6,41)
 41   FORMAT(T13,'TIME',T27,'STRAIN', T40,
     + 'STR. RATE',T55,'LN(STR. RATE)')
      WRITE(6,43)
 43   FORMAT(T13,'(MIN)', T26, '(DLT L/L0)', //)


      DO 50 I=1,101
 50   WRITE(6,51) XX(I),YY(I),YYD(I),ALGY(I)
 51   FORMAT(T4, 3F15.5, 1X, F15.5)
      WRITE(6,60)
 60   FORMAT(//////// T7, 'COEFFICIENTS:', / T7, 13('-'), //)
      WRITE(6,61)AK
 61   FORMAT(T7, 'K =', F9.5,/)
      WRITE(6,62)A,A1
 62   FORMAT(T7,'A =',F9.5,T24,'ALPHA =',F9.5,/)
      WRITE(6,63)B,B1
 63   FORMAT(T7, 'B =',F9.5,T24,'BETA  =',F9.5,//)


      WRITE(6,64)
 64   FORMAT(/ T7, 'MECHANICAL PARAMETERS:', / T7, 22('-'), //)
      WRITE(6,65)
 65   FORMAT(T10, 'M1', T18, 'ETA1', T27, 'M2', T34, 'ETA2', /)
      WRITE(6,66)RM1, E1, RM2, E2
 66   FORMAT(T6, F8.4, T15, F8.4, T23, F8.4, T31, F8.4, /)


      WRITE(6,67)
 67   FORMAT(// T7, 'INITIAL ESTIMATES:', / T7, 18('-'), //)
      WRITE(6,68)Q(1)
 68   FORMAT(T7,'P(1) = K =',F8.4, /)
      WRITE(6,69)Q(2), Q(3)
 69   FORMAT(T7,'P(2) = A.K =',F8.4, T31,'P(3) = ALPHA =',F8.4, /)
      WRITE(6,70)Q(4), Q(5)
 70   FORMAT(T7,'P(4) = B.K =',F8.4, T31,'P(5) = BETA  =',F8.4, /)
      WRITE(6,71) P(4), TB
 71   FORMAT(////T7, 'FINAL VALUE OF P(4) =', F9.5,/T21,
     + 'HENCE B =', F9.5)
      STOP
      END
```

```
      DO 100 I=1,N
      R(I)=P(1)-P(2)*DEXP(-P(3)*X(I))-(P(1)-P(2))*DEXP(-P(5)
     + *X(I))-Y(I)
100   CONTINUE
      RETURN
      END

      FUNCTION STRAIN(P,X)
      IMPLICIT REAL*8(A-H,O-Z)
      DIMENSION P(7)

      STRAIN = P(1)-P(2)*DEXP(-P(3)*X)-(P(1)-P(2))*DEXP(-P(5)*X)
      RETURN
      END

      FUNCTION EPSDOT(P,X)
      IMPLICIT REAL*8(A-H,O-Z)
      DIMENSION P(7)

      EPSDOT = P(2)*P(3)*DEXP(-P(3)*X)+(P(1)-P(2))*P(5)
     + *DEXP(-P(5)*X)
      RETURN
      END

      SUBROUTINE CALCR(N,M,P,NF,R,IPARM,RPARM,FPARM)
      IMPLICIT REAL*8(A-H,O-Z)
      DIMENSION P(M),R(N)
      COMMON X(60),Y(60)
```

APPENDIX B

An unit step input can be explained mathematically by

$$\epsilon = X\sigma \qquad \qquad \text{........ 1}$$

where

$$\epsilon = \text{strain (output)}$$
$$\sigma = \text{stress (input)}$$
$$\text{and } X = \text{transfer function}$$

The applied step input was normalized to a given reference strain† or

$$\sigma = \frac{\sigma_{applied}}{\sigma_{ref}} U_c(t)$$

$$\text{where } U_c(t) = \begin{matrix} 0 & \text{for } t \leq 0 \\ 1 & \text{for } t > 0 \end{matrix}$$

A differential equation for the system can be found by applying the Laplace transform to equation (1)[76] (represented by capital letters):

$$E = X\Sigma \qquad \qquad \text{........ 2}$$

where

$$E = L(\epsilon(t)) = \frac{K}{S} - \frac{KA}{S+\alpha} - \frac{KB}{S+\beta}$$

$$= \frac{K(S+\alpha)(S+\beta) - KAS(S+\beta) - KBS(S+\alpha)}{S(S+\alpha)(S+\beta)}$$

and

$$\Sigma = L(U_c(t)) = \frac{1}{S}$$

Therefore, the Laplace transform of the transfer function is found to be (taking into consideration that at t=0, $\epsilon(t)$=0, i.e., A + B = 1)

$$\frac{E}{\Sigma} = X = \frac{SK(A\alpha + B\beta) + K\alpha\beta}{S^2 + (\alpha+\beta)S + \alpha\beta} \qquad \qquad \text{........ 3}$$

---

†Note that when $\sigma_{eff} = \sigma_{app}$, the input is just a unit step function $U_c(t)$. The reference chosen for this work was ($\sigma_{ref} = 20$ MPa)

137

which can be rearranged to give

$$E\left[S^2 + (\alpha + \beta)S + \alpha\beta\right] = \Sigma\left[SK(A\alpha + B\beta) + K\alpha\beta\right] \qquad \text{........ 4}$$

Taking the inverse Laplace transform of equation (4) produces the differential equation

$$\frac{d^2\epsilon}{dt^2} + (\alpha + \beta)\frac{d\epsilon}{dt} + \alpha\beta\epsilon = K(A\alpha + B\beta)\frac{d\sigma}{dt} + K\alpha\beta\sigma \qquad \text{........ 5}$$